Vysoké učení technické v Brně
Fakulta strojního inženýrství
Ústav konstruování

Brno University of Technology
Faculty of Mechanical Engineering
Institute of Machine and Industrial Design

EXPERIMENTAL INVESTIGATION AND NUMERICAL MODELLING OF TOP OF RAIL PRODUCTS

Ing. Daniel Kvarda
Autor práce
Author

prof. Ing. Martin Hartl, Ph.D.
Vedoucí práce
Supervisor

Disertační práce
Dissertation Thesis

Brno 2022

ABSTRACT

This dissertation thesis deals with experimental and numerical study of top or rail products. These products are used to reduce wear, noise and improve energy efficiency of wheel and rail contact. In the last two decades, extensive experimental research has been conducted on the use of top of rail products. However, very little research has focused on the fundamental mechanisms of these products, especially causes of low adhesion. Application of mathematical models to this field was also not yet examined. The aim of this thesis is to explain the frictional behaviour and low adhesion conditions of the top of rail products with the use of a mathematical model. The model assumes both friction arising from solid asperity interaction and separation by a fluid film. The validation of this model was carried out on an experimental tribometer with the ability to measure film thickness to validate the accurate prediction of surface separation. A commercial tribometer was used to investigate the influence of individual components in oil-based top of rail product on the coefficient of adhesion. A set of rheological tests in combination with the model showed that the solid particles had very little effect in increasing adhesion after application. Subsequently, different types of top of rail products were tested using a high pressure torsion device. The boundary friction of these substances was evaluated by the model. The positive frictional characteristics that these products should provide are found to be a result of sliding friction changing the composition of the interfacial layer. In addition, the low coefficient of friction due to overapplication occurred at the same amount applied for all tested substances. This thesis presents original research expanding on the knowledge of top of rail products.

KEYWORDS

ABSTRAKT

Tato disertační práce se zabývá experimentálním a numerickým studiem maziv pro temeno kolejnice. Tyto maziva se používají ke snížení opotřebení, hluku a zlepšení energetické účinnosti kontaktu kola a kolejnice. V posledních dvou desetiletích byl proveden rozsáhlý experimentální výzkum týkající se použití maziv pro temeno kolejnice. Avšak velmi málo výzkumu bylo zaměřeno na základní mechanismy těchto produktů, zejména na problémy s nízkou adhezí. Aplikace matematických modelů v této oblasti také nebyla dosud zkoumána. Cílem této práce je pomocí matematického modelu vysvětlit třecí chování a problémy s nízkou adhezí maziv pro temeno kolejnice. Model předpokládá jak tření vznikající interakcí nerovností pevných látek, tak separaci mazacím filmem. Validace tohoto modelu byla provedena na experimentálním tribometru se schopností měřit tloušťku filmu pro ověření přesné predikce separace povrchu. Komerční tribometr byl použit ke zkoumání vlivu jednotlivých složek v mazivu pro temeno kolejnice na bázi oleje. Sada reologických testů v kombinaci s modelem ukázala, že pevné částice měly velmi malý vliv na zvýšení adheze po aplikaci. Následně byly testovány různé typy maziv pro temeno kolejnice pomocí vysokotlakého torzního zařízení. Mezný režim tření těchto látek byl hodnocen představeným modelem. Bylo zjištěno, že pozitivní třecí vlastnosti, které by tyto produkty měly poskytovat, jsou výsledkem velké skluzové vzdálenosti, která mění složení třecí vrstvy. Nízký koeficient tření v důsledku nadměrné aplikace se vyskytl při stejném aplikovaném množství u všech testovaných látek. Tato diplomová práce představuje původní výzkum rozšiřující znalosti o produktech pro temeno kolejnice.

KLÍČOVÁ SLOVA

Kontakt kolo-kolejnice, Řízení tření, Maziva pro kolejový svršek, Numerický model, Tribologie

BIBLIOGRAPHICAL REFERENCE

KVARDA, Daniel. *Experimental investigation and numerical modelling of top of rail products.* Brno, 2022. 120 p., PhD thesis. Brno University of Technology, Faculty of Mechanical Engineering, Institute of Machine and Industrial Design. Supervisor prof. Ing. Martin Hartl, Ph.D.

ACKNOWLEDGEMENT

Firstly, I would like to express my gratitude to prof. Ing. Martin Hartl, Ph.D. for his support during my study. A big thanks belong to Ing. Milan Omasta, Ph.D. for his guidance and help as co-supervisor and leader of our group. My sincere thanks also goes to Ing. Radovan Galas, Ph.D., who made great efforts to help me in all aspect of my research.

I also have to mention a group of colleagues and great friends that I have met and shared my office with during my study. You have kept me sane and without you I would probably not be able to finish this work. I do not dare to name all of you as there are many and I fear to forget someone. I also have to thank all my other friends, to whom I could rely on bringing happiness and motivation. And lastly, the most important thanks go to my family. My father, mother, sister and brothers who always helped me and supported me.

STATEMENT

I hereby declare that I have written the PhD thesis *Experimental investigation and numerical modelling of top of rail products* on my own according to advice of my supervisor prof. Ing. Martin Hartl, Ph.D., and using the sources listed in references.

…………………………….

Daniel Kvarda

CONTENTS

1 INTRODUCTION

Railway transportation network has high demands in terms of energy savings, reliability and safety. The movement of people and goods between cities, as well as city public transportation is highly represented by the railway sector. This is the result of the continuing pressure for environmentally friendly and sustainable transportation. Furthermore, the growing popularity of high-speed trains gives rise to new advances in the field of railway research and development.

A key role in the operation of railway vehicle is the contact area between the wheel and rail where traction and braking forces are transferred. Contact mechanics affect not only the acceleration and deceleration of the vehicle, but also the dynamic behaviour. The dynamics greatly influence passenger comfort, running safety and service life. Issues such as derailment, high level of noise and wheel-rail failure can be traced back to the contact interface between wheel and rail. The most important property of wheel-rail contact is friction, also referred to as adhesion in the field of railway industry. In the simplest case, high friction causes excessive wear of the surfaces, while too low friction can lead to issues with traction and braking of the vehicle. In terms of dynamics, frictional forces can cause excitation of vibration in different machine parts and lead to passenger discomfort and machine part failure.

As a result of the contact being an open system with a wide range of external influences, it is not feasible to control the friction in a simple manner. In past, the most common problem was low adhesion caused by environmental causes such as fallen leaves, rain or snow. The application of an abrasive material such as sand helps with adhesion forces as well as removing the contamination layer from surfaces. Nevertheless, hard particles promote surface damage and wear. Low adhesion is desirable in the contact between the wheel flange and the rail gauge. To reduce wear and geometrical changes in this high sliding area, grease lubrication systems are widely used. In recent decades, top of rail lubrication management, which aims to provide optimal frictional conditions in wheel-rail contact, has been gaining popularity. Top of rail products applied into wheel-rail contact increase fuel efficiency, reduce maintenance cost and mitigate noise emission. Understanding the possible risks of using these products and defining their proper use could bring benefits in increasing the effectiveness of railway transportation, as well as ensuring safety and comfort of not only passengers, but also people and residents in areas that use railway network.

The aim of this doctoral thesis is to clarify the frictional properties of top of rail products using experimental and numerical methods. Special attention is paid to the causes of low adhesion issues when applying these materials, which could cause problems with traction and braking.

2 STATE OF THE ART

The first signs of the use of wheeled vehicles that run on paved tracks can be traced back to ancient Greece and Roman Egypt. Later, the use of wooden rails and wagonways hauled by animal power was introduced in the 16th century Europe. The modern form of railway transportation started at the end of the 18th century with the invention of a steam locomotive.

Since the first deployment of railway transportation, the wheels and rails have undergone a substantial evolution. Nevertheless, the main principles remained the same. In the present day, the running surface of the wheel has a conical shape and slowly changes its geometry to a wheel flange at the inner side that prevents the wheels from derailing. Generally, during a rolling of two bodies, there are four main dimensions that define the contact geometry. The rolling radius of the wheel is r_{1x} and the radius of lateral profile is r_{1y}. For the rail, the radius in the direction of rolling is r_{2x}, which for a straight rail is equal to infinity, and in the lateral direction r_{2y}. The first index defines the body it refers to and the second index defines the direction as shown by the Cartesian system in Fig. 2.1. The wheel rotates with an angular velocity ω_1 resulting in velocity of the vehicle v_1. The velocity of the moving surface of wheel is $\dot{x}_1$ and if we take the ground as a reference, then the stationary rail has a surface velocity $\dot{x}_2$ equal to zero. The wheel is loaded by a normal force F_N resulting in a contact area with semi-axes a and b in the x and y direction, respectively. The resulting forces in x, y and z direction are longitudinal, lateral and normal respectively. The longitudinal forces are also referred to as tangential or creep forces.
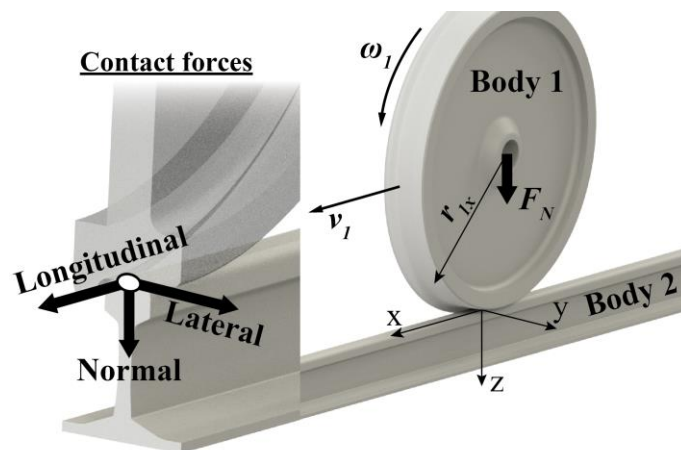

Fig. 2.1 Wheel-rail geometry and kinematics.

This description is limited to simple forward motion. In reality, the kinematics of the vehicle also include lateral movement and spin. These motions naturally occur due to the tracks not being perfectly straight. Especially when the vehicle is driving through a sharp curve, these movements arise. For simplicity, this thesis only deals with the longitudinal direction that is detrimental to the transfer of traction and braking forces.

2.1 Friction and adhesion in wheel rail contact

Friction is a phenomenon that every person deals with every day. It can be described as a resistance to relative motion of objects sliding against each other. The laws of friction were published by Amontons in 1699 even thou the discovery is attributed to Leonardo da Vinci. These laws state that the friction force is proportional to the normal load applied to the object and is independent of the apparent area of contact. These laws were later verified by Coulomb, who added that the frictional force is independent of the object velocity. Based on these properties, the friction is characterized by coefficient of friction. It is defined as a ratio between the tangential frictional force F_F and normal force F_N in contact between two surfaces, see Eq. (2.1).

$$f = \frac{F_F}{F_N}$$

(2.1)

This is true for an object that performs purely translational motion where the surfaces either stick together or slide against each other. For a wheel-rail contact, the conditions are more complex due to the combination of translational and rotational motion of the wheel. When a torque is applied to the wheel, there is a frictional force in the contact that can result in traction or braking depending on the direction of the torque. This frictional force is in the field of railway referred to as adhesion force F_T (not to be mistaken for adhesion force in general tribology). Therefore, the ratio between adhesion force and normal force in wheel rail contact is defined by coefficient of adhesion as described in Eq. (2.2).

$$\mu = \frac{F_T}{F_N} \leq f$$

(2.2)

The original laws provide a simplification that is reasonable for a general understanding of friction. At microscopic level we see that the true contact area is realized through asperity interactions. In wheel-rail contact, the combination of nonuniform contact pressure distribution and rolling-sliding kinematics makes the understanding of traction forces more difficult. The mathematical explanation of tangential traction (shear stress distribution) in wheel-rail contact was first given by Carter [1]. His work showed the division of contact area into part where the contacting surfaces are locked together, also referred to as area of stick or adhesion, and part where the contact is under micro-slip. This is due to the surface shear stress being too high to be supported by the pressure. The resulting shear stress has a limiting value which cannot be exceeded by the contact surfaces. Subsequently, this was observed and confirmed by a stress freezing method [2].

The increase in shear stress is closely linked with the increase in relative velocity between surfaces expressed as the slip value. For laboratory experiments, a term called slide-

to-roll ratio (SRR) is used due to the kinematics of laboratory devices. Both slip and SRR define the ratio between relative motion of surfaces and running speed, see Eq. (2.3) and Eq. (2.4).

$$slip = \frac{v_1 - \omega_1 r_{1x}}{v_1} \tag{2.3}$$

$$SRR = \frac{\dot{x}_1 - \dot{x}_2}{(\dot{x}_1 + \dot{x}_2)/2} \tag{2.4}$$

Slip is defined based on the velocity of the vehicle v_1 and the vehicle wheel surface speed $\omega_1 r_{x1}$. The SRR is defined based on the surface velocities $\dot{x}_1$ and $\dot{x}_2$ divided by their mean value. In both cases, the number that is being divided represents the relative velocity between the two surfaces. Plotting the coefficient of adhesion versus slip gives a traction curve, as illustrated in Fig. 2.2. Looking closely, the contact area is divided to adhesion and microslip areas. At zero slip the bodies are in pure rolling conditions where no micro-slip conditions occur. With increasing slip between the two bodies, the coefficient of adhesion increases as area of slip also increases. At some point, the area of adhesion vanishes, and the contact is transferring tangential forces through full slip area. At this point, the coefficient of adhesion reaches the theoretical value of coefficient of friction, which is defined for full sliding conditions.
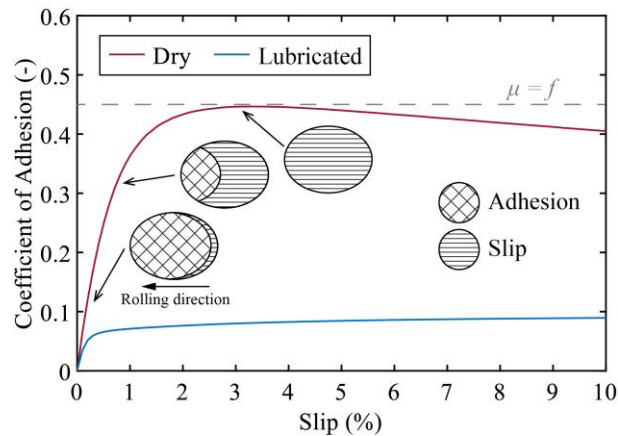

Fig. 2.2 Traction curve for dry and lubricated wheel-rail contact.

In Fig. 2.2 the traction curves for dry and lubricated contact conditions represent a real behaviour. With a higher slip, the coefficient of adhesion decreases for dry conditions. This is called a negative trend of the traction curve and is a result of increased temperature. For lubricated contact conditions, the traction curve reaches stable values, resulting in a negative or positive trend. The trend of the traction curve is important for the dynamic behaviour and stick-slip oscillations that occur under negative traction conditions.

In the presence of lubricant, the coefficient of adhesion is lower compared to clean

and dry contact. Lubrication can be done with either solid or liquid lubricant. In the case of solid lubricant, the slip is accommodated by a layer of solid lubricant that has low shear strength. For liquid lubrication, we must consider the hydrodynamic effect that creates surface separation, as well as lubricant viscosity. This is best illustrated by the Stribeck curve in Fig. 2.3. The film parameter Λ describes the ratio between surface separation and surface roughness. At very low film parameters, the shear stresses are transferred mostly through asperity contacts. This is called a boundary regime, and the lubricant itself can have properties that create a very thin molecular film that help lower the coefficient of adhesion. With an increasing film parameter, the shear stresses are taken partly by asperity contact and partly by the lubricant film in mixed lubrication regime. Going higher with film parameter transitions to the elastohydrodynamic regime, and the hydrodynamic regime where full separation of surfaces is achieved. At this point, friction is driven by the shear stress in the lubricant film, which is related to the viscosity of the lubricant.
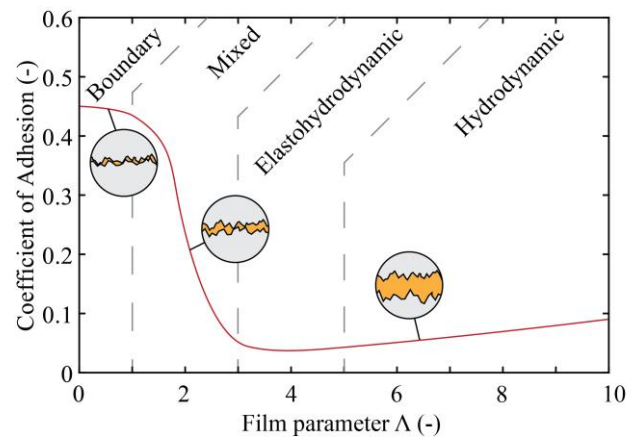

Fig. 2.3 Illustration of Stribeck curve.

2.2 Friction modification

The general categorization of products used for wheel-rail contact friction modification is based on articles [3–5]. Friction management at the wheel-rail interface can be looked at in different ways. In the contact of the wheel flange and rail gauge, the use of low coefficient of friction (LCF) modifiers, such as greases, decreases wear. On the top of the rail, the increase in coefficient of adhesion by adhesion enhancers (very high positive friction modifiers – VHPF) is used in conditions that endanger traction and braking. In case of dry conditions when friction is too high for efficient operation, the use of top of rail management products is justified. These products are often classified as high positive friction (HPF) modifiers.

Managing the friction by HPF top of rail products leads to benefits in reduction of energy consumption, noise and damage to contacting surfaces such as wear, corrugation and

rolling contact fatigue. Different types of products are applied to the contact interface for this purpose. We can differentiate these products based on the medium used to carry the components. Water-based substances are called friction modifiers (FM) and are meant to dry out after the substance is spread along the rail. Oil-based products are referred to as top of rail lubricants (TOR lubricant). In addition, products that use the benefits of both water and oil can be used (TOR hybrid). TOR hybrid products are often classified as TOR lubricants. Lastly, a solid material in the form of an interlocking blocks of sticks (solid FM) is available on the market. All these categories will be referred to as top of rail (TOR) products.

The effectiveness of TOR products has been reported in studies on vehicle dynamics [6–8], reduction of wear [9–15], corrugation [6, 16–20] and noise [21–24]. These studies might not be primarily focused on friction, which is the main aim of this thesis, and thus will not be described in further detail.

2.2.1 Frictional properties

The purpose of a TOR product is to lower the coefficient of adhesion to a desirable level. A typical coefficient of adhesion for TOR product is between 0.3 and 0.4 [3]. However, this can differ for field and laboratory experiments and is greatly influenced by the conditions of the surface and the used device. The study [25] compared the experimental results of various measuring devices for dry, wet and lubricated conditions. As seen in Fig. 2.4 for dry conditions, we get a wide range of measured coefficient of friction from 0.4 to 0.8. For friction modifier conditions, the data suggest more stable values around $0.15 - 0.25$. For this reason, it is not easy to transfer the measured data between devices or even to real field conditions.
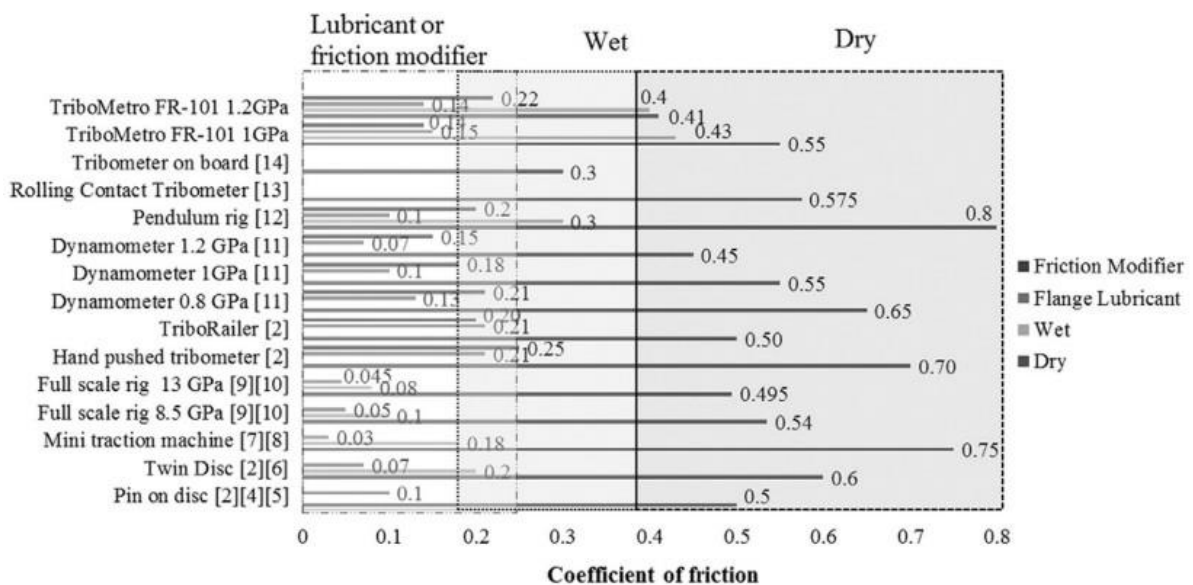

Fig. 2.4 Comparison of frictional values for different measuring devices and conditions [25].

The first investigation on the TOR product was conducted for the Vancouver mass transit system [26] in the early 1990s. This study was motivated by excessive corrugation problems, and TOR solid stick was selected as one of the solutions. The corrugation problem was virtually eliminated with the use of TOR product, as well as changing the tolerance of wheelset alignment and regauging the track. The study itself does not report field measurement of the coefficient of adhesion. However, an Amsler twin disc was used to test the solid stick under a contact pressure of 700 MPa and 400 rpm with discs of wheel-rail material. Under a light application pressure of solid stick, the coefficient of adhesion measured was 0.17 and 0.32 at 2.5% and 30% slip, respectively.

Matsumoto et al. [27] tested FM on a 1/5 scaled roller rig at 10 km/h. The FM was applied by brush and the experiments started after drying of the composition. This meant that there was no control over the amount applied. Fig. 2.5 shows the results for clean and FM conditions at a normal load of 1000 N. The saturation point for clean conditions was at 0.7% slip after which there was a decrease in coefficient of adhesion causing a negative trend of the traction curve. The maximum value of the coefficient of adhesion was 0.46. Using the application of FM, the traction curve showed increasing trend throughout the range of the measured slip ratio. The initial increase had a much lower slope with no clear saturation point resulting in a positive traction characteristic. At 1.2% slip, the measured coefficient of adhesion was 0.16 compared to around 0.43 in dry conditions. Similar trends were observed for the lateral traction curves, where a reduction in the lateral force was achieved.

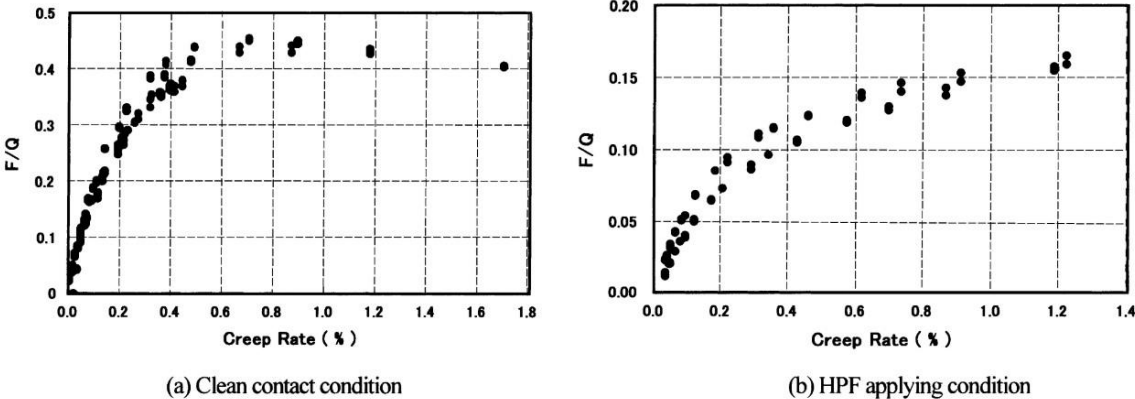(a) Clean contact condition　　　　　　　　　(b) HPF applying condition

Fig. 2.5 Traction curves for clean and FM conditions at normal load of 1000 N [27].

The continuation of the previous study was published two years later by Matsumoto et al. [28]. This time the authors used an on-board spraying system for the application of FM KELTRACK[TM] HPF SPRAY. In the first stage the authors used a 1/10 scaled model vehicle to assess the curving performance when FM was applied. A reduction in lateral forces was found as a well as lower lateral displacement of the axle, as seen in Fig. 2.6a. Furthermore, twin-disc experiments were conducted using a 172 mm disc diameter, where the rail disc had a lateral radius of 100 mm. FM was sprayed onto the rail disc by a spray nozzle. The results showed the dependency of coefficient of friction on the spraying time. Increasing the spraying time and thus increasing the applied amount led to a reduction of the coefficient of

friction below 0.1. Evaluating the effect of duration showed that increasing slip consumes the FM faster. The interval of spraying and thus the amount of FM applied is important to proper frictional characteristics. In combination with the slip, it determines the rate of FM consumption.
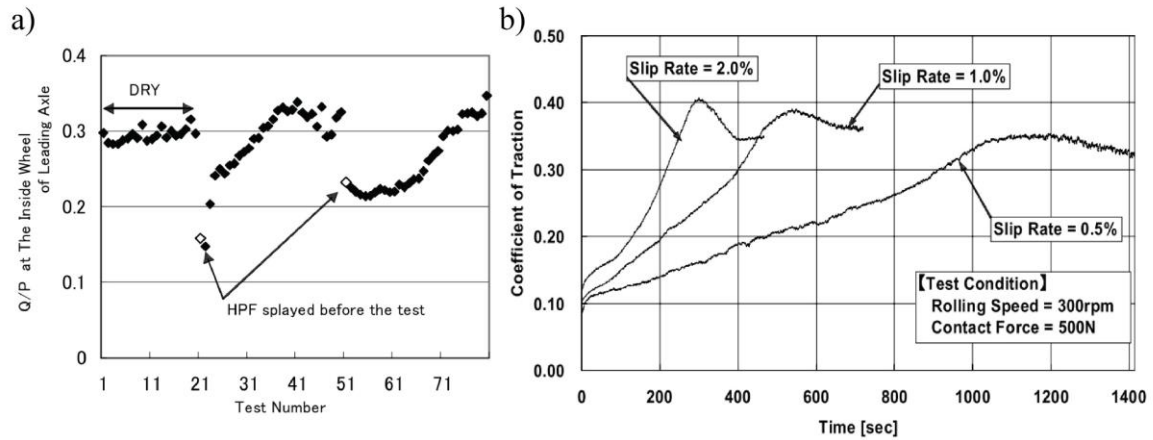

Fig. 2.6 Lateral coefficient of friction in scaled vehicle test (a), removal of FM during twin-disc test (b) [28].

A study by Tomeoka et al. [29] used the same twin-disc apparatus as [28] to investigate the influence of the HPF application method. Painting the HPF product onto the disc surface yielded a low coefficient of adhesion in the first cycle, as shown in Fig. 2.7a. Subsequent cycles increased the frictional values until a measurement similar to dry contact was reached. These results correspond to the study [28] by showing that the total slip distance that the lubricant undergoes is linked to the increase in frictional values. To suppress the low adhesion conditions after application, the authors suggested a method to spread the product more evenly by a spraying mist. The results in Fig. 2.7b showed a desirable frictional characteristic even after the first application by spray nozzle. An on-board HPF spraying system developed by the authors was tested, which resulted in good performance lowering the contact forces and squeak noises.
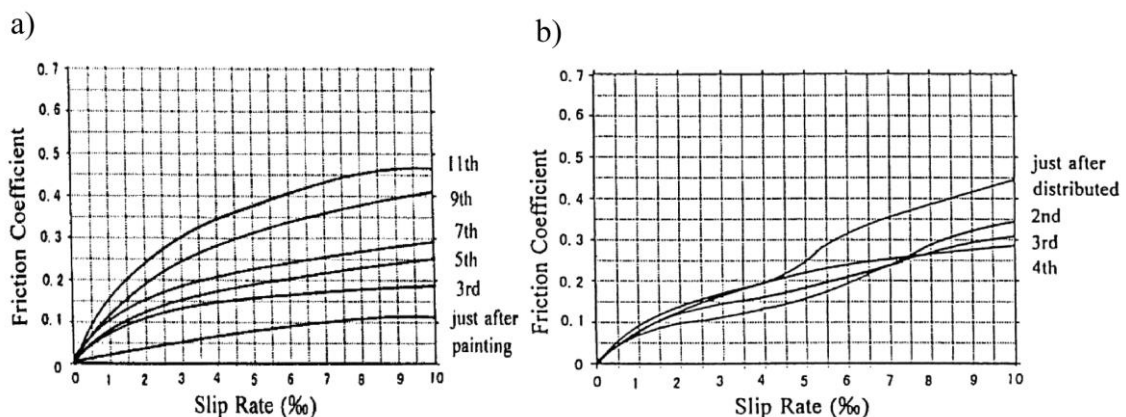

Fig. 2.7 Traction curves for painted HPF (a), sprayed HPF (b) [29].

Ishida et al. [30] used a twin-disc machine to assess the frictional properties of two developed friction modifiers as well as other lubricants. Subsequently, a friction modifier was applied

on a curve with 200 m radius, where a portable tribometer was used to measure the coefficient of friction. Twin-disc testing used a realistic wheel and rail material for the specimens. The circumferential speed was set to 40 km/h and the radial load to 3.5 kN, resulting in a maximum Hertzian pressure of 672 MPa. The root mean square roughness of the samples prior to the test was measured to be 1 μm. The results are shown in Fig. 2.8a. The developed friction modifiers provided the highest coefficient of adhesion, while oil with solid lubricant and natural graphite reached low values of 0.05. The friction modifier is made of carbon-based particles with additional coating. Using this friction modifier on a track resulted in a reduction of coefficient of friction as measured by a portable tribometer. The results shown in Fig. 2.8b suggest frictional values of 0.2. With three passes of a train, the removal of frictional layer caused an increase to about 0.4.
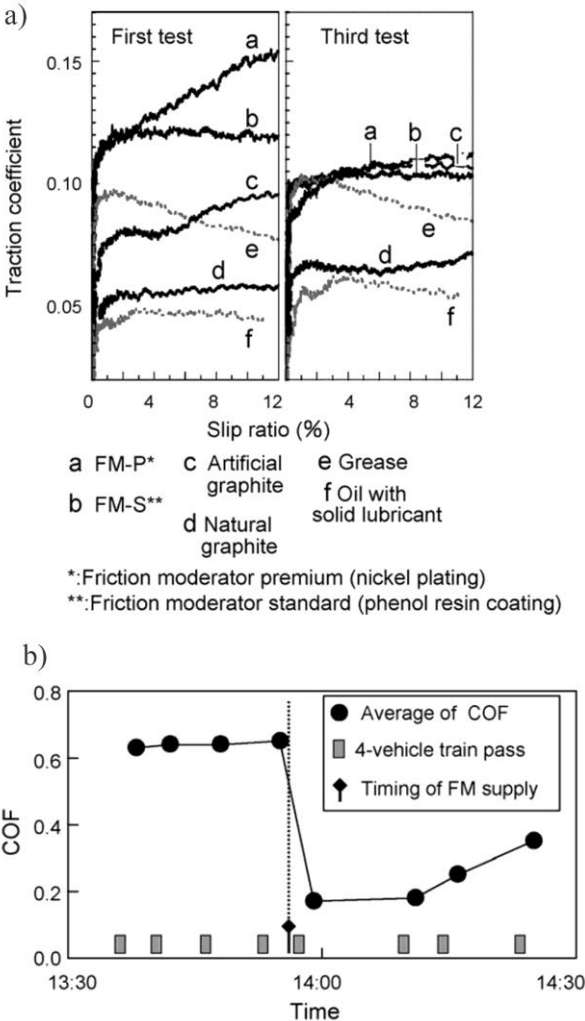

Fig. 2.8 Comparison of tested lubricants (a), field measurement of coefficient of friction (b) [30].

A similar field study was conducted by Areiza et al. [25] with commercial and custom-made friction modifier, as well as grease for flange lubrication. Frictional testing was done by a hand-pushed tribometer TriboMetro FR 101. This device uses a measurement wheel that applies braking torque and simultaneously measures the angular velocity, allowing it to measure the traction curve with changing slip. The coefficient of friction was measured on

18

a 90 m rail curve on a low-density traffic line. The average roughness of the rail was measured at 3 µm ± 0.6 µm. The pressure influence from the average of 20 measurements in Fig. 2.9 shows a decreasing trend with increasing pressure. The commercial "Friction modifier 1" reduces the coefficient of friction to levels similar to the flange lubricant at both tested pressures. Custom made "Friction modifier 2" provided a higher level of coefficient of friction around 0.2.
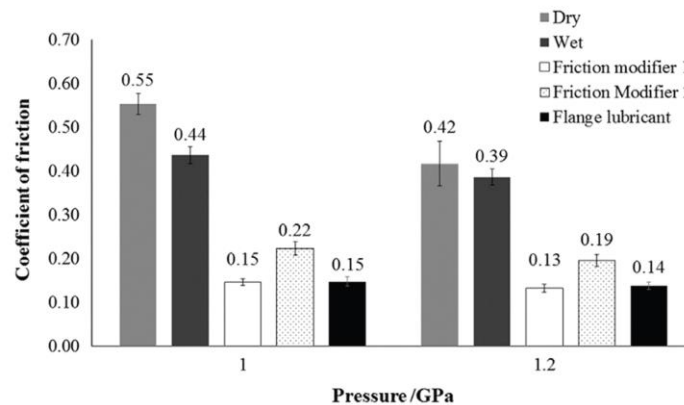

Fig. 2.9 Influence of pressure on tested substances (a), measurement of friction modifier (b) [25].

Measurement of different TOR products using two types of field tribometers was done by Harrison et al. [31]. In this study, a vehicle-propelled TriboRailer device was compared with a hand-pushed tribometer developed by British Rail Research. The tested products were water-based VHPF, HPF and LCF all manufactured by Kelsan Technologies. A hot-air dryer was used to ensure that the products dried before commencing the tests. The results for TriboRailer are shown in Fig. 2.10a, and the hand pushed tribometer in Fig. 2.10b. It is evident that the TriboRailer measured lower values of the coefficient of adhesion than the hand-pushed tribometer in all tested conditions. The tested HPF product helped achieve a positive trend of the traction curve compared to dry conditions that had a negative trend for the TriboRailer and a neutral trend for the hand-pushed tribometer. Aging process of HPF product was carried out with a run time of 60 minutes. During this test, the frictional film was slowly removed, which resulted in an increase in the coefficient of adhesion. However, dry conditions were not achieved even after the test was completed. This means that some of the lubricant content was still present in a very small amount, causing a decrease in the coefficient of adhesion.

Lundberg et al. [32] conducted a full-scale field approach with IORE locomotive used for heavy iron ore. The locomotive was equipped with a measurement system for frictional forces and sliding velocity. Additionally, tests with a commercial hand-pushed tribometer were conducted. The applied TOR product was Whitmore TOR Armor LT based on a glycol-water solution, which makes it a TOR hybrid product. The application of the product was done manually using a brush. Before lubrication, the tribometer estimated coefficient of friction between 0.5 – 0.7. The train measurement for dry conditions showed

much lower values between 0.3 – 0.4, as highlighted in Fig. 2.11. After lubrication, the tribometer measured the coefficient of friction around 0.2, while the train measurements varied between 0.05 – 0.25. In the second run, the values measured by the locomotive were higher and mostly above 0.1. This is explained by the influence of the sliding distance on the coefficient of friction. The first set of wheels ran into larger amount of applied TOR film. The variation of the results is related to the measurement being averaged on each bogie separately. Compared with the hand-pushed tribometer, influences such as scaling factor, different contact geometry and different pressure needs to be accounted for.
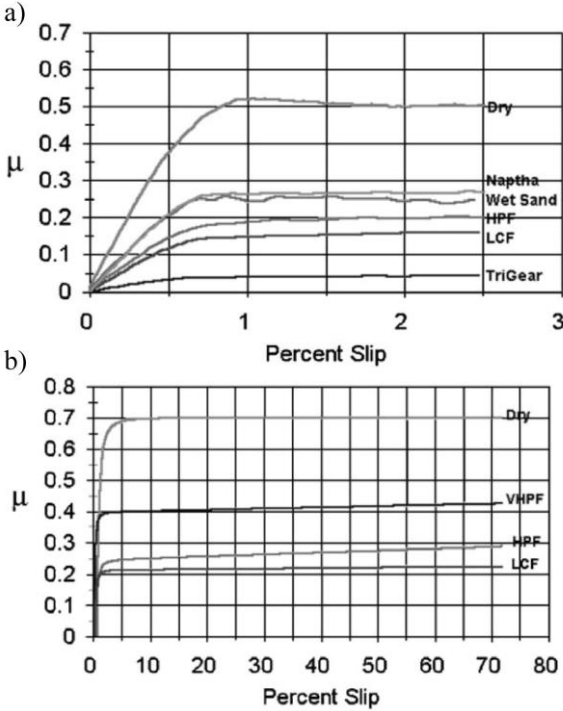

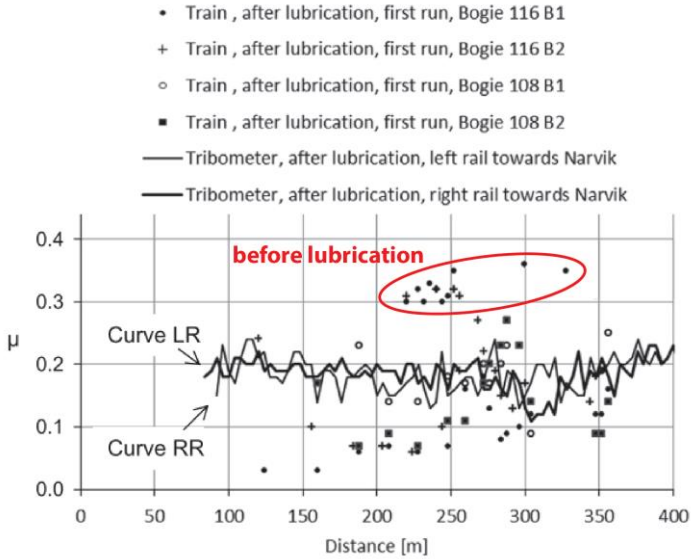Fig. 2.10 Field measurement with TriboRailer (a), and hand-pushed tribometer (b) [31].

Fig. 2.11 Train and tribometer measurements of friction under TOR lubricated conditions [32].

20

Liu and Meehan [22] conducted a study focused on the generation of squeal noise in the wheel and rail contact. The authors used a twin-disc experimental device with discs of diameters of 0.426 and 0.6 m. The normal load was set to 1000 N. The upper smaller disc is held by leaf springs with strain gauges that allow measurement of contact forces. The device uses a change in the angle of attack between the discs to create lateral slip. Only the upper wheel is driven so as the longitudinal slip is neglected. The experiments used one FM and two TOR lubricants. The FM was brushed onto the wheel tread and dried out. The results are shown in Fig. 2.12, where FM provided a coefficient of adhesion around 0.3 compared to 0.35 for dry conditions. Both TOR lubricants achieved very low coefficient of adhesion around 0.07. The results were fitted by a slip-dependent model for the coefficient of friction and further noise analysis was conducted.
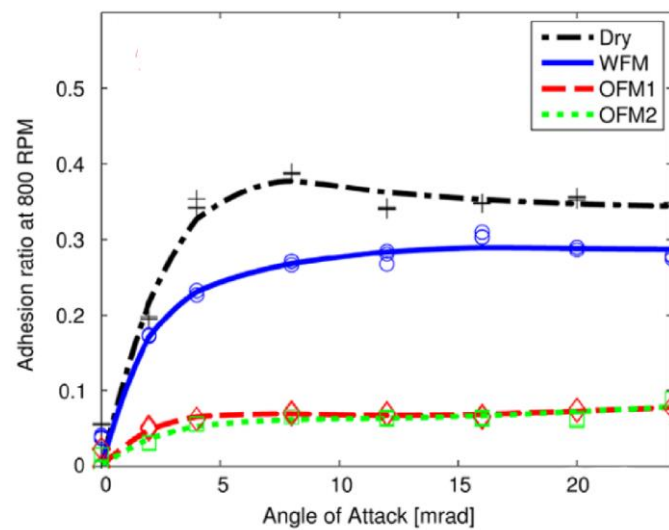

Fig. 2.12 Experimental results for dry conditions and TOR products at 800 rpm [22].

A set of laboratory studies focused on frictional properties of TOR products was conducted by Galas et al. [11, 12, 33]. The effect of TOR lubricants on the coefficient of adhesion [12] was investigated using a commercial ball-on-disc device Mini Traction Machine from PCS Instruments. The products were tested under 750 MPa maximum Hertzian pressure and 0.3 m/s speed. Two commercial TOR lubricants based on plant (FMA) and ester (FMB) oil were used. The product FMA contained solid particles of copper and zinc, while the FMB contained copper and aluminium. SEM photographs showed that the particles for both products are of a flake shape. Laser particle analysis showed that FMA contains 40x more solid particles larger than 4 μm than FMB. The results showed that this causes higher sensitivity to applied amount for FMB, as seen in Fig. 2.13. Using only 1 μl did not provide significant benefit, because the coefficient of adhesion quickly climbed to values similar to dry conditions for both TOR lubricants. Increasing the applied amount decreased the slope of frictional curve until there was only a small change in the coefficient of adhesion after application. The fact that the coefficient of adhesion does not drop below 0.1 is a good indicator that with over-lubrication there is no significant impact on traction and braking for

the test setup. Based on particle analysis, the product with higher particle content shows faster recovery and lower time below coefficient of adhesion 0.15. Furthermore, Stribeck curves for both TOR lubricants and castor oil were measured under fully flooded conditions. The results showed that both TOR lubricants behave very similarly to castor oil in transitioning from mixed lubrication regime to elastohydrodynamic. This suggests that solid particles do not help to increase friction at fully flooded conditions. However, these conditions cannot be compared with a single application test.
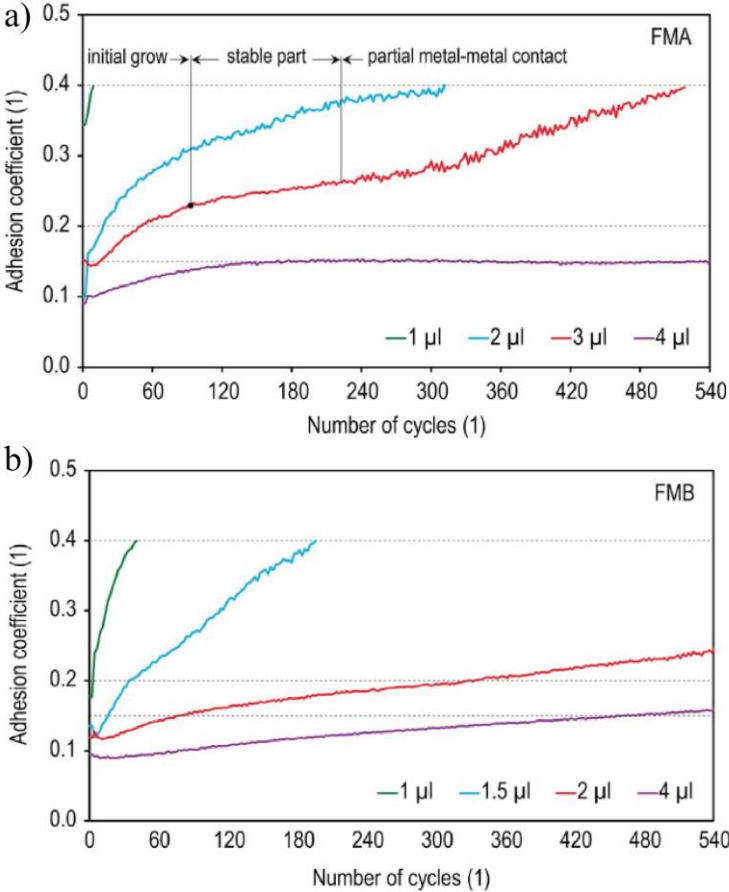

Fig. 2.13 Experiments with applied amount: FMA (a), FMB (b) [12].

The study [33] uses the same FMA as in [12] for the twin-disc evaluation of adhesion and noise. The experimental data were measured using 80 mm diameter discs made of bearing steel 100CrMn6 with a hardness of 60 HRC. The lower disc had a profile with a radius of 50 mm. The initial roughness of the discs was Ra 0.4 µm. The maximum Hertzian contact pressure was set at 800 MPa, the mean speed 1 m/s and the SRR 0.08. The tested product was applied by a micropipette into the contact. The results showed similar initial trend to the ball-on-disc testing [12], as seen in Fig. 2.14. Increasing the applied amount above 4 µl did not cause an additional reduction in the coefficient of adhesion and prolonged the effective area of intermediate adhesion. Lower amounts of 1 µl and 2 µl were not sufficient to provide intermediate values for an extended period of time. The larger contact dimensions and running surface of twin-disc required higher amounts of TOR lubricant to achieve similar over-lubrication as smaller scaled devices. During these experiments, the level of sound

22

pressure was also measured. The application of TOR lubricant reduced the sound pressure level from 97 dBA at dry conditions down to 68 dBA right after application. The sound pressure measurement also provided information on when the frictional layer breaks up and returns to conditions of dry contact. For the tested amounts, the coefficient of adhesion of 0.35 represents the point where sound pressure level climbed back to 97 dBA of dry contact. From Fig. 2.14, the value 0.35 is where the experimental data change slope to a faster increase of the coefficient of adhesion. To provide the benefits of reducing noise, this would be the point of reapplication to suppress noise emission.
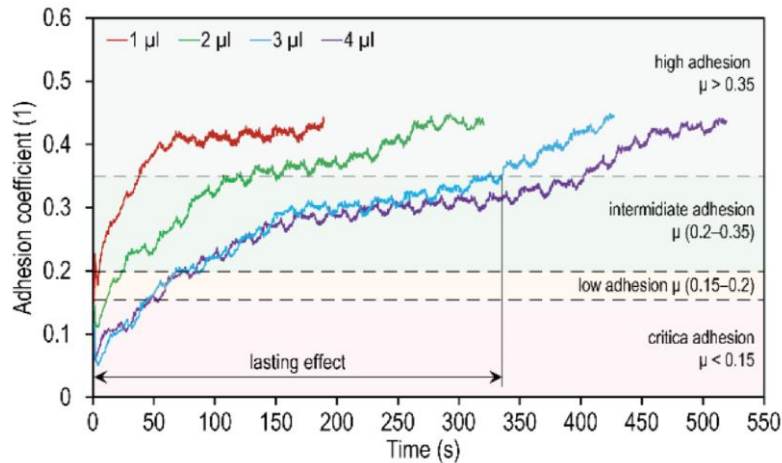

Fig. 2.14 Twin-disc testing of commercial TOR lubricant under different applied amounts [12].

The last publication of Galas et al. [11] focuses on the frictional properties of custom-made TOR FMs. The aim of this study was to investigate the influence of different components and materials of the water-based TOR product. The same ball-on-disc device as in [12] was used. All tests were carried out under 750 MPa contact pressure, 0.3 m/s speed and SRR 0.05. The final compositions tested consisted of water, 7.5 wt% bentonite, 5 wt% talc or zinc oxide as solid particles and 5 wt% molybdenum disulphide or graphite as a solid lubricant. Initial results showed that excessive viscosity of the substance will cause it to squeeze out and not allow for replenishment of the contact. This leads to faster removal of the frictional film and restoration of dry contact conditions. In this case, over 10 wt% of bentonite thickener in 1 ml of composition was enough to cause the mentioned replenishment problem. This was not the case for particles of talc that could control friction for long period of time even at 25 wt% content.

The final compositions were tested in both the "wet" and "dry" states, which means that the test was carried out right after application or after drying the base medium. Results for the best-performing compositions are shown in Fig. 2.15. The wet conditions in Fig. 2.15a suggest that the initial first seconds are controlled by the water medium and cause a coefficient of adhesion of 0.1. After the water was evaporated by the sliding contact, the values increased over 0.15 and then slowly up to 0.2. These are values similar to the results of dry film seen in Fig. 2.15b. The dry film provided a coefficient of adhesion around 0.2

from the start of the test. This drying effect is something that the previous publication did not take into account. The use of harder zinc oxide led to suppression of the initial adhesion drop. The correct selection of these particles for friction modification is important to provide suitable adhesion conditions.
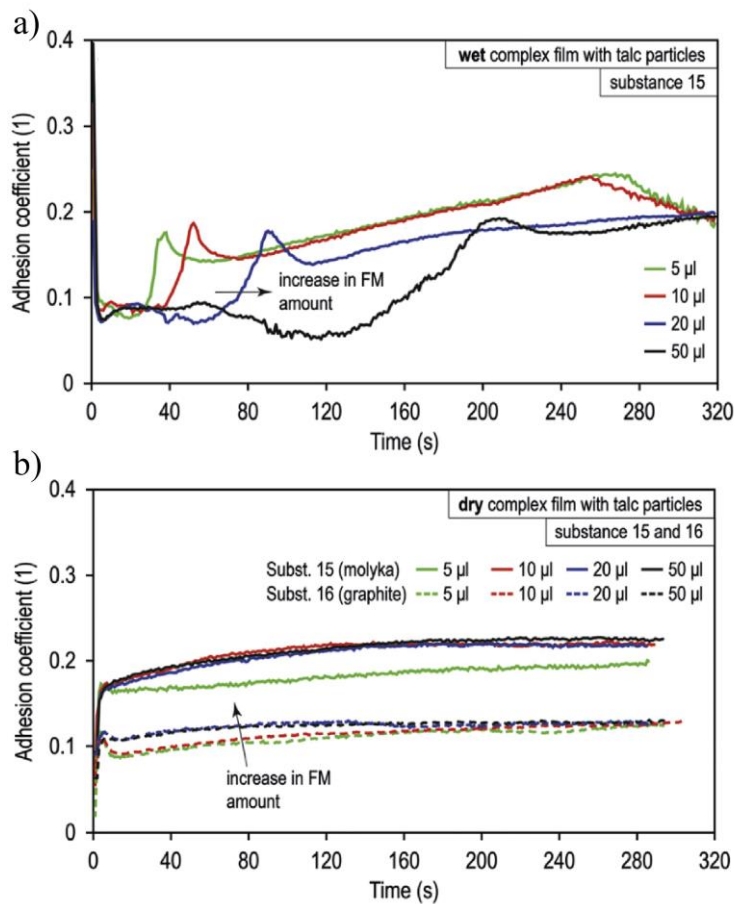

Fig. 2.15 Wet composition with talc and molybdenum disulphide (a), dry compositions with talc (b) [11].

A TOR hybrid was studied by Seo et al. [10] using a twin-disc machine with specimens made of KS60 rail and RSW wheel. The specimen had 60 mm diameter and resulted in line contact with a maximum Hertzian pressure of 1.1 GPa. The speed was set to 1.5 m/s with varying slip conditions. The used TOR hybrid is not specified, however, the microscope photographs suggest the content of solid metal particles of size less than 3 μm. The product was applied using a spraying device with a nozzle located 30 mm above the surface of the rail specimen. The results of the spraying time in Fig. 2.16a show a similar trend to the study [28]. The initial application moment caused a drop in coefficient of adhesion to very low values around 0.05. This drop appeared to be independent of the spraying time, while the stabilized part provided a higher coefficient of adhesion for a shorter duration of spraying of the TOR product. It took around 30 cycles to increase the coefficient of adhesion from the initial drop to the stable part. The longer spraying time of 1 s also caused a visibly slower transition to the stable part right after application.

The measured traction curves shown in Fig. 2.16b show intermediate levels of

24

coefficient of adhesion for the TOR hybrid. The results also indicate a positive trend of the traction curve compared to dry conditions and water contamination. Between 0% and 0.5% slip, the TOR product behaved similar to water contaminated conditions. After 0.5% slip, the water did not show any change while the TOR product provided steady increase with increasing slip.
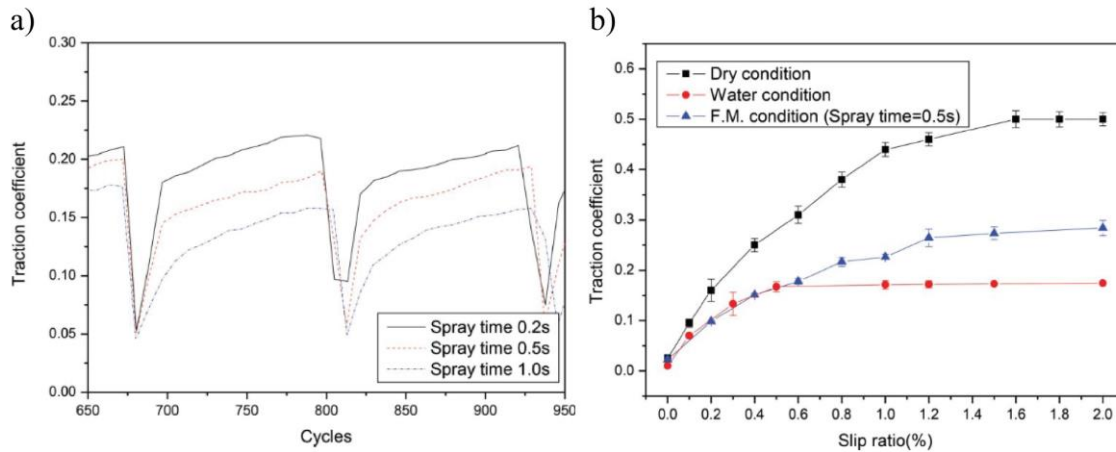

Fig. 2.16 The effect of spraying time under 0.6% slip (a), traction curves fo 0.5s spraying time (b) [10].

Hardwick et al. [34] conducted a study focused on the effect of TOR products on rolling contact fatigue, however some frictional results of interest are provided. The experiments were carried out on a twin-disc machine with R8T wheel and R350HT rail material, both with an initial roughness of 1 μm. The discs had a diameter of 47 mm and a width 10 mm. The mean speed was set to 1 m/s, maximum Hertzian contact pressure 1.5 GPa and 1% slip ratio. The tested products included FM, TOR hybrid and two types of TOR lubricant: low viscosity oil and high viscosity grease. No detailed description of these products is given. The application of these products was done using a small brush with an applied amount of 0.05 g per 500 cycles.

The results for all tested products are shown in Fig. 2.17. The FM provided the highest average coefficient of adhesion of 0.12. The TOR lubricant (oil) and TOR lubricant (grease) decreased the coefficient of adhesion to 0.07 and 0.06, respectively. The TOR hybrid had the worst performance with average values of 0.02. As seen in Fig. 2.17a, the FM caused the fastest recovery after application compared to the other tested products. This is due to the drying process and the removal of created film from the surfaces. However, with subsequent applications, the coefficient of adhesion decreased. Both non-drying TOR lubricants behave stable during the whole experiment with minor coefficient of adhesion increase for TOR lubricant (oil) at around 13 000 cycles. The TOR hybrid, as a partially drying substance, behaves in a similar way to the FM by slowly increasing the coefficient of adhesion after application. Nevertheless, the results suggested that the hybrid substance had great lubricating properties and the drying process and recovery were too slow to provide a coefficient of adhesion similar to FM. The application rate for this product needed to be much lower to prevent low adhesion conditions.
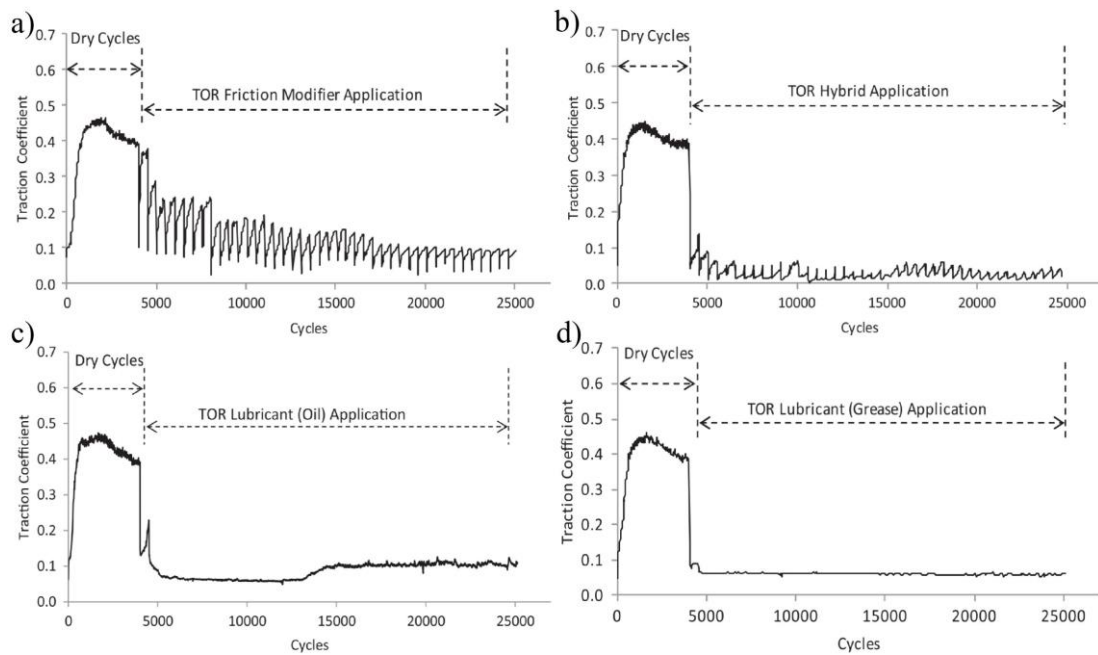
Fig. 2.17 Time tests: TOR FM (a), TOR hybrid (b), TOR lubricant (oil) (c) and TOR lubricant (grease) (d) [34].

Only a handful of studies used solid FMs for frictional testing. The first investigation [26] was already mentioned, but subsequent studies focused primarily on TOR lubricants and FMs. Eventually, Lewis et al. [35] and Hardwick et al. [36] studied the effect of wheel and rail electrical isolation when solid FM is used. The twin-disc testing machine consisted of 47 mm diameter discs resulting in line contact of 10 mm width. An application device pressed the solid FM against the wheel disc using a preloaded spring. The results, as seen in Fig. 2.18, show that the coefficient of adhesion saturates at 0.3. In study [35] a 3% slip was used at 900 MPa with the resulting coefficient of adhesion 0.3. This is in line with the initial study [26], where at 30% slip the coefficient of adhesion of 0.32 was reached.

Slip %	Average friction (dry)	Average friction (HPF)
0.0	0.0	0.0
0.1	0.19	0.14
0.2	0.25	0.16
0.3	0.35	0.23
0.5	0.40	0.27
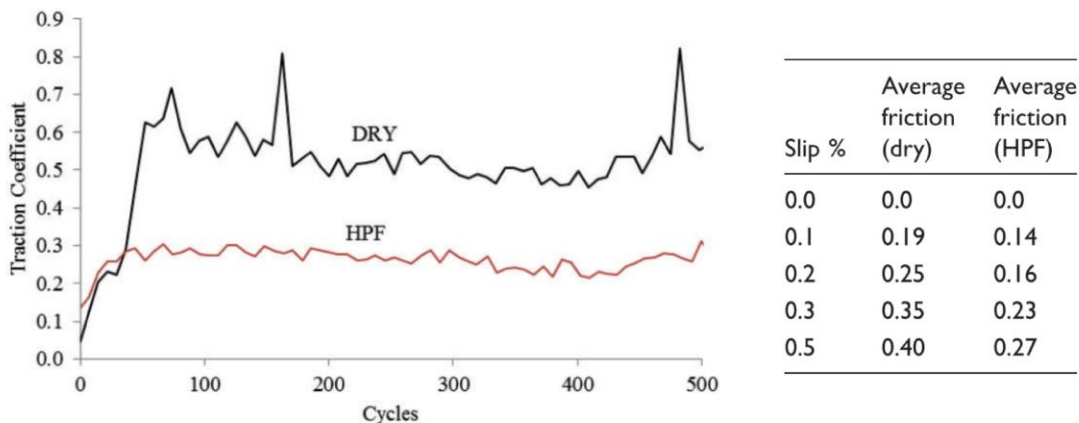
Fig. 2.18 Traction measurement of solid FM (HPF) at 0.5% slip, 400 rev/min and 470 MPa [36].

A publication [37] used a twin disc machine with discs diameter of 40 mm and 5 mm width. The discs were made of CL60 wheel tread and U75V rail head. The discs were loaded to a set contact pressure of 900 MPa and tests were carried out with 200 revolutions per minute. In this study, the solid stick was custom-made from 40 wt% polytetrafluoroethylene, 30 wt%

molybdenum disulfide, 10 wt% talcum and 20 wt% carbon fibre. A loading mechanism with a dead weight was used to press the stick against the wheel disc. The results, shown in Fig. 2.19, confirm results of previous studies [26, 35, 36] with a coefficient of adhesion reaching maximal values around 0.29. During the application time the coefficient of adhesion is very stable. After the solid FM was removed, a transition to dry conditions occurs. This transition phase is shorter for higher slip values.
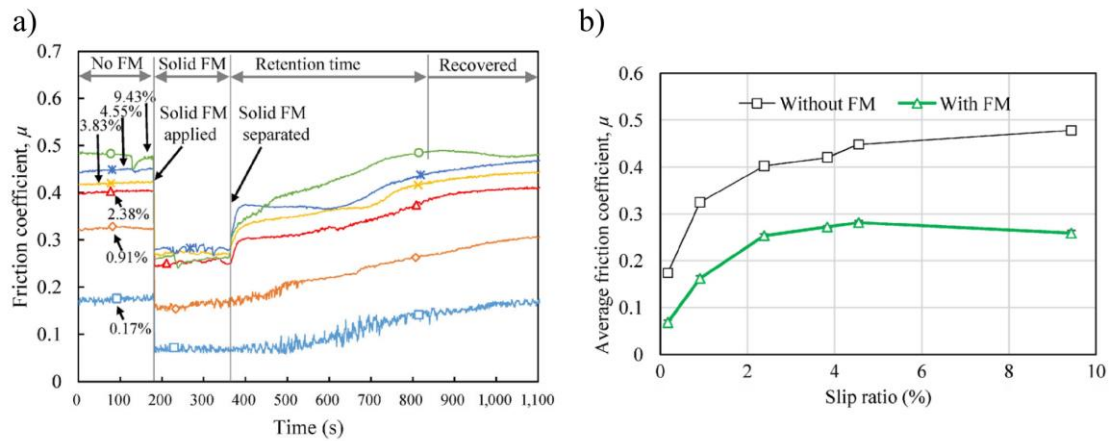

Fig. 2.19 Coefficient of friction for solid FM as a function of: time (a) and slip (b) [37].

2.2.2 Rheological properties

The wheel-rail contact can be seen as a combination of base bodies, natural third body and artificial third body. This concept of the third body layer was introduced by Godet [38] and plays important role for the case of wheel and rail contact, as the tribological system is of open nature. TOR products act as an artificial third body and greatly influence both friction and wear. The study of the rheological properties of third body layer is an important part in understanding friction mechanisms. The rheological properties represent the shear response of the surface to displacement in the case of solid-to-solid contact or shearing of liquid separating the surfaces.

Hou et al. [39] studied common natural and artificial materials in powder form. These powders were oxidized wear debris (magnetite), sand, clay and molybdenum disulfide. The rheological properties were characterized by shear stress versus displacement of the third body layer. The experimental pin-on-disc device consisted of two stationary pins pressed against anvil that was fixed to a rotating turntable. The slow rotation of the turntable caused a displacement between the pin and the anvil. The tested powders were brushed onto the surface of the anvil using ethanol to create an easily applied paste. The authors do not clearly state detailed descriptions of the experiments such as contact geometry or applied pressure. However, based on the results, a contact pressure of around 1 GPa seems reasonable. The results of the tests are shown in Fig. 2.20. Based on the results, two main parts of the curve can be identified. In the first micrometres of deformation, the shearing process behaved

elastically and then slowly transitions to pseudo-plastic deformation, where sliding between surfaces occurs. Between magnetite, clay and sand, three types of shear behaviours were identified. After reaching the elastic limit, the clay increased shear stress with further displacement, magnetite stabilized, and sand caused a decrease in shear stress. Molybdenum disulfide accommodated very low shear stress with negligible elastic deformation.
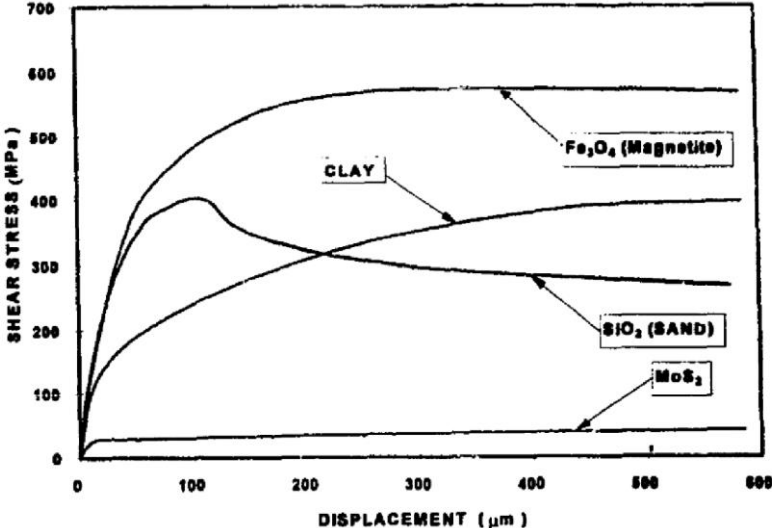
Fig. 2.20 Shear stress curves for tested materials [39].

The same pin-on-disc device was also used by Harrison [31] to evaluate TOR products. The applied materials were LCF, HPF and VHPF TOR products. As in the previous study, authors did not state the experimental conditions. Only that the experiments were carried out under nominal Hertzian contact stress encountered in giver rail application. The tested LCF provided a very low and stable coefficient of friction, similarly to molybdenum disulfide [39]. Between the tested HPF and VHPF it is clear that VHPF is meant to provide the highest possible coefficient of friction. These substances generally contain hard solid particles that help with the removal of contaminant, such as leaf layers. HPF products are used for bringing benefits of intermediate levels of friction. Between 2 mm, and 4 mm the HPF layer underwent changes that caused an increase in coefficient of friction.

Fig. 2.21 Coefficient of friction versus displacement for tested TOR products [31].

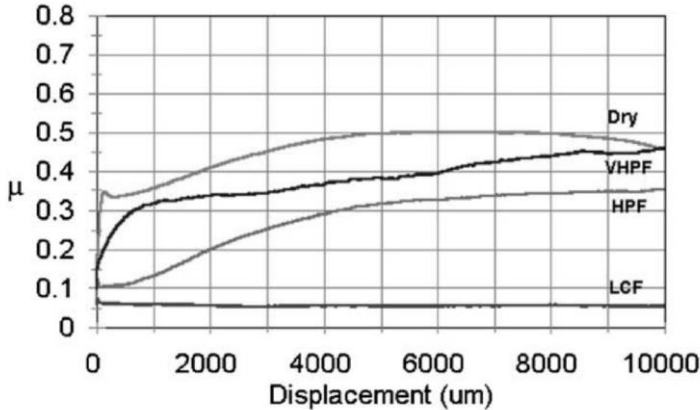The third publication using the pin-on-disc device [40] dealt with contamination of TOR FM developed by the company KELTRACK. The contaminants used were hematite (Fe_2O_3) and grease (Shell Cardura® WS). The contact pressure was set to 880 MPa and the sliding speed 2.67 μm/s. The results of iron oxide contamination can be seen in Fig. 2.22a. The use of FM provided a very low shear strength comparable to that of molybdenum disulfide [39]. Increasing the amount of iron oxide caused an increase in shear stress. However, a significant change was seen only after the composition contained 50 wt% and more iron oxides. For tested compositions with 90 wt% and 75 wt% iron oxide, a decrease in shear stress was observed after reaching the peak value at the end of the elastic part of the shear stress curve. Contamination with grease is shown in Fig. 2.22b. Pure FM showed a distinctive peak in the initial part of the shear stress curve and slowly increased to around 60 MPa at 1 mm displacement. Coating the surface first with FM and grease on top of it (SFG) or first with grease and then FM (SGF) caused a lower shear stress of around 50 MPa at 1 mm displacement and supressed the initial peak.

a)

b)
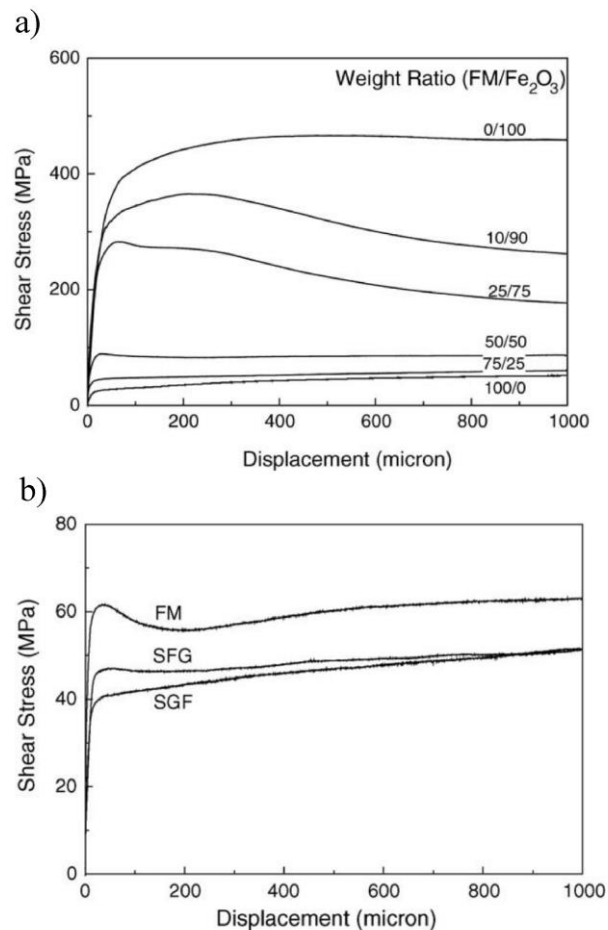
Fig. 2.22 Shear stress curves for FM contaminated with iron oxides (a) and grease (b) [40].

Advanced methodology for the evaluation of shear stress in wheel and rail contact was proposed by Evans et al. [41]. The methodology described the use of a high pressure torsion (HPT) device previously used for evaluation of water/iron oxide mixture [42] as well as dry contact [43, 44]. The HPT device used a specimen with an annulus contact area pressed

against a flat specimen. A slow rotation of the upper specimen causes displacement at the effective radius. This allows to study interfacial properties of materials and third body layers. Due to the dimensions of the specimen, it is possible to create a contact area and contact pressure similar to real wheel and rail contact conditions.

Part of this study dealt with FM, its application amount and the drying process. The results regarding the application amount of dry FM at 600 MPa normal stress are shown in Fig. 2.23a. Even the lowest dose of 16 mL/mile applied was able to reduce the coefficient of friction below 0.3. A further increase in dosage up to 2048 mL/mile reduced the coefficient of friction to around 0.1. Compared to dry conditions, the FM caused a sudden increase with initial displacement. This increase was much steeper compared to dry conditions. The lower coefficient of friction was achieved with excessive overapplication as seen in Fig. 2.23b. The coefficient of friction dropped to about 0.05 with both dry and wet FM film.

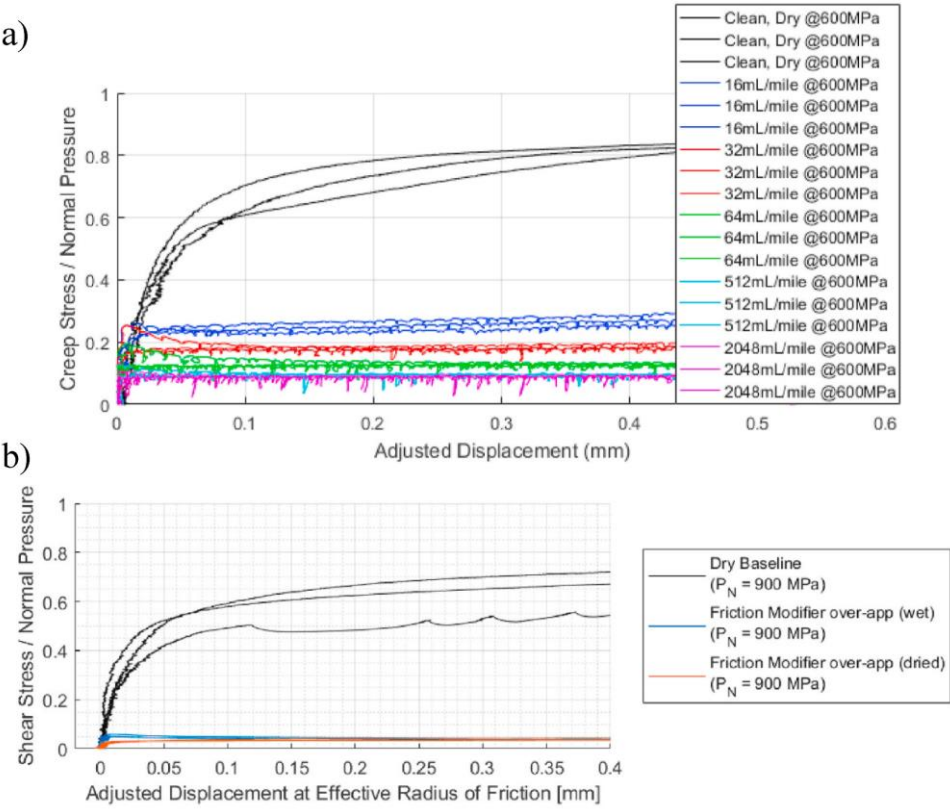Fig. 2.23 Shear stress curves for applied amounts of TOR FM (a) and overapplication of TOR FM (b) [41].

2.3 Wheel-rail contact models

Models of wheel and rail interaction can be divided into different types and scales. In terms of types, there are models such as simple lookup table models to physics-based calculations. When dealing with scale, the geometry of wheel and rail can shrink down to the size of

contact patch and even further to the level of asperity contact. The use of models for wheel-rail contact is important in understanding the driving physical processes and proving a tool or concept without additional costs that are linked with experimental and field testing. When dealing with wheel-rail contact, the key role is played by frictional forces. Since managing friction is the topic of this thesis, the models discussed in this chapter will thus be dealing with prediction of traction curves, as illustrated in Fig. 2.5. More information about wheel-rail models and future challenges can be found in review articles [45, 46].

2.3.1 Normal contact

The rolling-sliding mechanics of two bodies loaded against each other is described by the normal and tangential contact models. Normal contact deals with the calculation of the contact area and the normal pressure distribution. The work by Hertz in 1882 [47] and its resulting normal contact mechanics theory is widely known and still used today. The theory is built upon some simplifying assumptions, such as elastic and linear material behaviour, homogenous material properties, perfectly smooth contact surfaces and much larger curvatures of bodies than the size of contact patch. These assumptions may not hold true to wheel and rail contact. Especially the fact that surface curvatures are not constant, and the wheel flange causes two-point contact. Thus, improved models have been developed. These models are categorized by [45] as:

- Kalker's non-Hertzian models
- Approximate multi-Hertzian models
- Approximate virtual penetration models

Kalker's solution to normal contact [48] is considered to be the most accurate while having higher computational demands. The model considers the wheel and rail as elastic half spaces. It is very accurate when solving non-elliptical multi-contact problems. Kalker's model has been implemented in the software CONTACT that solves both normal and tangential problem. The approximate models [49] provide faster calculation with a trade-off being differences to Kalker's more accurate solution in some specific cases.

2.3.2 Tangential contact

The tangential contact describes the shear stresses and the resulting tangential forces in the contact area. The basic explanation on the existence of adhesion and slip areas in contact was given in subchapter 2.1. In this subchapter, models and approaches to predict shear forces will be given. Since this thesis deals with understanding friction management products, a primary focus will be on models that help describe contact with interface consisting of third body material. However, a short description of the original models for tangential contact is provided below.

One of the first analytical theories was given by Johnson and Vermeulen [50] for quasi-identical bodies with elliptical contact area. This theory divided the tangential contact into areas of adhesion and slip as described above. However, an assumption was made that the area of adhesion is of elliptical shape, located adjacent to the leading edge of the contact ellipse. Thus, the resulting formula is an approximate one with an error up to 25% [45]. Another analytical theory was later in 1990 given by Polach [51]. His approach provided a much faster calculation compared to numerical models, which also caused a lower accuracy, especially for high spin conditions. Similarly to Johnson and Vermeulen, Polach assumes an elliptical contact area divided into areas of adhesion and slip. The shear stresses in the contact area arise from the leading edge and increase linearly until a traction bound is reached. When the traction bound is reached, the area of slip appears. Using a transformation from the ellipsoid tangential stress distribution to a hemisphere and subsequent integration gave the formula for calculating the tangential force. Using the assumption of a linear increase in shear stress, but neglecting the area of slip, covers Kalker's linear theory [52]. This theory provides good accuracy at lower slips where area of adhesion covers most of the contact area and with slender contact ellipses [45].

In the late 20th century, due to the boom of computers, numerical approaches for calculation of contact forces became possible. The two most important theories were given by Kalker. These are FASTSIM (based on simplified theory) [48, 52, 53] and exact 3D theory CONTACT [48, 54]. The exact theory is considered to be a benchmark for contact theories, as it provides the most accurate solution. It is based on half-space approximation and the principle of virtual work applied to the contact problem. It can also provide a solution for unequal base materials, which is a requirement for a simplified theory. However, it has a very high calculation time, and the algorithm itself is more complex than other theories. The FASTSIM algorithm [48, 52, 53] divides the contact area into longitudinal strips. It assumes a linear traction-displacement relationship with an increase in shear stress from the leading edge of the contact area in each strip. This linear relationship is defined by the compliant parameters, also called contact flexibility coefficients. These are determined based on the linear theory and Kalker's creepage coefficients. The FASTIM algorithm assumes all kinematic motions – longitudinal, lateral and spin. This makes the FASTSIM very accurate in a wide range of situations. Kalker estimates the error to be around 15% [48].

The original theories try to describe the ideal contact with smooth geometry and no roughness or contamination. This causes a disagreement with the experimental findings, where the initial increase in the traction curve is more gradual. Also, original theories use a limiting coefficient of friction when the contact area reaches full slip. When this occurs, there is no further change in the coefficient of adhesion. In reality, thermal effects and more substantial surface changes with high slip conditions cause a negative slope of the traction curve after the saturation point in dry conditions. When a TOR product is present in the contact interface, a neutral to positive trend of the traction curve is expected. The following pages will focus on studies that try to consider the effects of the interfacial layer in prediction

models.

Already mentioned study by Hou et al. [39] used a bilinear rheological model of the solid layer. As shown in Fig. 2.24a, during the third body layer deformation, the surface displacements are accommodated by elastic deformation until a limiting shear stress is reached. After that, a sliding occurs in the third body layer as illustrated by the third body layer collapse on the right side of Fig. 2.24a. The model input data were measured by a pin-on-disc device. As seen in Fig. 2.24b, the interfacial layer model in contact can elastically deform in the area of adhesion or plastically slide when a critical stress is exceeded. The calculation assumed a Hertzian line contact, where the frictional force comes from integration of the shear stress in contact area. Incorporating the bilinear material characteristic into the frictional force calculation resulted in an equation with 7 parameters representing the bilinear model, Hertzian contact and slip conditions. The model was demonstrated using a typical locomotive wheel-rail contact with sand separating the surfaces. The results of the model predicted a coefficient of adhesion of 0.355. This was compared to a previous study [55] and resulted in a good agreement.
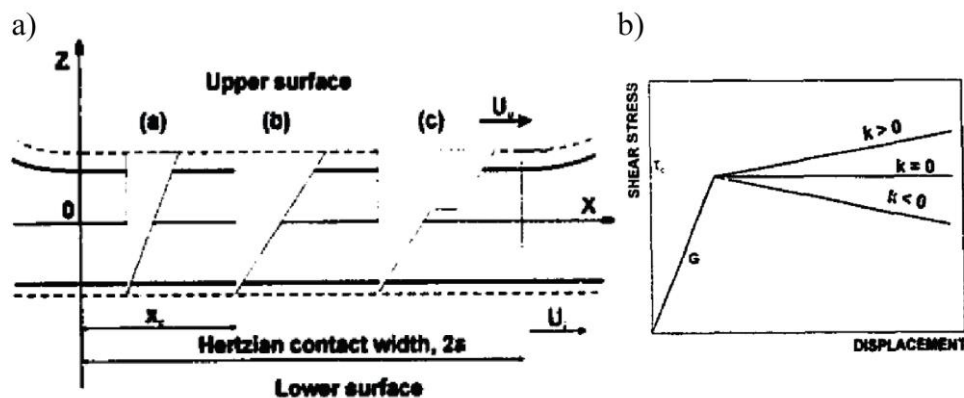

Fig. 2.24 Rheological model of solid layer (a) and bilinear material properties (b) [39].

Ertz and Bucher [56] proposed a model that considers the effect of surface roughness and temperature. This provided a more accurate solution with a more gradual initial increase of the coefficient of adhesion in the initial part of the traction curve and decrease after saturation, as shown in Fig. 2.25a. The model is based on Shen, Hedrick and Elkins non-linear creep force law [57]. The driving factor for the roughness influence is the ratio between the real contact area of the asperities and the nominal contact area. The ratio of real contact area is then added as a parameter to the initial calculation of the frictional forces. This resulted in a less steep increase of the coefficient of adhesion at low slip, as is demonstrated for various roughness in Fig. 2.25b. The decrease in the coefficient of adhesion at high slip conditions is attributed to the increase in contact temperature caused by the generation of frictional heat. A temperature-dependent coefficient of friction was then introduced into the calculation. The temperature is calculated using an analytical

approximation of the average contact temperature. The benefit of this model is that it is based on the physical phenomenon of roughness and temperature. It is viable for both longitudinal and lateral slip, as well as small spin conditions.
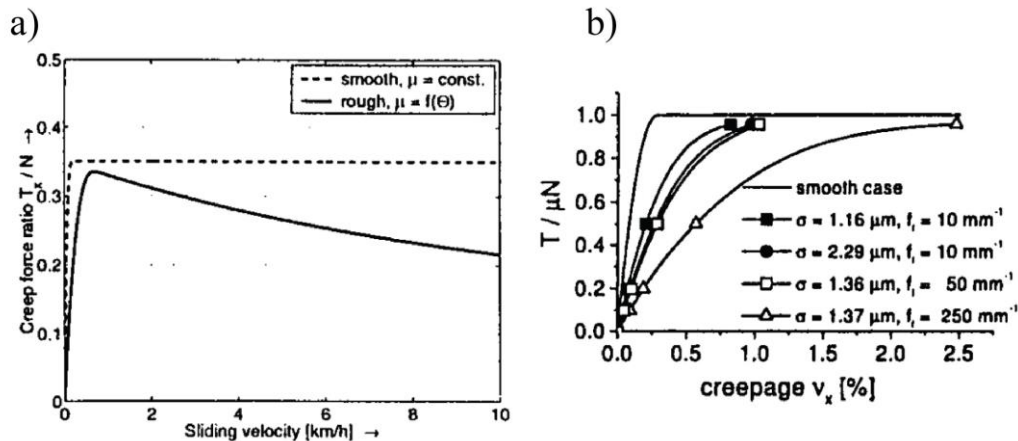

Fig. 2.25 Comparison of smooth and rough model (a) and results for different roughness [56].

Polach [58] introduced a slip velocity dependent coefficient of friction to his previously published model [51]. The constant coefficient of friction is replaced with equation describing decreasing coefficient of friction with increasing slip velocity. However, this addition did not help change the initial slope of traction curve. It was previously suggested that decreasing the Kalker's coefficients helps lowering the initial slope. Nevertheless, a clear agreement with locomotive measurements was still not met, as shown in Fig. 2.26a. Polach suggested a two-parameter reduction factor for Kalker's coefficients in his model. One parameter deals with the reduction in the area of adhesion and the second parameter in the area of slip. Both the slip velocity dependent friction and two-parameter reduction factor helped accurately represent field measurements as seen on an example in Fig. 2.26b. The improved model maintains its fast computational time and provides a better experimental representation compared to Polach's original theory, making it a valuable tool for vehicle dynamics simulations.
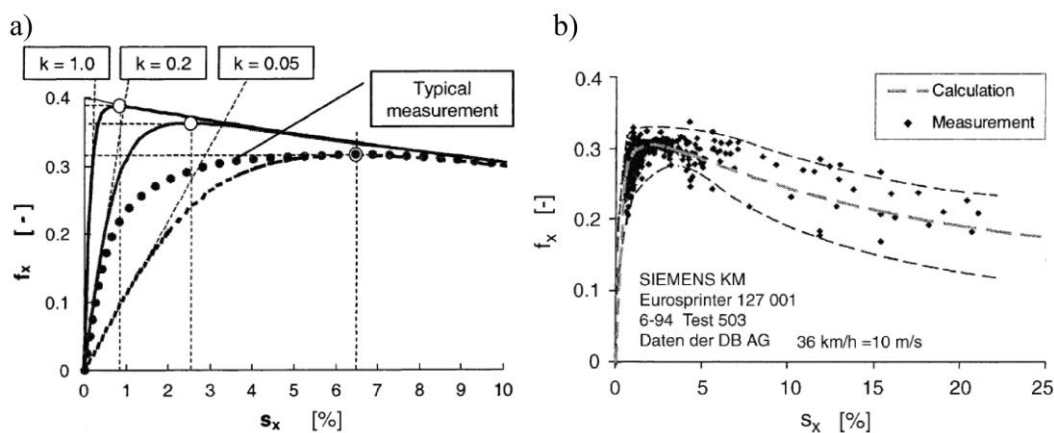

Fig. 2.26 Comparison of single reduction factor for Kalker's coefficients (a), model of traction curve for locomotive Siemens Eurosprinter 127001 (b) [58]

34

Spiryagin et al. [59] used the same slip velocity dependent variable coefficient of friction as Polach [58] in Kalker's FASTSIM algorithm. In addition, a similar reduction factor was implemented to provide better accuracy in predicting the transition to saturation point on the traction curve. The reduction factor was calculated in such a way that it increases the contact flexibility coefficients used in FASTSIM calculation and thus leads to a change in initial slope of the traction curve. The parameters introduced by the authors change based on the slip conditions with different ratio between the area of adhesion and slip. The results shown in Fig. 2.27 compare the presented model with Polach's model [58] on a SD45X locomotive measurements [60]. Both models agree well with the measurement for both wet and dry conditions. The FASTSIM calculation also provides the shear stress distribution in the contact area.
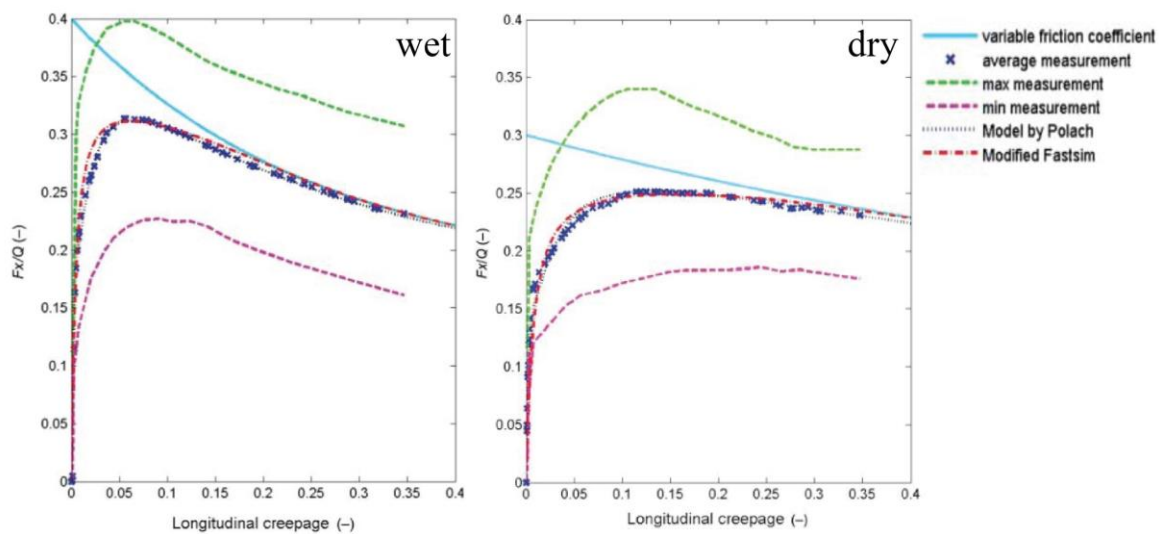

Fig. 2.27 Comparison of model by Spiryagin [59], Polach [58] and SD45X locomotive measurements [60].

The use of FASTSIM for various contamination conditions was also proposed by Rovira et al. [61]. The authors propose three different slip dependent coefficients of friction: three-parameter exponential function, four-parameter exponential function and piecewise linear function consisting of two linear parts with three parameters. Similarly to Spiryagin [59], a reduction factor is used for change in contact flexibility. Fig. 2.28a demonstrates the physical meaning behind the contact flexibility coefficient for ideal contact and real contact conditions with roughness and contamination. The parameters for variable coefficient of friction and the change in contact flexibility were identified from experimental measurements of traction curve on twin-disc device. The experimental and model results are shown in Fig. 2.28b. A good fit for different types of contaminants was achieved. The same approach was also applied to traction enhancers. The results were then used to analyse wear based on energy dissipation.

Meierhofer et al. [62] used experimental twin-disc results to identify the parameters of third body layer and their implementation in an analytical model. The maximum third body layer thickness of 50 μm, shown in Fig. 2.29a, was observed for maximal Hertzian

pressure 1500 MPa and slip 5% at 0.5 m/s speed. Decreasing the pressure to 900 MPa resulted in a much thinner third body layer made up mainly of cracks. The analytical model consisting of two integral equations was then proposed. The third body is represented by a bilinear characteristic, similarly to the work of Hou et al. [39]. Parameters identified based on the twin-disc experiments were used in prediction of traction curves. Fig. 2.29b shows the inaccuracy of not using the third body in the model, which corresponds to the results expected from Kalker's exact theory for line contact. The use of third body properties greatly increased the accuracy of predicted traction curve, especially around the saturation point near 1% slip.
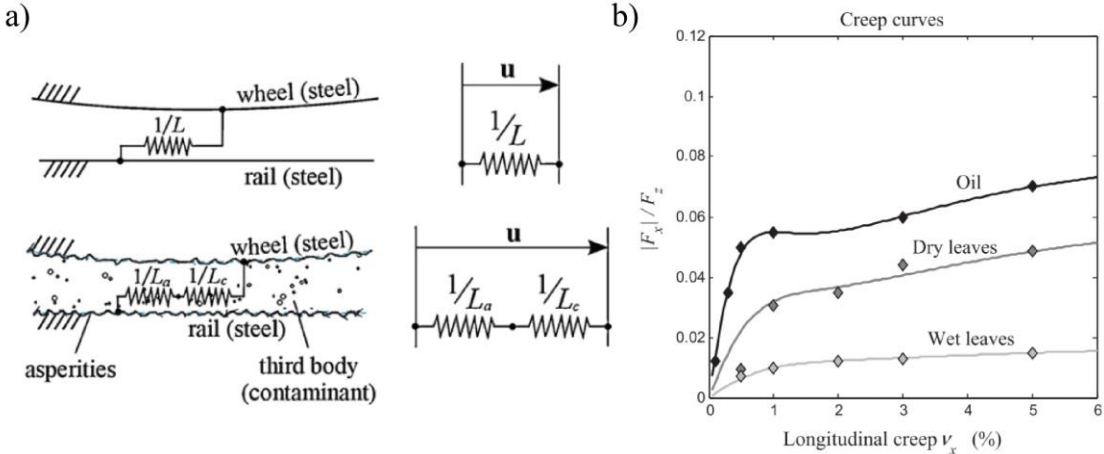
Fig. 2.28 Rheological model of interfacial layer with contact flexibility coefficients (a), comparison of model with experimental data (b) [61].
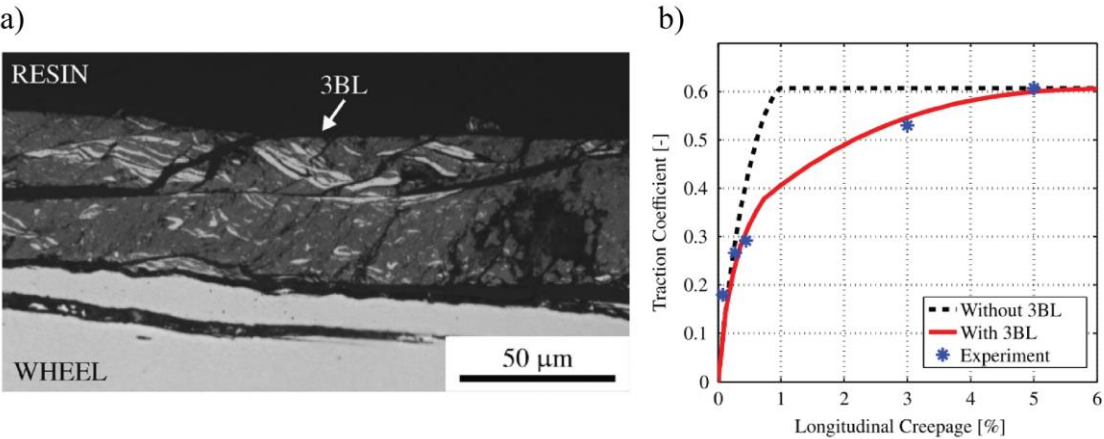
Fig. 2.29 Third body layer from experiments on twin-disc (a), comparison of model results and twin-disc experiments [62].

FASTSIM-based model that uses a shear-displacement properties of contact interface was proposed by Six et al. [43, 44]. The core of the third body layer model is based on the work of Meierhofer [63] called the ECF model. The third body layer is modelled using Voce's hardening law [64]. Additionally, the behaviour is parametrized based on pressure and temperature influence. The pseudo-plastic deformation of the third body layer in the model

changes the resulting frictional response. The shear-displacement behaviour is acquired by means of HPT testing as described in the previous subchapter. This allows a direct physical connection between the properties of the contact interface and frictional results predicted by the model. The results of the ECF model are shown in Fig. 2.30. The model prediction corresponds well with vehicle tests, especially under dry conditions. Additionally, the results were used in wear and damage estimation.

Fig. 2.30 Results of ECF model for dry conditions (a) and wet conditions (b) [44].

The above-mentioned studies focus on models that describe the traction that arises due to surface displacements and the resulting tangential forces. When we consider application of FM or TOR lubricant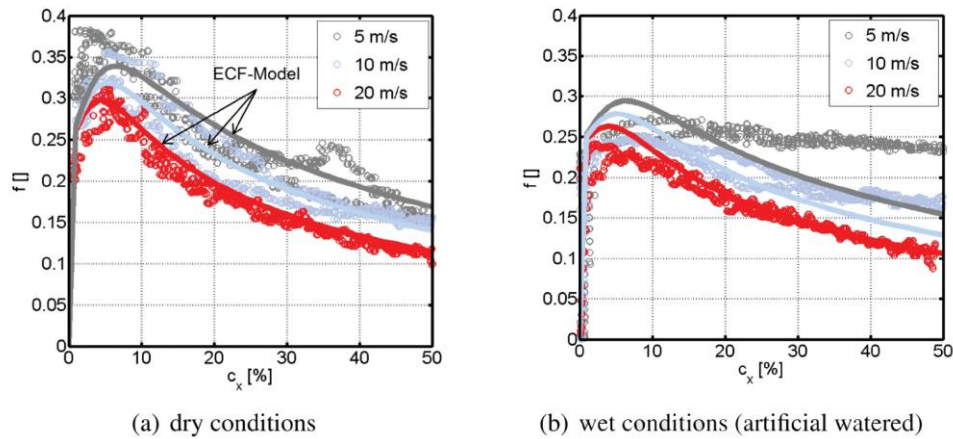 into contact, as well as contamination with oil and water, it is reasonable to assume that the hydrodynamic effect can influence the friction. This is more significant with increasing vehicle speed. Chen et al. conducted several studies [65–69] motivated by water contamination in high-speed railways. The developed model is based on the assumption that a portion of the normal load is carried by asperity contact and a portion by hydrodynamic film. The asperity contact is related to boundary friction, while the hydrodynamic film is related to hydrodynamic friction. The transition phase is characterized by the ratio between the asperity contact and the surface separation in the contact area. For this, Greenwood and Williamson statistical model [70] was used. The boundary coefficient of friction is set based on experimental data. The coefficient of friction for the hydrodynamic film is calculated using Newton's viscosity law and formulas for film thickness prediction. The results can identify how surface roughness influences the coefficient of adhesion, as seen in Fig. 2.31a. Decreasing the roughness for single value of speed (or equally single value of film thickness), causes decrease in coefficient of adhesion due to less asperity contact. Compared with the experimental data in Fig. 2.31b, it is evident that precisely determined boundary coefficient of friction is also important. Even though the transitioning area is estimated correctly, the level of adhesion is misrepresented with a higher boundary coefficient of friction. Pressure and temperature influence on water viscosity was also used to estimate how it changes the coefficient of adhesion.
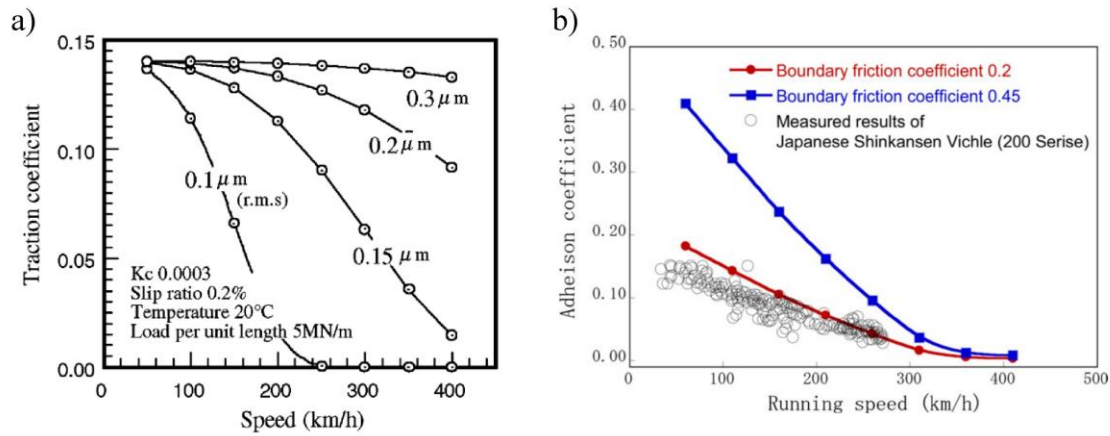
Fig. 2.31 Influence of roughness on traction coefficient (a) [68], effect of boundary friction coefficient on model prediction (b) [66].

Wu et al. [71] employed a similar approach for water and oil contaminated conditions. Additionally, the effect of surface orientation on flow equation was implemented. For estimation of film thickness, a numerical solution to Reynolds equation is used. The asperity problem is solved using Greenwood and Tripp [72] model. The general idea of the modelling approach is similar to the work of Chen et al. [68]. The results and trends are also in line with the predictions of Chen et al. [65–68]. The model was later improved in the publication of Wu et al. [73] using the advanced asperity model by ZMC [74] and finite element analysis [75] that considers plastically deforming asperities. The viscosity equation is extended by the influence of temperature, which is calculated from heat generated by the contact. The results showed that the effect of a more accurate ZMC asperity model was not significant. The use of thermal model had visible influence, especially in the boundary regime. The results of the model were compared with experimental results as shown in Fig. 2.32. A good agreement was achieved for both water and oil contaminated conditions in a wide range of speeds.

Fig. 2.32 Comparison of model prediction with results from experimental wheel/rail facility [73].

38

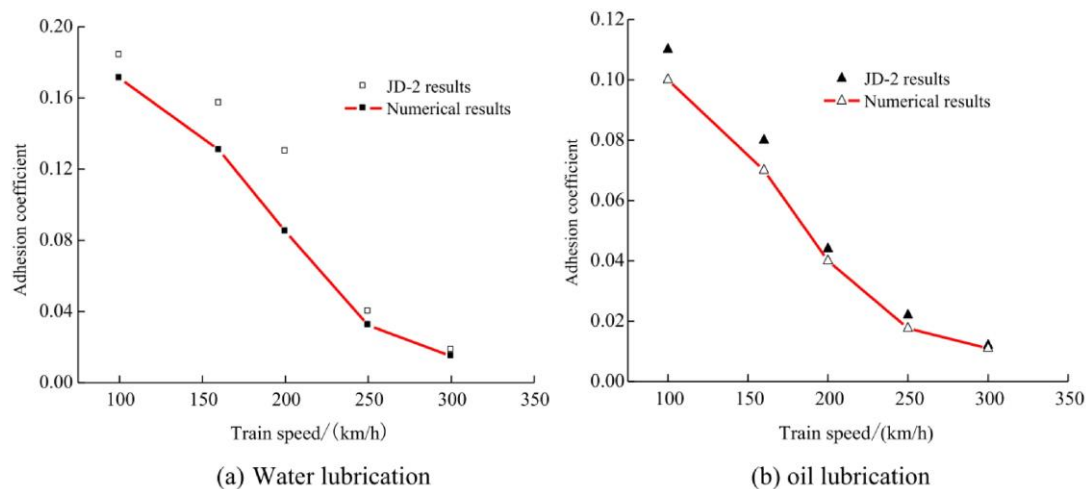Tomberger et al. [76] proposed a complex model assuming asperity microcontact, interfacial fluid and temperature effects. The modelling idea is based on a contact area divided into a grid where each grid point represents a cell with height dimension. Portion of the cell is occupied by the asperity and liquid. The asperity microcontact is based on statistical method by Greenwood and Williamson [70]. The statistical distribution is used to define the parameters of each cell of the calculation grid. The fluid model is based on the principle of mass conservation and pressure-mass flow. In Fig. 2.33a, a longitudinal section shows traction bounds for close to zero speed, where effects of fluid pressure are negligible. At higher speeds, the surface separation causes part of the cells to reduce the tangential traction by means of fluid film separation. The temperature is calculated across the contact area and can use arbitrary heat source distribution, which is determined based on frictional power. These three parts of the calculation are connected with the tangential model that is based on FASTSIM algorithm. The tangential shear stress distribution assumes a varying coefficient of friction across the calculation grid. The effect of temperature is evident for dry conditions, especially at higher speeds, as shown in Fig. 2.33b. An increase in temperature causes a decrease in yield stress of asperities and thus a decrease in the coefficient of adhesion.
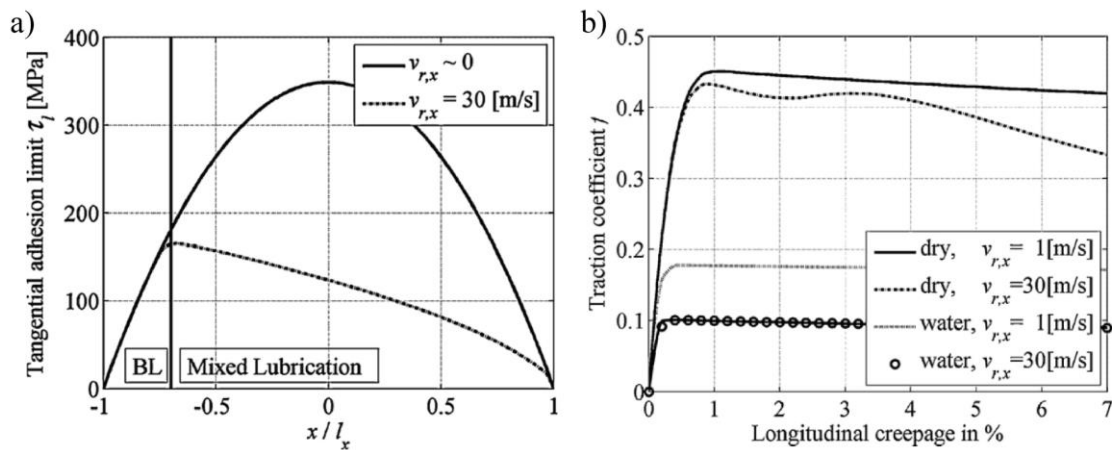

Fig. 2.33 Tangential adhesion limit for different vehicle speeds (a), calculated traction curves for dry and water conditions (b) [76].

3 ANALYSIS AND CONCLUSIONS OF LITERATURE REVIEW

3.1 Analysis of literature review

The introductory part of subchapter 2.2 points out the idea behind using friction management in railway operation. The main properties of TOR friction management products are the ability to provide an intermediate (optimal) level of adhesion and neutral to positive traction curve characteristic. It should be noted that friction management products are available in three main forms: FMs, TOR lubricants (or TOR hybrid) and solid FMs. The working principle of these products differs and as such should be taken into account when analysing and discussing results of publications using different types of TOR products.

The first study that brought to light the benefits of using friction management [26] used a solid FM product. However, the following studies to present day were mostly focused on water-based FM products and, only in some cases, TOR lubricants/hybrid products. Only a handful of studies [35–37] used solid FM in experimental testing. Studies [35, 36] are also primarily focused on electric isolation that could be dangerous for the detection of trains. Interestingly, all the mentioned studies that used solid FM for frictional tests [26, 35–37] report a coefficient of friction of around 0.3 at higher slip ratio. For FMs, studies report coefficient of friction from 0.1 [25, 29, 40] up to 0.3 [22, 31], with the most occurring values being around 0.2 [11, 27, 29, 32]. TOR lubricants are not as thoroughly researched as FMs. Studies report values of around 0.1 [22, 34] up to 0.3 [12, 33]. However, the coefficient of adhesion for FM and TOR lubricant are dependent on the experimental device, methodology and application method. Normally, after application, the coefficient of adhesion drops to low values and slowly climbs to the optimal level where it should remain the longest time. After that, the film created from TOR product is removed and close to dry conditions are reached. When considering the dry FM film, the effect of initial drop is suppressed [11]. The TOR lubricant is more sensitive to applied amount and over-lubrication as suggested by studies [3, 12, 33, 34]. This is also true for TOR hybrid compositions [3, 34]. Taking into account studies dealing with VHPF and adhesion restoration [77, 78], it seems that the use of a higher hardness of particles or a higher amount of particles leads to faster recovery from low adhesion values after application.

The neutral to positive traction curve characteristic of TOR products is agreed upon by the studies in subchapter 2.2.1. Intermediate levels of adhesion are experimentally confirmed under laboratory and field conditions. However, the application methodology plays a key role in the resulting coefficient of adhesion. Painting a TOR FM product with a brush caused low values of the coefficient of adhesion compared to spraying [29], where more stable values were achieved. The spraying process provides a more spread and thinner

layer, while brushing can leave an excessive amount of product on the surface. A decrease in coefficient of adhesion was also observed with high applied amounts of FM in HPT tests by Evans et al. [41]. Using moderate amounts of non-commercial FM, Galas et al. [11] measured very stable intermediate levels of the coefficient of adhesion. With TOR lubricants and hybrid products, studies [10, 12, 33] showed a decreasing trend in the coefficient of adhesion with an increasing applied amount. Lower values were also seen in comparison with FMs in study by Hardwick [34]. This is reflected in review study by Stock. [3]. For solid FMs, the currently published papers focus primarily on traction curves with single application parameters. Direct comparison in coefficient of adhesion from published studies is not adequate due to different testing methodologies. Difficulty also being that the effect of applied amount is tied to the application method, experimental device, geometry of the specimen and contact area. Studies [10–12, 28, 33, 34] show that the coefficient of adhesion for TOR products is changing with running time of experiment. Based on selection of the time window for evaluation of the one point of traction curve, the results can vary considerably. On the other hand, using a continuous change in slip [29, 31] to measure the traction curve in one measurement run changes the interfacial layer by continuous removal of TOR product during the change of slip. This means that the state of contact interface constantly changes, and it is not valid to assume that same amount of TOR product is present at different slip conditions. This is supported by the study [29] in which subsequent tests without reapplication of FM resulted in a continuous increase in values of the traction curves.

Studies that focus on rheological properties provide shear stress-displacement characteristics for interfacial layers. This characteristic is key for modelling, as it provides information about the response of the contact interface to deformation caused by rolling-sliding motion. The first study [39] that introduced an approach based on the shear stress-displacement demonstrates a theoretical basis for predicting friction in contact with an artificial interfacial layer. This study used a pin-on-disc rheometer to measure the elasto-plastic behaviour of common contaminants. The same device was also used for TOR products in [31, 40]. Results from Harrison [31] show that HPF FM results in a low coefficient of friction in the initial low displacement. With further sliding, the coefficient of friction reaches around 0.35 where is stabilizes. At high displacements the dry conditions started to decrease in coefficient of friction which was not observed for TOR products. The results by [40] suggest a low coefficient of friction for FM below 0.1. No evident increase is seen for higher displacements as reported by [31]. These low values of the coefficient of friction seem to be the result of applying an excessive amount of FM. This is seen in study [41] where overapplication of FM dropped coefficient of friction below 0.05. The lower amounts applied reached values around 0.2 to 0.3 and with an increase in applied amount, the coefficient of friction decreases. In the more recent use of shear stress-displacement characteristic for modelling of wheel and rail contact [41, 43, 44], a parametrization by Voce's hardening model [64] was used. The use of high pressure torsion device has been recently employed [41–44] to assess the shear response of various contact conditions.

Models for tangential contact forces need to be separated into two main areas: boundary and elastohydrodynamic friction. In the wheel and rail contact, studies mostly focus on expanding the boundary lubrication effects as the contact conditions point to the boundary regime. Experimental investigations showed that the original models [48, 50, 51, 53] do not predict the traction curve accurately. The two main deviations are in the initial slope of the traction curve and the decreasing trend at high slips. To resolve this, the original models were extended to accommodate for an accurate representation of experimental results. The modelling algorithm that is most built upon is Kalker's FASTSIM [48, 52, 53] that is used in studies [43, 44, 59, 61]. These studies show a good agreement between extended model predictions and experimental data under various contact conditions and contamination. The main improvements come from using a variable coefficient of friction, either as a frictional function [59, 61] or by using material properties of the third body layer [43, 44]. In the study [62], the use of the material properties of third body layer in analytical model also yielded a good agreement with experimental data. The decrease in coefficient of adhesion is attributed to the increase in temperature. This is also taken into account in studies [43, 44, 56], where the estimation of contact temperature is shown in study [79].

As previously mentioned, FMs and TOR lubricants are based on liquid carrying medium. When modelling these materials, the effect of hydrodynamic lubrication should not be put aside. This was shown in the study [12] where excessively overlubricated contact with TOR lubricant behaved similarly to pure castor oil. It could also be the answer to very low adhesion conditions immediately after application of liquid TOR product, as seen in studies [10, 12, 33, 34]. Studies concerned with the elastohydrodynamic effect were mostly focused on water contaminated contact [65–69, 76]. The lubrication regime for wheel and rail contact can, in some cases, extend to mixed lubrication. In this case, the effect of roughness is important for accurate prediction of the coefficient of adhesion. The most commonly used models for asperity contact are statistical models of Greenwood and Williamson [70] and Greenwood and Tripp [72]. The study [73] used a newer model ZMC [74] that expands upon elasto-plastic deformations of asperities. However, the results were compared to Greenwood and Williamson model [70] with minimal differences for the selected conditions. The calculation of the coefficient of friction for mixed lubrication regime in these studies is based on the calculation of load portion carried by asperity and lubricant film. Both these portions have assigned coefficient of friction, which results in total coefficient of friction for the whole contact area. The coefficient of friction for lubricant film is mostly based on Newton's law of viscosity and the estimation of film thickness either by analytical formulas [65, 68] or using Reynold's equation [71, 73]. The coefficient of friction for asperity contact is assumed to be equivalent to friction in the boundary regime. However, studies [65, 68, 71] use a fixed coefficient of friction for asperity. The study [76] uses FASTSIM with varying coefficient of friction for asperity contact, allowing it calculation of different slips.

3.2 Conclusions of literature review

The analysis of state of the art shows that a significant effort has been put into research of TOR products, mainly water-based FMs. Studies that use experimental methods to evaluate coefficient of adhesion for TOR products show that these products are able to reach optimal levels of adhesion and neutral to positive trend of traction curve that is linked with benefits such as better vehicle dynamics, fuel effectiveness, reduction of wear and noise. Nevertheless, the positive trend of the traction curve might not be a result of the product properties, but rather a reduction in the amount present in contact interface by means of increased slip. This results in non-steady-state conditions where the amount of TOR product in contact constantly changes. Using this information in a boundary model could explain the true shape of the traction curve under conditions of a set amount present in contact. In terms of low adhesion, the use of TOR lubricant is commonly associated with a low coefficient of adhesion, especially after application, as reported by studies [12, 22, 33, 34]. The exact causes for these low adhesion conditions are not yet fully explained. In terms of FM, the results diverge into studies reporting optimal adhesion levels [11, 27, 31], but also low levels [29, 32, 34] and in some cases even very close to dry conditions [22]. The use of different testing methodologies and applications results in inability to compare and deduce clear conclusions. However, it seems to be clear that FMs are much less sensitive to applied amount compared to TOR lubricants [3]. The drying process appears to be important [11], but has not yet been studied compared to different amounts and TOR lubricants. Such comparisons should be made on an experimental device using basic frictional principles to minimize the effect of application methodology and rolling-sliding contact. Lastly, solid FM was studied by only a handful of studies [26, 35, 37] that report very similar frictional values. However, the sensitivity of the applied product to the coefficient of adhesion was not yet examined.

Current frictional models that use elastohydrodynamics for wheel and rail contact focus mainly on water contamination [65–69, 76]. The limitation of these studies is the need for a boundary coefficient of friction that is based on estimation to fit experimental results [66, 68] or uses original boundary friction theories with a parametrized coefficient of friction [76]. Promising approach has recently been proposed, where purely boundary friction of various third body layers is represented by material properties of the contact interface [43, 44, 62]. The connection between boundary and elastohydrodynamic models is mostly done by means of statistical asperity models [70, 72, 74]. Nevertheless, a complete model using rheological properties for both the elastohydrodynamic and boundary regimes was not yet used and validated. Such model could use inputs from viscosity and surface shearing measurements to predict the coefficient of adhesion under various kinematic and loading conditions. This approach has also not yet been applied to the frictional properties of TOR products, where it could bring benefits in finding optimal use based on fundamental frictional properties.

4 AIM OF THESIS

The aim of this doctoral thesis is to use experimental and modelling methods to clarify the frictional behaviour of top of rail products. The main focus is to explain the causes of low adhesion conditions when using these products. The modelling approach will consider both boundary and elastohydrodynamic regime. As a result of the higher sensitivity to over-lubrication, a TOR lubricant will be used to assess the effect of composition and lubrication regime. Experimental methodology will be used to explain the characteristics of different types of TOR products currently available: FM, TOR lubricant and solid FM. The conditions leading to the risk of low adhesion will be evaluated. Subsequently, the model will be used to assess the traction curves of these products.

To achieve the main goal of this thesis, the solution of following sub-goals will be necessary:

- Frictional investigation of a TOR lubricants and use of model to assess the effect of boundary and elastohydrodynamic effects.
- Comparison of different TOR products by the application amount dependency on coefficient of friction.
- Development of a numerical model that considers both boundary and elastohydrodynamic lubrication regimes based on the rheological properties of the third body layer.
- Validation of the model using an experimental method with a model fluid.
- Assessment of causes leading to low adhesion conditions when using TOR products.
- The use of a model for the evaluation of steady-state traction curves of TOR products.

4.1 Scientific questions and hypotheses

Q1. How can the rheological properties be used with third body concept to predict the coefficient of adhesion in contaminated rolling-sliding contact?

H1.1 Knowing the shear response of solid-to-solid contact and lubricant viscosity can be used in Kalker's theory and general theory of elastohydrodynamics, combined with the asperity model to predict traction curves in contaminated rolling-sliding contact.

The use of elastohydrodynamic theory [65, 68, 73] proved to be useful when assessing water contamination. However, these studies assume a limiting coefficient of friction either by fitting it to experimental data or in a few cases applying original theories, which are seen to not be accurate under most realistic conditions [56, 59]. Only in study [76], the parametrized coefficient of friction was used that can provide more accurate results. Nonetheless, all these simplifications of boundary friction in the models disconnect the physical properties of the

contact interface from the resulting friction. In recent years, several studies [43, 44, 62] have been published with the aim of using original boundary friction models and material properties of the third body layer. This new rheological approach combined with already established elastohydrodynamic theories could result in a model that uses rheological inputs of both liquid and solid creating a third body layer. Such an implementation into the model could describe complex third body under various conditions.

Q2. What is the cause of the low adhesion drop after application of the TOR lubricant and how can it be suppressed?

H2.1 Low adhesion after application of TOR lubricant is caused primarily by the hydrodynamic effect that shifts the contact to the mixed lubrication regime.

H2.2 Using large solid particles, which ensure asperity-particle-asperity interaction, will reduce initial drop and promote fast increase to optimal levels of adhesion after application of TOR lubricant.

Previous studies [12, 34] show that the application of TOR lubricant in excessive amounts can cause a coefficient of adhesion on a level similar to pure oil or grease lubricant. For optimal amounts, a typical adhesion drop is observed immediately after application [12, 33], followed by an increase in the coefficient of adhesion. Since the initial adhesion drop results in similar values to pure grease or oil, it is valid to assume that the asperities and particles of friction modification cannot provide enough solid to solid interaction. Therefore, the resulting friction response is thus driven by the base oil, causing surface separation and a low shear strength of interfacial film. This assumption can be answered with the help of estimating lubrication regimes by a numerical model considering the rheology of both solid interaction and lubricating film.

The study [12] suggests that a higher amount of particles should lead to a lower sensitivity to the application amount. However, the comparison was made with a product using different material of particles for friction modification. Nevertheless, several studies [77, 78] dealing with adhesion recovery suggest that larger and harder particles will lead to a faster increase in water contaminated contact. This should also translate to TOR lubricants as the film separation caused by the oil medium is significantly smaller than the scale of particles for friction modification.

Q3. What conditions pose a risk of low adhesion conditions for FM and solid FM?

H3.1 The presence of liquid in FM will cause low adhesion, but after evaporation the undesirable conditions occur only when an excessive amount is applied.

H3.2 The composition of solid FM should provide a greater resilience to the applied amount compared to TOR lubricant.

The use of FM is inherently linked to the effects of drying the water-containing medium. Review of current research suggests that FM should provide optimal levels of adhesion even at higher applied amounts [3]. Studies using rolling-sliding testing devices report results from very low coefficient of adhesion [29, 32, 34], intermediate levels [11, 27, 31] and some even very close to dry conditions [22]. Even though some studies report whether the product was dried prior to the test, the studies still do not give clear answer to why the low adhesion occurs in some cases. Comparison of these results is not easy to make due to the different testing methodologies used. The only paper studying the drying process [11] suggests that lower values of adhesion are expected when water is present in the substance. This finding does not seem to be explained by the hydrodynamic effect, as water cannot create sufficient surface separation for the experimental conditions. However, the small-scale device used cannot be equally compared to real wheel and rail contact. Spraying FM onto the surface in study [28] resulted in similar values as in the wet state reported in [11] suggesting that presence of water causes lower values of the coefficient of adhesion. Rheological studies of dry FM [31, 40, 41] suggest that a very low frictional value is expected upon application. A case study of the applied amount of dry FM [41] indicates that excessive amounts can cause extremely low coefficient of friction. In terms of solid FM, there is not a lot of research. Three studies that report values of coefficient of friction [26, 35, 37] are in agreement on intermediate levels of friction. The application parameters were not studied currently. Assuming a similar composition of particles for friction modification and solid lubricant as in water-based FM, only excessive amounts compared to TOR lubricant should result in low coefficient of friction. The use of a high pressure torsion device, similarly to [41], could help answer these hypotheses as it provides a realistic contact area and does not cause scaling problems as small rolling-sliding devices do.

Q4. What is the true shape of the traction curve under non-transient contact conditions of the applied product without the effects of time dependent TOR product removal?

H4.1 The use of TOR product does not result in a positive trend of traction curve as it only reduces the effects of temperature that causes a negative trend in dry contact.

The often-reported distinct positive trends of the traction curve [10, 29, 30] seem to be a result of the removal of TOR product film causing an increase in coefficient of adhesion, as seen in [12, 28, 29]. Studies showing the rheological properties of FM films [40, 41] suggest that after full slip occurs, additional displacement of the surfaces does not result in an increase in the coefficient of friction. Only after excessive displacement, when film removal occurs, the coefficient of friction increases [31]. As the negative trend is linked with increase in temperature, it is valid to assume that the TOR product will suppress the effect of temperature on coefficient of friction causing a neutral trend of the traction curve. The effects of temperature were not previously studied, and the use of a modelling approach can explain this phenomenon.

4.2 Thesis layout

This thesis is composed of three papers published in peer-reviewed journals. **Paper A** deals with the modelling approach of boundary and elastohydrodynamic friction. The model is compared with frictional measurements on the ball-on-disc tribometer. Film thickness measurements were conducted to validate the prediction of asperity contact. The traction curves for various speeds were measured and compared with the model prediction. **Paper B** aims to investigate the properties of a custom-made TOR lubricant. The effects of different components are examined, and rheological measurements were conducted for selected compositions to acquire inputs into the numerical model. The model is then used to evaluate the low adhesion conditions that occur immediately after application. The selected compositions were also compared with the commercial TOR lubricant. **Paper C** uses a high pressure torsion device to assess the boundary lubrication properties of FM, TOR lubricant and solid FM. Different application amounts were used to understand the sensitivity of these products to the amount applied. The numerical model is extended with thermal effects, which were also measured by the experimental device. A wheel-rail contact model was used to assess the traction curves of different products.

Paper A

KVARDA, D., R. GALAS, M. OMASTA, L.B. SHI, H.H. DING, W.J. WANG, I. KRUPKA and M. HARTL. Asperity-based model for prediction of traction in water-contaminated wheel-rail contact. *Tribology International*, 2021, 157, 1–11.
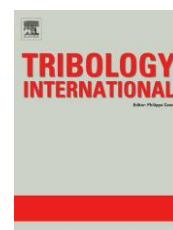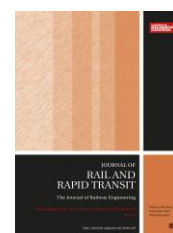
Paper B

KVARDA, D., S. SKURKA, R. GALAS, M. OMASTA, L.B. SHI, H.H. DING, W.J. WANG, I. KRUPKA and M. HARTL. The effect of top of rail lubricant composition on adhesion and rheological behaviour. *Engineering Science and Technology, an International Journal*. 2022, 35, 1–9.

Paper C

KVARDA, D., R. GALAS, M. OMASTA, M. HARTL, I. KRUPKA and M. DZIMKO. Shear properties of top-of-rail products in numerical modelling. *Proceedings of the Institution of Mechanical Engineers, Part F: Journal of Rail and Rapid Transit*. 2022, 0, 1–10.

5 MATERIALS AND METHODS

This chapter is divided into three parts. First part describes the experimental devices used, second part focuses on the mathematical model and third part provides details of methodology for all three papers. A graphical illustration of this thesis is shown in Fig. 5.1.
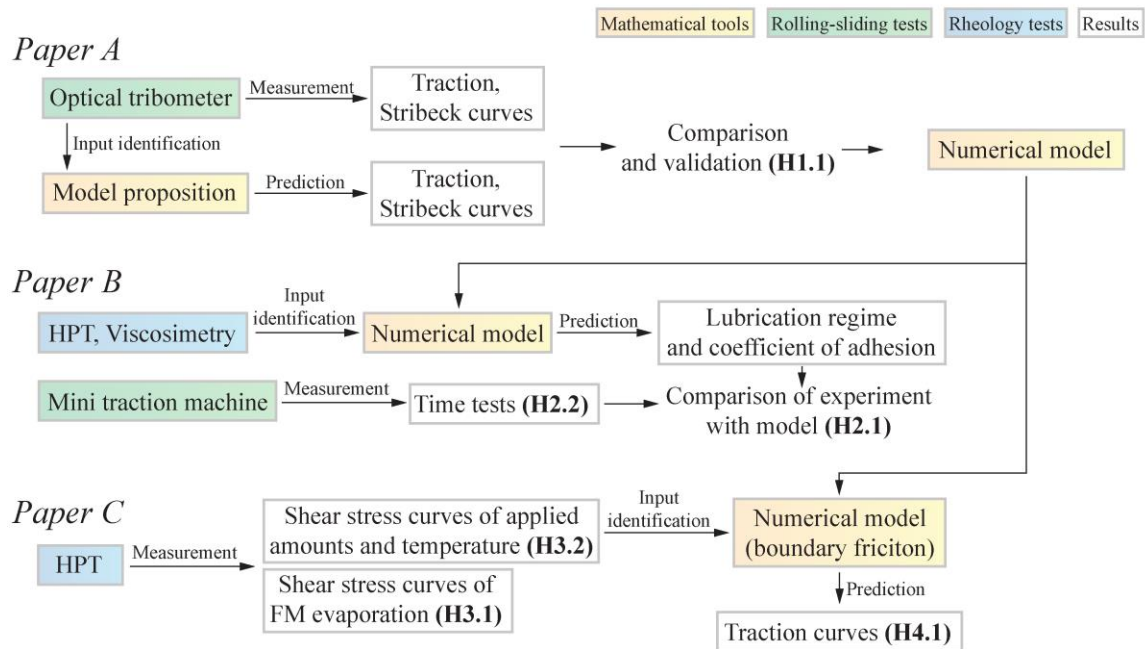

Fig. 5.1 Schematic illustration of link between methods, results and hypotheses.

5.1 Laboratory experimental devices

5.1.1 Optical ball on disc tribometer

An optical tribometer, as shown in Fig. 5.2, was used to measure the coefficient of friction and film thickness between contact of a 25.4 mm diameter bearing steel ball and a BK7 glass disc. Both ball and disc are separately driven by servomotors allowing a precise control over rolling-sliding conditions. The disc is mounted with a lever arm that loads the disc against the ball and a force transducer is used for accurate measurement of normal load. A torque transducer is connected to the ball drive shaft for the measurement of coefficient of adhesion with a frequency of 1 kHz. The device uses a principle of colorimetric interferometry to measure the film thickness in the contact area. A light source enters the microscope, where it is directed into the lens that is focused into the contact area. The glass disc has a thin chromium coating that causes part of the light beam to reflect. The rest of the light beam enters into the contact and reflects from the surface of the ball. The part reflection from the

chromium layer and part reflection from the ball surface cause an interference image that is recorded by the CCD camera and analysed by the software. The exact film thickness is calculated based on a calibration of static contact.
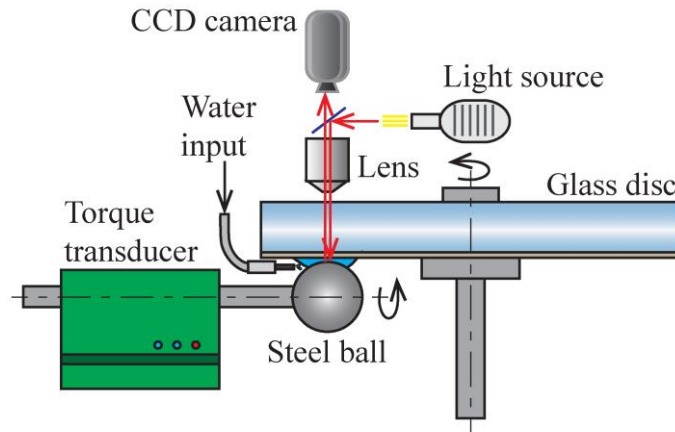

Fig. 5.2 Ball on disc optical tribometer.

5.1.2   Mini traction machine ball on disc tribometer

The ball on disc tribometer is a commercial device Mini Traction Machine (MTM) produced by PCS Instruments Ltd in the United Kingdom. The device enables measurement of coefficient of adhesion between 19.05 mm diameter ball and 46 mm diameter disc, see Fig. 5.3. Alternative specimens and equipment are available, however, only the above-mentioned specimen dimensions were used. Both the ball and the disc are independently driven by a servomotor, enabling precise control over the rolling-sliding contact conditions. The driving mechanism of the ball is mounted on a lever arm, which enables the loading of the ball against the disc. The lever arm is equipped with a force transducer that measures the loading force. A second force transducer is used to measure the frictional force. The normal load can be set from 0 to 70 N, resulting in a 0 to 1.25 GPa maximum Hertzian contact pressure.
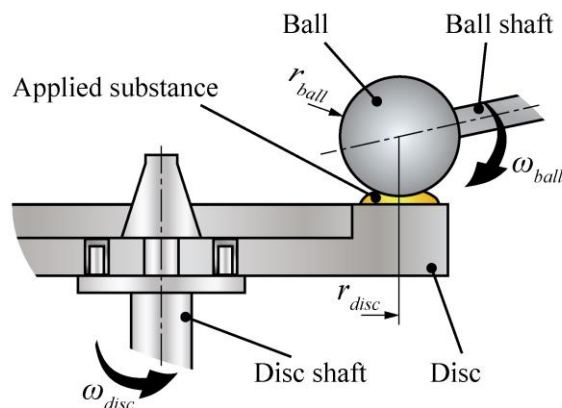

Fig. 5.3 Ball on disc tribometer Mini Traction Machine.

The speed is controlled from -4 to 4 m/s and SRR from -200% to 200%. The software records all the parameters, as well as temperatures and wear rate with a frequency of 1 Hz.

5.1.3 Torsion rheometer

A high pressure torsion (HPT) rheometer, see Fig. 5.4, is a device used for measuring rheological properties of interfacial layers. The device is designed by the author of this thesis and is based on devices used in studies [39, 42–44]. The construction of the device comes from a friction and wear testing station R-MAT 3, originally developed at Brno University of Technology. The device uses a lower specimen with a flat surface and an upper specimen with an annulus with outer diameter of 12 mm and inner diameter of 6 mm. This results in a contact area of 85 mm^2. The lower specimen is held in a specimen holder that is fixed to a loading platform that can move up and down. The loading platform is loaded with hydraulic cylinder, resulting in a maximum loading force of 100 kN. The loading platform is made of a metal plate with high stiffness in the torsional loading direction, but is able to slightly bend in the normal direction. An alignment washer is used between the hydraulic cylinder and the loading platform to allow a slight correction of parallelism between the upper and lower specimen. The upper specimen is held in a specimen holder that is fixed to a shaft with a loading arm. The loading arm uses a screw jack to rotate the upper specimen. Between the screw jack and the loading arm is a force transducer that measures the force exerted on the arm, which is recalculated to torque. The maximum torque allowed is limited by the force transducer to 400 Nm. The shaft is equipped with a rotary encoder that is used to calculate the displacement at the effective radius of the contact specimen. In addition, the rotational position of the worm screw driving motor is used to obtain a more accurate angle of the loading arm. The arm angle resolution is 0.00045 degrees, which corresponds to around 20 nm of displacement at the effective radius. Additionally, a heating segment can be attached with cartridge heating elements. This allows measurements at increased temperatures up to 100 °C.
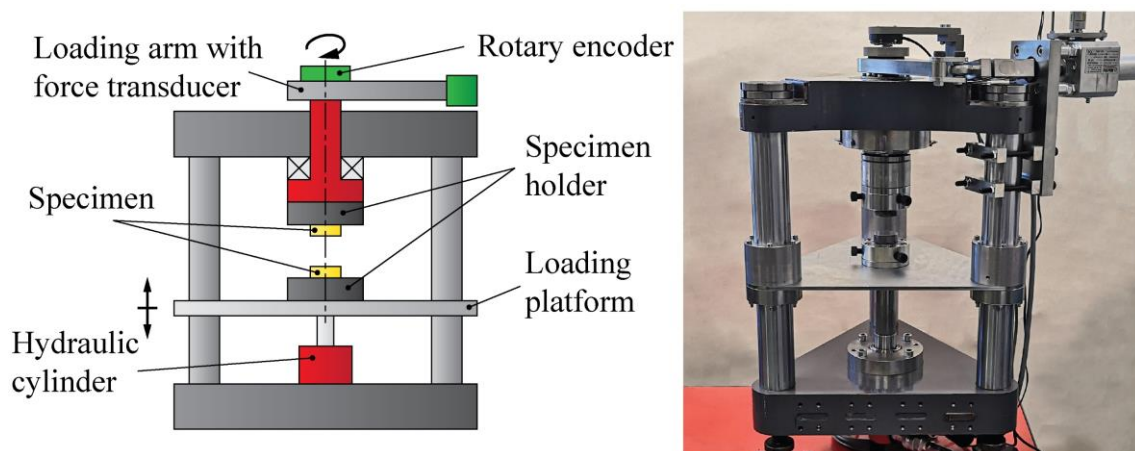

Fig. 5.4 High pressure torsion rheometer.

The HPT device measures the dependency of the coefficient of friction on the displacement of the contact surfaces. Normal stress is calculated based on the set loading force F and the contact area of the specimen S, see Eq. (5.1). The shear stress in Eq. (5.2) is calculated from the measured torque M_k, effective radius r_e (see Eq. (5.3)) and contact area S. The resulting coefficient of friction is a ratio between the shear stress and normal stress, as described by Eq. (5.4).

$$\sigma = \frac{F}{S} \tag{5.1}$$

$$\tau = \frac{M_k}{r_e S} \tag{5.2}$$

$$r_e = \frac{2(r_2^3 - r_1^3)}{3(r_2^2 - r_1^2)} \tag{5.3}$$

$$f = \frac{\tau}{\sigma} \tag{5.4}$$

5.1.4 Optical profilometer

A Bruker ContourGT-X was used for non-contact surface topography measurements. The device uses the principle of light interferometry measuring principle. A piezo-electric motion control moves the scanning head away from the surface with a precisely defined step. A beam splitter with a reference mirror is used to create an interference pattern that is recorded and analysed by the evaluation software. Different types of evaluation methods are available, such as vertical scanning interferometry and phase-shifting interferometry. Vertical measurement resolution reaches up to 0.01 nm.

5.1.5 High pressure viscosimeter

Viscosity measurements were conducted using a custom-made high pressure viscosimeter. The device is built on the principle of a falling element that is placed in a pressurized cartridge with measured oil sample. The falling position of the element is measured by linear a variable differential transformer sensor. Based on the velocity of the falling element, the viscosity is calculated. The maximum lubricant pressure that the device allows is 0.3 GPa. Based on different pressure measurements, the pressure-viscosity coefficient can be identified.

5.1.6 Laboratory balance

The precise weighing of the samples and components was done with analytical laboratory balance KERN ABJ 320-4NM. The maximal weight of a measured sample is 320 g. The readability of the measurement is 0.1 mg.

5.2 Numerical model

The numerical model consists of three main routines. The first routine calculates the parameters of elastohydrodynamic friction. The second routine calculates boundary friction parameters. The third routine connects both the elastohydrodynamic and boundary solution with the asperity contact model. The calculation scheme that explains the algorithm is shown in Fig. 5.5.
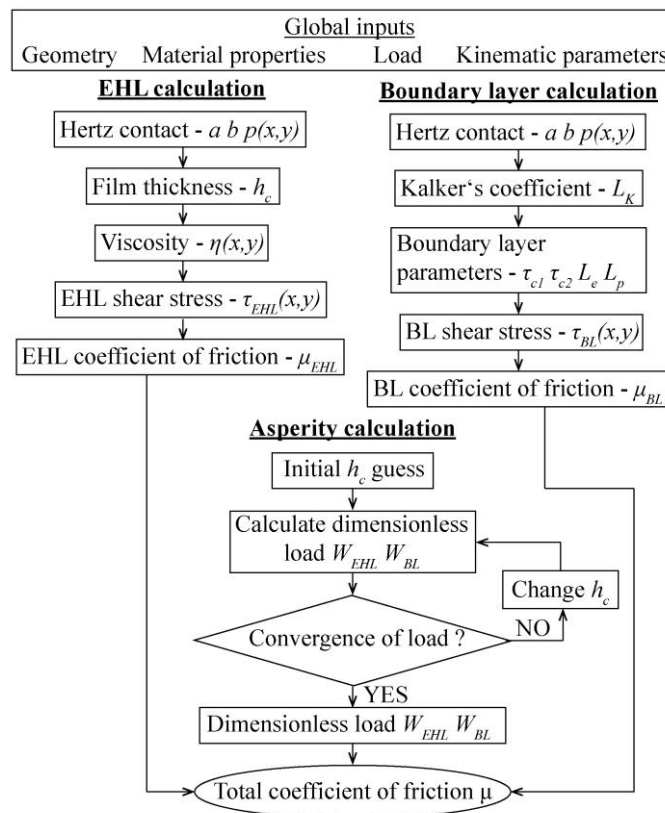

Fig. 5.5 Calculation scheme of numerical model.

5.2.1 Normal contact

The calculation of normal contact follows the Hertzian theory [80]. An approximate solution described in [81, 82] is used. Firstly, the principal curvatures of the contact are calculated, see Eq. (5.5) and Eq. (5.6). The reduced contact radius R is then defined by Eq. (5.7).

$$1/r_x = 1/r_{1x} + 1/r_{2x} \tag{5.5}$$

$$1/r_y = 1/r_{1y} + 1/r_{2y} \tag{5.6}$$

$$1/R = 1/r_x + 1/r_y \tag{5.7}$$

The approximate solutions to the axis ratio k (Eq. (5.8)) and the elliptical integral θ (Eq. (5.9)) are based on [81].

$$k \approx 1.0339(r_x/r_y)^{0.636} \tag{5.8}$$

$$\theta \approx 1.0003 + 0.5968(r_y/r_x) \tag{5.9}$$

The reduced elastic modulus E^* is described by Eq. (5.10). E_1 and E_2 are the values of Young's modulus and v_1 and v_2 are the values of Poisson's ratio.

$$\frac{1}{E^*} = \frac{1 - v_1^2}{E_1} + \frac{1 - v_2^2}{E_2} \tag{5.10}$$

The resulting semi-axes of the contact area are then calculated using Eq. (5.11) and Eq. (5.12).

$$a = \left(\frac{3k^2\theta F_N R}{\pi E^*}\right)^{1/3} \tag{5.11}$$

$$b = \left(\frac{3\theta F_N R}{\pi k E^*}\right)^{1/3} \tag{5.12}$$

The contact pressure at each point of contact area is given by Eq. (5.13). The origin of the coordinate system is placed in the centre of contact area. At this point $(x,y)=(0,0)$ the contact pressure reaches the maximum value.

$$p(x, y) = \frac{3F_N}{2\pi ab}\sqrt{1 - (x/a)^2 - (y/b)^2} \tag{5.13}$$

5.2.2 Boundary friction

The calculation of the boundary coefficient of friction is based on the FASTSIM [48, 52, 53] algorithm. Extension of the theory is made by assuming the third body layer, in a similar way as described in [43, 44], and frictional heating. Full theory analysis and equation derivation will not be given as it can be found in [48, 52, 53]. As mentioned previously, only a simple longitudinal rolling is assumed.

To determine the tangential stresses in contact, we first need to define the relative motion of particles of opposite surfaces in contact. The relative velocity of these two particles in contact is defined as slip s. This relative velocity is composed of rigid slip w between contacting bodies and contribution of surface deformations u. If we assume opposite surface particles that enter the contact area, as depicted in Fig. 5.6, the particles x_1 and x_2 move with velocity $\dot{x}_1$ and $\dot{x}_2$. These particles also undergo a displacement caused by surface deformation u_1 and u_2.
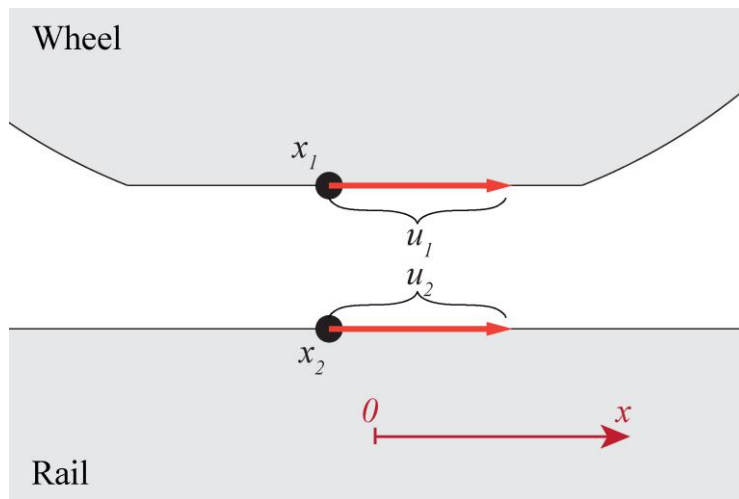

Fig. 5.6 An illustration of contact surface kinematics.

The derived equation that describes this process is Eq. (5.14). In this equation, the rigid slip w is corresponding to the term $(\dot{x}_1 - \dot{x}_2)$, v is the rolling speed and the surface displacement difference u is equal to $(u_1 - u_2)$ as noted in Fig. 5.6.

$$s = (\dot{x}_1 - \dot{x}_2) - v\frac{\partial u}{\partial x} + \frac{\partial u}{\partial t} \qquad (5.14)$$

In the case of steady state rolling, we can neglect the time dependent term $\partial u/\partial t$ and the Eq. (5.14) is transformed into Eq. (5.15).

$$s = (\dot{x}_1 - \dot{x}_2) - v\frac{\partial u}{\partial x} \qquad (5.15)$$

In the simplified theory used by the FASTSIM algorithm [48, 52, 53] it is assumed that the surface displacements and the arising shear stresses have a linear relationship, as described by Eq. (5.16). The linearity is given by Kalker's coefficients of flexibility L. These coefficients are also noted as L_1, L_2 and L_3 for longitudinal, lateral and spin respectively. As this thesis only deals with the longitudinal direction, the coefficient of flexibility L refers to L_1.

$$u = L\tau$$

(5.16)

The calculation of L_1 is based on the assumption of Kalker's linear theory [52] given by Eq. (5.17). The coefficient C_{11} is given by Kalker [48] and G is the shear modulus of material.

$$L_1 = \frac{8a}{3C_{11}G}$$

(5.17)

Here we introduce the concept of third body layer. An elasto-plastic behaviour using Voce's hardening law [64], as shown in Fig. 5.7, is considered. The third body layer is characterized by limiting shear stress of elastic deformation τ_e, limiting shear stress of pseudo-plastic deformation τ_p, elasticity parameter L_e and plasticity parameter L_p. As explained by [43, 44, 61], the resulting coefficient of flexibility in elastic region is given by sum of each individual coefficients of flexibility as given by Eq. (5.18).
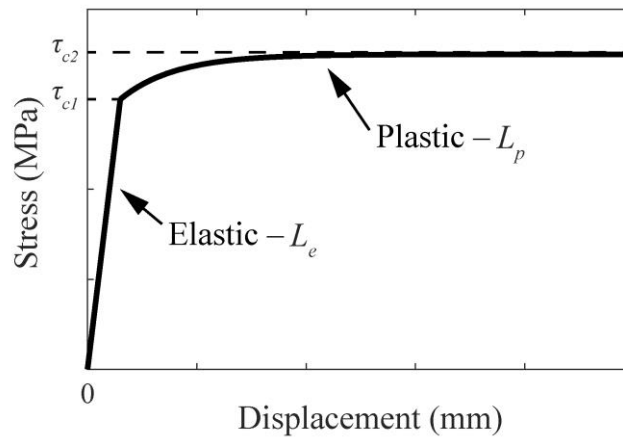

Fig. 5.7 Hardening material model.

$$L = L_1 + L_e$$

(5.18)

Now we rewrite the Eq. (5.15) assuming a time instants t and t', where $t' < t$. Result is Eq. (5.19). The term Δt comes from combination of rolling velocity v divided by the differential $x(t) - x(t')$.

$$s = w + \frac{u(t) - u(t')}{\Delta t} \tag{5.19}$$

Combining Eq. (5.16) and Eq. (5.19) gives Eq. (5.20).

$$s = w + L\frac{\tau(t) - \tau(t')}{\Delta t} \tag{5.20}$$

As we are interested in the shear stresses the Eq. (5.20) is rewritten into Eq. (5.21).

$$\tau(t) = \tau(t') + \frac{\Delta t}{L}[s - w] \tag{5.21}$$

To solve this equation, a discretization of the contact area is done as shown in Fig. 5.8. The contact area is divided into n number of longitudinal strips with Δy width. Each strip is then divided into m number of points with distance of Δx. The algorithm runs through each strip where the solution in each point is acquired. In the following equations, the y_j coordinate is not provided if not necessary, as all parameters dependent on x_i are also dependent on the coordinate of corresponding strip y_j. This makes the equations more readable.
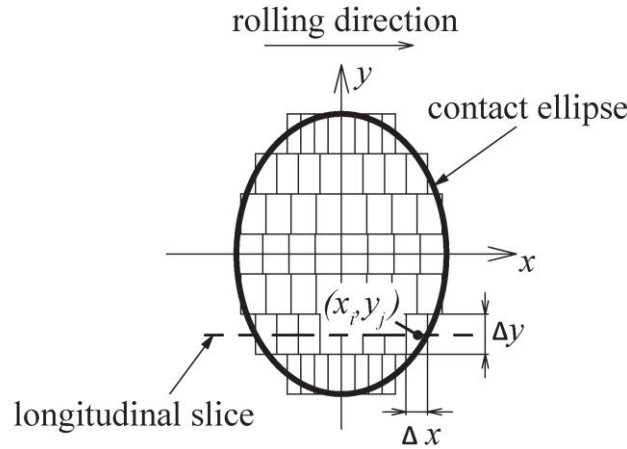

Fig. 5.8 Contact area discretization.

The term Δt is calculated according to Eq. (5.22) based on the length of the strip at specific y_j coordinate and running velocity v, which is defined as a mean speed of surfaces $(\dot{x}_1 + \dot{x}_2)/2$,. We also transform the equation to use x coordinates instead of time. It is assumed that no slip s is present in the first calculation point which results in Eq. (5.23). At the leading edge of the strip, the normal stress from contact pressure and shear stress are equal to zero. The first step of the calculation thus neglects the term $\tau_{BL}(x_{i-1})$, which is equal to zero. Each subsequent step then uses the previous solution of shear stress in the calculation. This

calculation continues for each subsequent time step until the elasticity limit $\tau_{c1}(x_i)$ is reached.

$$\Delta t(y_j) = \frac{2a(y_j)}{vm} \tag{5.22}$$

$$\tau_{BL}(x_i) = \tau_{BL}(x_{i-1}) - \Delta t \frac{w}{L(x_i)} \tag{5.23}$$

After the elasticity limit is reached, the calculation follows the Voce's hardening law as described by Eq. (5.24). Where the deformation u is defined by Eq. (5.25).

$$\tau_{BL}(x_i) = \tau_{c1}(x_i) + (\tau_{c2}(x_i) - \tau_{c1}(x_i))(1 - e^{(-u(x_i) + \tau_{c1}(x_i)L)(x_i)/L_p(x_i)}) \tag{5.24}$$

$$u(x_i) = u(x_{i-1}) - w\Delta t \tag{5.25}$$

Since the pressure and temperature changes in the contact area, it should also be reflected by the elastoplastic third body layer. Assuming a simple Coulomb's law, the limiting shear stresses are defined by Eq. (5.26) and Eq. (5.27). The elasticity parameter is inversely proportional to the normal stress as defined by Eq. (5.28). This is based on the assumption that with higher pressure the third body layer gets stiffer and thus less flexible. The plasticity parameter L_p is assumed to not change its value with change in pressure, see Eq. (5.29).

$$\tau_{c1}(x_i) = (\mu_{c1}p(x_i))exp(\mu_{c1}{}^T(T(x_i) - T_A)) \tag{5.26}$$

$$\tau_{c2}(x_i) = (\mu_{c2}p(x_i))exp(\mu_{c2}{}^T(T(x_i) - T_A)) \tag{5.27}$$

$$L_e(x_i) = L_{\mu e}/p(x_i) \tag{5.28}$$

$$L_p = L_{\mu p} \tag{5.29}$$

The resulting coefficient of adhesion for boundary friction is a ratio between the calculated sum of shear stresses and normal stresses in the contact, as seen in Eq. (5.30).

$$\mu_{BL} = \frac{\tau_{BL}}{p} \tag{5.30}$$

5.2.3 Elastohydrodynamic friction

The calculation of elastohydrodynamic friction uses a Newton's law of viscosity. A critical parameter is the separation of surfaces, which is also referred to as film thickness. The calculation of the film thickness can be done by using one of many approaches. However, in this model, an analytical formula is used. It provides a good enough accuracy with the benefit of a much faster calculation time. Two equations are used here, one for the iso-viscous regime and the second one for piezo-viscous regime. In the iso-viscous regime, no change of viscosity with pressure is assumed. This is relevant for simple models of water, where the change of viscosity with pressure is much smaller compared to oil. For the iso-viscous regime the formula for central film thickness by Esfahanian and Hamrock [83] in Eq. (5.31) is used. For the piezo-viscous regime the formula of Hamrock and Dowson [84] is used (Eq.(5.32)).

$$h_c = 5.08 U^{0.66} W_{EHL}{}^{-0.21} r_x \tag{5.31}$$

$$h_c = 2.69 U^{0.67} G^{0.53} W_{EHL}{}^{-0.067}(1 - 0.61 e^{-0.73D}) r_x \tag{5.32}$$

Parameter r_x is the reduced rolling radius defined in Eq. (5.5) and D is the ellipticity parameter defined in Eq. (5.33). The formula uses non-dimensional parameters U, G and W_{EHL}, which are defined by Eq. (5.34), Eq. (5.35) and Eq. (5.36). Note that these equations use the effective modulus $E' = 2E^*$.

$$D = a/b \tag{5.33}$$

$$U = \frac{\eta_0 v}{E' r_x} \tag{5.34}$$

$$G = \alpha E' \tag{5.35}$$

$$W_{EHL} = \frac{F_{EHL}}{E' r_x{}^2} \tag{5.36}$$

In these equations, η_0 is the viscosity at ambient conditions, α is the pressure-viscosity coefficient and F_{EHL} is the normal load carried by EHL film. To calculate the shear stress in the lubricant film, the same discretization as shown in Fig. 5.8 is used. In each point, the shear stress is calculated using Eq. (5.37).

$$\tau_{EHL}(x_i, y_j) = \eta(x_i, y_j)\frac{w}{h_c} \tag{5.37}$$

The viscosity in each point is calculated using Roelands pressure-viscosity dependency [85], as described in Eq. (5.38). However, if the iso-viscous regime is considered than $\eta(x_i, y_j)$ is equal to η_0. The Barus equation (Eq. (5.39)) is a simpler formula which is used to experimentally find the pressure-viscosity coefficient α, that is needed in Eq. (5.35)(5.32).

$$\eta(x_i, y_j) = \eta_0 e^{[ln\eta_0 + 9.67]\{(1 + 5.1 \cdot 10^{-9}p(x_i, y_j))^z - 1\}} \tag{5.38}$$

$$\eta(x_i, y_j) = \eta_0 e^{\alpha p(x_i, y_j)} \tag{5.39}$$

The resulting coefficient of friction in elastohydrodynamic regime is defined as sum of shear stresses divided by sum of normal stresses, as seen in by Eq. (5.40).

$$\mu_{EHL} = \frac{\tau_{EHL}}{p} \tag{5.40}$$

The hydrodynamic friction calculation does not use the temperature dependency. As the temperature dependency is closely linked to frictional power. Due to the low coefficient of adhesion in the elastohydrodynamic regime, the frictional power generated is also low compared to that in the boundary regime where asperities are in contact. This is a simplification that is assumed to cause a negligible error in the calculation.

5.2.4 Asperity contact

Now that the calculation of friction in both the boundary and elastohydrodynamic regime is defined, a model for a mixed lubrication regime will be explained. The calculation is based on the theory of Greenwood and Tripp [72], that estimates the pressure p_a carried by asperity interaction. The theory assumes paraboloidal asperities with Gaussian height distribution. The parameters that define these asperities are height standard deviation ψ, curvature of asperity peak β and density of asperity peaks γ. The parameter defining the roughness characteristic of the surface is $K = \psi\beta\gamma$. Two models of asperity deformation are used: elastic and plastic. The elastic model is defined by Eq. (5.41) and plastic model by Eq. (5.42).

$$p_a = \frac{4}{3}\frac{K}{2}E^* F_{3/2}\left(\frac{h}{\psi}\right)\sqrt{\frac{\psi}{\gamma}} \tag{5.41}$$

$$p_a = \frac{2}{3}\pi^2 H K^2 F_4\left(\frac{h}{\psi}\right) \tag{5.42}$$

In the plastic deformation model, the term H is mean pressure related to the hardness of material. An approximation is made, where this is equal to around 6 times the yield shear stress [86]. The function F_n is defined by Eq. (5.43) and it is solved by numerical integration. The upper bound of the integral is set to 30 and the integral is divided into 1000 steps. This was found to give very good accuracy with low computational time.

$$F_n(h) = \frac{1}{\sqrt{2\pi}} \int_{h/\psi}^{\infty} (u - h)^n e^{-u^2/2} \mathrm{d}u \tag{5.43}$$

The calculation process starts with an initial guess of h that is taken from the prediction of film thickness by Eq. (5.31) or Eq. (5.32). This initial guess assumes that all load is carried by lubrication film, thus $F_{EHL} = F_N$. Then the mean asperity pressure p_a is calculated either by Eq. (5.41) or Eq. (5.42) based on the deformation regime (elastic, plastic) that is considered. Using the mean asperity pressure, the non-dimensional load carried by asperities is determined using Eq. (5.44).

$$W_{BL} = \frac{p_a \pi a^2}{E' r_x^2} \tag{5.44}$$

The non-dimensional loads are then used to estimate the error by Eq. (5.45). The non-dimensional load W refers to the total load carried by the contact as defined by Eq. (5.46).

$$\varepsilon = \left| \frac{W^2 - (W_{EHL} + W_{BL})^2}{W^2} \right| \tag{5.45}$$

$$W = \frac{F_N}{E' r_x^2} \tag{5.46}$$

The terminating condition for the error calculation is set to 0.1%. If the first iteration does not meet this condition, a change of surface separation $h = h - h_c/1000$ is done. This provides first two point which are then taken by the Newton-Raphson numerical method. The calculation then continues until the convergence condition defined by Eq. (5.45) is met. At the end of the calculation, the non-dimensional load carried by asperity W_{BL} and non-dimensional load carried by lubrication film W_{EHL} are known. Using these parameters, the coefficient of adhesion is calculated using Eq. (5.47). The shear stress distribution is determined by Eq. (5.48).

$$\mu = \frac{\mu_{EHL}W_{EHL} + \mu_{BL}W_{BL}}{W_{EHL} + W_{BL}} \tag{5.47}$$

$$\tau(x_i, y_j) = \frac{\tau_{EHL}(x_i, y_j)W_{EHL} + \tau_{BL}(x_i, y_j)W_{BL}}{W_{EHL} + W_{BL}} \tag{5.48}$$

5.2.5 Contact temperature

The temperature calculation is based on the solution provided by Ertz and Knothe [79]. The frictional power dissipation rate is a result of shear stress and rigid slip in the contact patch as defined in Eq. (5.49). The resulting temperature is then calculated using Eq. (5.50). The parameter λ is thermal conductivity, ρ is density and c is specific heat capacity. All parameters in the model use values from [87].

$$\dot{q}_i(x_i, y_j) = \tau(x_i, y_j)w \tag{5.49}$$

$$T(x_i, y_j) = \frac{2}{\sqrt{\lambda \rho c}} \sqrt{\frac{a(y_j)}{\pi v}} \sum_{k=1}^{i} \dot{q}_i(x_i, y_j)(\sqrt{x_i - x_{k-1}} - \sqrt{x_i - x_k}) \tag{5.50}$$

Firstly, the shear stresses are found, as described in previous sub-sections. Then the power dissipation rate and the temperature distribution are calculated. The temperature distribution is then used again in a new calculation of shear stress where temperature dependent variables change. Since both shear stress and temperature are dependent on each other, an iterative process is needed to reach convergence. This convergence cycle is repeated until the change in temperature is smaller than 0.1 °C.

5.3 Design of experiments and methodology

5.3.1 Paper A

This paper deals with the description and validation of a numerical model for the prediction of friction in liquid-contaminated contact. The model is described in subsection 5.2. It neglects the temperature dependency mentioned in subsection 5.2.2 and uses iso-viscous film thickness prediction defined by Eq. (5.31). The experimental validation is done using an optical ball on disc tribometer with the ability to measure film thickness by means of colorimetric interferometry. Water is used as a reference liquid. It was chosen mainly to

provide a wider range of mixed lubrication in the measurement speed range. Due to the very low roughness of the contact specimen the film thickness needs to be very low and thus oils were not suitable.

A 25.4 mm diameter ball made of bearing steel AISI 52100 with 53HRC (standard deviation 0.3HRC) hardness was used. This corresponds to 6 GPa for parameter H. Two types of surface roughness conditions were used in this study. A smooth surface of the ball was prepared by polishing with a diamond paste. A rough surface was prepared by a run-in procedure with maximum Hertzian pressure 0.75 GPa, 5% SRR and 500 mm/s speed. The resulting parameters of the surface measured by the optical profilometer are stated in Tab. 5.1. The calculation uses only these parameters, as the roughness of the glass disc with chromium coating has roughness less than 1 nm. These procedures were selected as they provided the most stable roughness condition during the experiment. The surface conditions were measured and evaluated after each experiment to confirm negligible changes. Also, the length of each measurement was made as short as possible. This was done to eliminate the effect of wear as well as damage to chromium layer.

Tab. 5.1 Surface parameters of ball specimen

Surface condition	Roughness standard deviation ψ (nm)	Asperity peak curvature β (mm)	Asperity peak density γ (1/mm²)	K (-)
Smooth	8.3	0.301	24 200	0.0605
Rough	9.56	0.373	21 500	0.0767

The water used as a lubricant was previously distilled to guarantee its pureness. It was applied using a needle placed 5 mm in front of the contact. The supply of water was continuous to provide fully flooded conditions. The viscosity of 1 mPa·s is taken from [88], based on the room temperature.

Three types of tests were conducted: traction tests, film thickness measurement and Stribeck test. All tests were carried out under maximum Hertzian pressure of 0.75 GPa. The first test measured the traction curve and was aimed at identifying the boundary layer parameters defined in Eq. (5.26)–(5.29). The results were fitted by four parameters in these equations. As mentioned before, the temperature dependency was neglected in the calculation. The second test measured the film thickness under 0% SRR. These measurements were used to compare the accurate prediction of film thickness by the model, which is important for the calculation of mean asperity pressure p_a. Stribeck tests were then measured for both surface conditions. These results of the rough and smooth surface were then compared with the coefficient of adhesion prediction by both elastic and plastic asperity model. Lastly, a traction test under 5 different speeds was conducted. Only a rough surface was used for this, as it resulted in a broader mixed lubrication regime. Values from negative to positive SRR were measured and transformed to positive values to confirm the

symmetrical behaviour with respect to 0% SRR. Each measurement point of the coefficient of adhesion is an average from a 4 second long interval at set measurement conditions. All types of tests with experimental conditions are shown in Tab. 5.2.

Tab. 5.2 Experimental parameters for all types of tests.

Test type	Roughness type	Speed (m/s)	SRR (%)
Dry traction	Rough	0.5	-10 – 10
Film thickness	Smooth	0 – 2	0
Stribeck	Smooth	0.1 – 2	5
Stribeck	Rough	0.1 – 2	5
Traction	Rough	0.25, 0.5, 1, 1.5, 2	-5 – 5

5.3.2 Paper B

The second paper uses both experimental and numerical tools to assess the frictional properties of TOR lubricants. The numerical model was extended with piezo-viscous elastohydrodynamic behaviour as described by Eq. (5.32), (5.38) and (5.39). The properties of the lubricants were measured by high pressure viscosimeter and HPT device. Different TOR lubricant components and compositions were tested using a ball on disc MTM machine. Custom TOR lubricants used a synthetic ester oil with bentonite thickener as a base medium. It was selected due to its good biodegradability. Additional constituents were friction modifier particles and solid lubricant. The list of all used components is seen in Tab. 5.3. All components were weighed using laboratory balance and mixed with shaft mixer for at least two hours before each experiment to ensure homogeneity of the composition.

Tab. 5.3 List of TOR lubricant constituents

Component	Name	Particle size (μm)	Mohs hardness (–)
Base medium	Synthetic ester oil with bentonite thickener	–	–
Friction modifier particles	Aluminium oxide	10, 44 (D99)	9
	Zinc oxide	5 (D99)	4.5
	Copper(I) sulfide	≈5	2.5
Solid lubricant	Graphite	7 (D90)	1–2
	Molybdenum disulfide	4.2 (D50)	1–2

For comparison, two commercial TOR lubricants were used. These are referred to as TOR A and TOR B. Both are hydrophobic biodegradable high pressure resistance lubricants. They are designed to reduce wear and squeal noise in railway curves.

Adhesion tests were conducted using MTM device with a specimen from bearing steel AISI 52100 with Vickers macro-hardness of 800–920 HV (ball) and 720–780 HV (disc). Hardened bearing steel does not represent real wheel and rail material. However, for comparative tests of TOR lubricants in a laboratory environment, the hardened steel provides minimal changes in surface topography during the tests. This ensures similar contact conditions during testing, which is desirable for quantitative comparison of tested substances. The tests were done under 800 MPa maximum Hertzian pressure, 2% SRR and 1 m/s speed. The contact pressure is typical for light-rail system. The speed was set based on the analysis of the lubrication regime and the parameter lambda, which corresponds to about 60 km/h in the train. The speed is also limited by the centrifugal effect, which removes the lubricant from the surface of the disc. The SRR was set to represent realistic conditions of wheel and rail contact. Higher values of SRR could cause excessive wear, which is a negative effect on stable surface conditions for all experiments. The experiments with different components were stopped at 20 minutes after application. The evaluation of the average coefficient of adhesion was taken after initial drop recovery until the end of the test, as shown in Fig. 5.9.
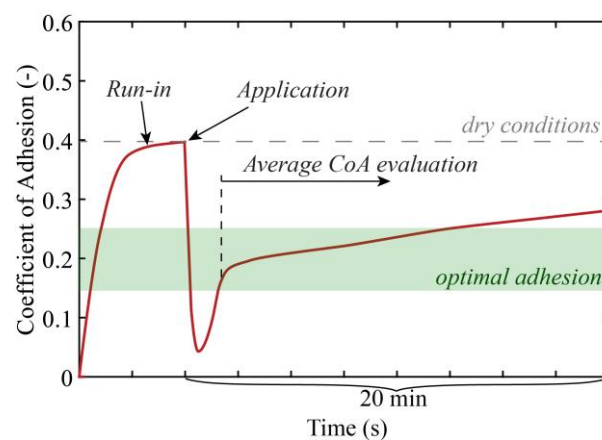

Fig. 5.9 Testing procedure for individual components of TOR lubricant.

Rheological tests were conducted using an HPT device to acquire boundary regime frictional properties. A high pressure viscosimeter was used for parameters of the base ester oil for the elastohydrodynamic part of the model. All HPT tests were done under 750 MPa normal pressure and displacement rate of 1 μm/s. The maximum shear displacement was set to 0.1 mm. The specimens used were made of DIN 100CrMn6 steel which has similar material properties to AIS 52100. The TOR lubricant was applied with a micropipette in 8 μl amount to ensure surface coverage. Before each HPT test a run-in was done. This run-in consisted of a 60 mm shear displacement at 500 MPa. The high pressure viscosimeter used only the

base ester oil for tests. The viscosity was measured at 50 MPa steps up to 300 MPa at ambient temperature 25 °C. The equations of Barus (Eq. (5.39)) and Roelands (Eq. (5.38)) were then used to estimate the pressure-viscosity coefficients.

5.3.3 Paper C

The last paper uses HPT device and boundary friction model to assess different types of TOR products and their performance. The tested TOR products are oil-based TOR lubricants (OFM 1 and OFM 2), water-based FM (WFM) and solid stick (SFM). Both OFM1 and OFM2 use ester oil as a base medium. OFM1 uses organic thickener and is classified as NLGI 0. OFM2 uses inorganic thickener and has NLGI number 00. WFM contains water, thickener, solid lubricant and solid particles. SFM is made of a polymeric base with solid lubricant and solid particles for friction modification.

Since the experimental results use an HPT device, the numerical model neglects any effects of elastohydrodynamic lubrication. The boundary calculation is extended with temperature dependent parameters as shown in Eq. (5.26) and Eq. (5.27). The calculation of temperature used in the model is described in sub-section 5.2.5. The calculation parameters were selected based on a representative wheel and rail contact. Input parameters for the calculation are shown in Tab. 5.4. The input parameters of the boundary friction of the TOR products are part of the experimental results.

Tab. 5.4 Calculation parameters

Parameter	Value	Unit
Longitudinal semi-axis a	3.7	mm
Lateral semi-axis b	3.3	mm
Rolling radius r	350	mm
Normal force F	20	kN
Maximum Hertzian pressure p_0	790	MPa
Thermal conductivity λ [87]	50	W/(K·m)
Density ρ	7850	kg/m^3
Specific heat capacity c [87]	450	J/(kg·K)

The contact specimens were made of DIN 100CrMn6 with 60HRC hardness. The material does not reflect the real material of the wheels and rails. However, this choice was selected to provide more stable and comparable surface conditions for comparison of different TOR products. The selected material also reduces wear and suppresses any oxidation effects that could cause different conditions for experiments. The specimen surface was reconditioned for each tested product by polishing to remove any residue on the surface. The resulting

surface roughness after polishing was 0.1 μm.

The application of the tested liquid products was done using a micropipette. The applied liquid was spread along the contact patch to cover as much asperity contact as possible. In case of testing WFM at dry conditions, the applied product was dried by a heat gun set at 60 °C. The solid stick was crushed into fine particles (particle size around 50 μm) and the precise applied amount was weighed using laboratory balance. This does not correspond to the application methodology of these solid products. However, it allows the most precise control over the applied amount.

HPT tests were carried out under 750 MPa normal pressure which roughly corresponds to the maximum Hertzian contact pressure of light-rail system. The displacement rate was set to 1 μm/s with a maximum displacement of 400 μm. The experiments under increased temperature used the same pressure and displacement rate. These tests were stopped after 200 μm displacement. Before each experiment, a run-in was conducted that was aimed at stabilizing the surface roughness around 0.3 μm. This run-in phase also allowed to control the initial dry coefficient of friction that was around 0.5 at 400 μm displacement. Whenever surface roughness exceeded 0.4 μm after experiment the reconditioning process was repeated. After each experiment, the specimens were unloaded, cleaned with acetone in ultrasonic cleaner and surface roughness was measured. Resulting coefficient of friction data points are taken from an average value of last 20 μm of displacement before reaching maximum displacement, as shown in Fig. 5.10.
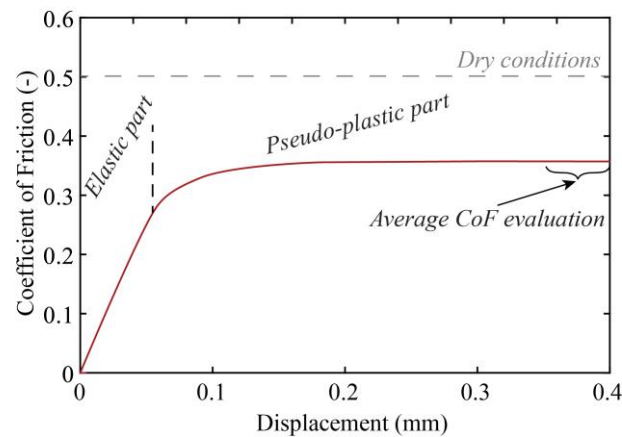

Fig. 5.10 HPT test illustration.

6 RESULTS AND DISCUSSION

This thesis aims to clarify the frictional characteristics of TOR products, especially focused on problems with low adhesion conditions. In the first part, a numerical model that calculates both boundary and elastohydrodynamic friction based on the third body model approach was proposed. Subsequently, this model was used to investigate the low adhesion conditions of TOR lubricants. Furthermore, the effect of different components of TOR lubricants was experimentally studied. Lastly, the boundary friction model is used together with experimental rheological measurements to assess the effect of amount of TOR products on coefficient of friction and low adhesion. The modelling approach helps identify the resulting traction curve characteristics. The findings can help with design of TOR products and defining strategy of their use and application.

The first step was to develop a numerical model that would use rheological inputs to predict coefficient of adhesion in contaminated rolling-sliding contact. **Paper A** presents a model for prediction of adhesion across the boundary, mixed and elastohydrodynamic regime. The model calculates the coefficient of adhesion based on the resulting shear stresses in the asperity contact and the lubricating film. The fact that the resulting friction is based on the rheological properties of the interface as a shear response to displacement (boundary regime) and rate of displacement (hydrodynamic regime) frees the solution from fixed values of the coefficient of friction.

The numerical model uses Kalker's FASTSIM algorithm to calculate surface displacements and resulting shear stresses based on third body layer rheology. This was previously proposed by Six et al. [43, 44] and similar approaches that use the parametrization of coefficient of friction proved to be applicable in various conditions [59, 61]. The elastohydrodynamic part uses the general law of viscosity to calculate shear stress in the lubricant film. Studies showed good agreement of this theory with experimental results [65, 66, 68, 73]. However, these studies also show that setting the correct coefficient of friction for the asperity contact is the key to obtaining relevant results. A workaround for these studies is to set this value in such a way that it corresponds to the experimental data, as shown in Fig. 2.31b. This is where the novelty of this study uses the results of improved FASTSIM to provide an accurate estimation of the boundary coefficient of friction in a simple calculation scheme. In this way, the calculation of shear stresses needs the rheological properties of the contact interface. The different running conditions can then be studied without knowing the coefficient of friction for each condition. The relative simplicity of the algorithm also allows for easy implementations of ideas such as lubricant shear thinning, temperature dependent parameters and different asperity models.

Initial experimental results using an optical tribometer under dry contact were used to identify boundary friction parameters. Saturated values of the coefficient of adhesion were relatively low, which was caused by the steel–glass configuration. During the main Stribeck

and traction experiments, the film thickness measurement was only used to verify that no contamination occurred, and the film thickness is in a correct range. If contamination occurred, the film thickness would rapidly increase above expected values, and the experiment needed to be redone. This approach helped control the contact conditions to ensure that parameters of the model prediction were correct.

The film thickness measurements verified a good accuracy of the analytical film prediction formula. The first Stribeck test with a smooth surface resulted in a very low coefficient of adhesion values across the measured speed range. Such a low coefficient of adhesion is a result of very low viscosity of water and very smooth surfaces. Similar values were observed in both the experimental and numerical works of Chen et al. [66, 68]. Under such a smooth surface as was used in this study, even a small surface separation enables the lubricating film to carry a large portion of the normal load. This is closely related to a modern topic in study of elastohydrodynamic superlubricity with low viscosity lubricants. The prediction using elastic asperity deformation heavily underestimates the coefficient of adhesion at low speed but gets more accurate with higher speed. The lower load carried by asperity using the elastic deformation model was also shown in the original study by Greenwood and Tripp [72]. The results of asperity models showed that the estimation of the load carried by the lubricant film is a complex problem that is not easily solved by formulas using general simplifications. A future direction in using state of the art models could improve the accuracy across various experimental conditions as presented in studies [73, 75].

The proposed model showed a new way to incorporate the extended FASTSIM model and elastohydrodynamic theory to estimate the coefficient of adhesion in contaminated wheel-rail contact. The input rheological properties of dry contact and water implemented into FASTSIM and the general theory of elastohydrodynamic lubrication were able to accurately represent the experimental data with the correct use of the asperity model (**HYPOTHESIS H1.1 CONFIRMED**). However, the asperity model was valid for the used conditions and surface topography and does not have to be reasonably accurate for different surface topography. The use of the model is not limited to water contaminated contact, but by using a third body concept for boundary friction, it is suitable for various natural and artificial substances present in the contact interface. It should be noted that the asperity model is key to an accurate prediction of the mixed lubrication regime. The problematic of asperity contact needs to be thoroughly considered for different cases of contact conditions.

The tools descried in **Paper A** were subsequently used together with experimental methods to answer the question regarding low adhesion conditions after the application of TOR lubricant in **Paper B**. The aim was to evaluate the low adhesion conditions of TOR lubricant composition while proposing a composition that reaches optimal levels of adhesion between 0.15–0.25 and is resilient to low coefficient of adhesion after application.

The initial experiments aimed to investigate the influence of individual components

and their different contents in TOR lubricant. Experiments with solid lubricants were in line with a previous study [11] on the same device. In was found that use of solid particles for friction modification of medium hardness does not directly result in higher frictional values in base medium. These results are in agreement with studies using zinc oxide in FM [11] and in water [78]. However, using a higher amount of medium hardness particles compared to high hardness aluminium oxide helped with lowering the sensitivity to application amount in study [12]. In this study, increasing the amount of solid particles did not lead to significant suppression of the initial drop. The addition of solid lubricant to the composition did not result in a significant reduction of effective coefficient of adhesion. Similar behaviour was shown in [40], where adding grease to FM did not result in an additional decrease in the coefficient of friction. This means that correct selection of friction modifier particles is key for the resulting frictional behaviour. It was also found that the use of excessive amounts of solid lubricant makes the composition a viscous paste, which causes problems with application with no additional benefits of coefficient of adhesion reduction. This needs to be taken into account when designing the product to ensure proper application in field use.

Based on the previous results, several compositions were compared with two commercial TOR lubricants. At the lowest applied amounts, all tested substances showed an increasing trend in coefficient of adhesion. This is typically observed with TOR products as a result of a low amount applied or high slip as seen in studies [12, 28, 33, 34]. With the higher amount, the commercial products resulted in over-lubrication as was also seen in [12, 34]. The custom-made substances stabilized at the optimal levels of adhesion with a very slow increase in the coefficient of adhesion until end of the experiment. This shape of time test results seem to be the most advantageous in achieving the optimal levels of adhesion for longer time. Similar trends were observed in studies [10, 12, 33]. However, the products that these studies use are much more sensitive to the applied amount, especially in [12]. Since this study uses the same small-scale ball on disc device, the geometry itself might be important in the low adhesion conditions seen.

The rheology measurements with the HPT device showed that the commercial product causes a low coefficient of adhesion in the boundary regime. This was not true for custom-made substances where the coefficient of friction reached optimal levels. The increasing trends in low application amounts are thus a result of removal of TOR product and increase in asperity contact. This would explain the slow increases seen in rheology testing of TOR products in [31]. Knowing the exact amount of product in the contact interface could help explain the transient effects of the coefficient of adhesion. A redistribution model could be built on this idea to simulate how long the applied product can be effective. Based on the model results, the initial drop for custom made substances seemed to be a result of not enough particles in the contact. Only the action of crushing the particles in combination with contact starvation will promote the boundary lubrication regime where the optimal levels of adhesion are reached.

Important conclusions are that the use of the model can help predict the coefficient of adhesion in boundary and elastohydrodynamic regime. Low adhesion conditions were the result of the solid particles providing not enough interaction between the surfaces (**HYPOTHESIS H2.1 CONFIRMED**). The commercial product was not able to provide optimal levels of adhesion even in the boundary regime. This means that if the product is not spread into thin film, a low adhesion conditions will occur. Increasing the amount of solid particles for friction modification did not lead to effective suppression of low adhesion drop (**HYPOTHESIS H2.2 FALSIFIED**). The application methodology and the focus on creating a thin film seems to be the key to provide the longest effect with minimal risk to traction or braking.

Based on the findings in **Paper B**, where the boundary lubrication was found to be an important parameter for assessing the coefficient of adhesion, the boundary properties of different TOR products were investigated in **Paper C**. The aim of this study was to evaluate the low frictional properties and the application amount dependence of different TOR products. The numerical model was then used to assess the resulting trend of the traction curves.

The experimental results with TOR products show similar behaviour to studies [40, 41] and low displacement results in [31]. The application of FM in a dry state caused low friction only at a higher applied amount as suggested by [40, 41]. However, no low frictional values were observed when water was present, even at high applied amounts. This contradicts the findings of the study [11]. Suggesting the hydrodynamic effect does not seem to be a realistic explanation, as ball on disc tests with water do not generate enough surface separation compared to the scale of asperities and particles contained in FM. The results with a high amount of dry FM in this and previous studies [40, 41] could be explained by the formation of a compacted thick film that separates the surfaces. On the other hand, when water is present, the movement of particles is not constricted, and upon loading surfaces against each other, the particles can disperse and squeeze out with the help of water. This results in a thin film that allows for asperity interaction with hard particles of FM. In practice, when FM is applied, the wet state helps spread FM on the rail and provides an intermediate level of coefficient of friction. The action of spreading the product creates a thin film that upon drying contains a small amount of FM that cannot result in low frictional values. The only possible case where such low friction can occur is when FM is applied by a stationary unit and the film dries locally before the wheels can spread it. This results in a high amount of FM on a short section of rail creating low adhesion before the action of the wheel can remove it.

When comparing the applied amounts, the approximate density of TOR lubricant and FM can be interpreted that microliter applied results in around one milligram of product in the contact. As a result, the same trends of application sensitivity were seen for all tested products. Assuming the same mass of the TOR product in the contact, the levels of friction

will be the same for the TOR lubricant, FM and solid FM. The explanation for the higher sensitivity of the TOR lubricant compared to FM [3, 34] could be a result of the effect described in the previous paragraph. After application of FM, the wet state provides high frictional values, and after drying, the film is too thin to create a thick layer that would cause low friction conditions. Regarding solid FM, even though the same sensitivity as that of the TOR lubricant was seen, the vehicle application methodology used is not likely to overdose the contact with solid FM. However, this area is still not fully explored, as no detailed study about the application parameters of solid FM was published.

The investigation into the influence of temperature showed that TOR products supress the effect of a decrease in coefficient of friction at a higher temperature seen in dry contact in this and other studies [89, 90]. However, the increased temperature does not cause an increasing trend in coefficient of friction. Similarly, the frictional tests do not show a prominent increase in coefficient of friction with higher displacement, as was also observed in [40, 41]. Since there is no process that would cause a dominant continuous increase in coefficient of adhesion with increase in slip, the traction curves shower a neutral trend. This means, that the reported excessively positive trends of traction curve [27–30] are a result of removal of the applied TOR product. As the friction of TOR product is dependent on the applied amount [10, 12], the measured traction curves do not exhibit purely slip-dependent behaviour, but also the influence of TOR product film removal. This could be especially important with the use of traction curves in dynamic modelling. Assuming a clearly positive trend of traction curve will not represent the reality of contact interface in discrete time instances.

The main findings of the last publication show that the presence of water medium in FM will not cause low adhesion conditions (**HYPOTHESIS H3.1 FALSIFIED**). If such conditions occur, it might be the result of used methodology, especially the use of small point contacts can lead to particles avoiding the leading edge of contact. When the mixture dried, low friction was observed with excessive amounts. However, if used correctly, this does not seem to hold true for wheel and rail application. All tested substances resulted in transition to low frictional values at the same amount present in contact. This means that FM and solid FM are not more resilient to the applied amount present in contact (**HYPOTHESIS H3.2 FALSIFIED**). It would be correct to state that it is easier to form a thin film and remove FM and solid FM, thus overall decreasing the amount in contact interface. It was found that the clearly positive trend of the traction curve is not a property of the TOR product, but it seems to be a result of decreasing the amount present in contact by increasing the sliding at higher slip (**HYPOTHESIS H4.1 CONFIRMED**).
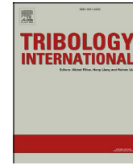
Asperity-based model for prediction of traction in water-contaminated wheel-rail contact

Daniel Kvarda [a,*], Radovan Galas [a], Milan Omasta [a], Lu-bing Shi [b,c], Haohao Ding [b], Wen-jian Wang [b], Ivan Krupka [a], Martin Hartl [a]

[a] *Faculty of Mechanical Engineering, Brno University of Technology, Technicka 2896/2, 616 69, Brno, Czech Republic*
[b] *Tribology Research Institute, State Key Laboratory of Traction Power, Southwest Jiaotong University, Chengdu, 610031, China*
[c] *Zhengzhou Research Institute of Mechanical Engineering Co., Ltd., Zhengzhou, 450001, China*

The effect of top of rail lubricant composition on adhesion and rheological behaviour

Daniel Kvarda [a,*], Simon Skurka [a], Radovan Galas [a], Milan Omasta [a], Lu-bing Shi [b,c], Haohao Ding [b], Wen-jian Wang [b], Ivan Krupka [a], Martin Hartl [a]

[a] *Faculty of Mechanical Engineering, Brno University of Technology, Technicka 2896/2, 616 69 Brno, Czech Republic*
[b] *Tribology Research Institute, State Key Laboratory of Traction Power, Southwest Jiaotong University, Chengdu 610031, China*
[c] *Zhengzhou Research Institute of Mechanical Engineering Co., Ltd., Zhengzhou 450001, China*

Shear properties of top-of-rail products in numerical modelling

Daniel Kvarda[1] , Radovan Galas[1] , Milan Omasta[1], Martin Hartl[1], Ivan Krupka[1] and Marian Dzimko[2]

7   CONCLUSION

The present dissertation thesis deals with the use of both experimental and numerical methods for evaluation of frictional performance of TOR products. The use of TOR products for reduction of wear, noise and energy requirements has been extensively studied in the last two decades. The current state of research shows that these benefits are linked to a reduction in coefficient of adhesion and a neutral to positive frictional characteristic. A large part of the published research used water-based FM products and less focus was aimed at TOR lubricants and solid FMs. The general conclusion can be made that the use of TOR lubricant poses a higher risk of over-lubrication and low adhesion conditions. However, even in some cases of FM use, there are lower than optimal levels of adhesion. To study these problems, the use of prediction models has not yet been extensively used. The main goal was to use experimental investigation and a numerical model to assess conditions that lead to low adhesion conditions when applying TOR product.

The results of this thesis are divided into three papers. The first paper dealt with introduction of the numerical model and its application on a model case of water contaminated contact. The model consists of a boundary friction part using Kalker's FASTSIM algorithm and elastohydrodynamic part governed by general Newton's law of viscosity. A statistical asperity model was used to provide connection between these two regimes to mixed lubrication. It was revealed that the correct use of the asperity model is detrimental to accurate prediction. The results showed that the combination of mentioned boundary and elastohydrodynamic models is usable for studying various third body contamination. The second paper used a commercial ball on disc tribometer and developed a numerical model to investigate the influence of TOR lubricant components on the coefficient of adhesion. Experiments with different types of particles in an oil-based medium showed that the hard solid particles have a dominant effect on the resulting friction. However, an important finding was that immediately after application, the particles were unable to rapidly increase the coefficient of adhesion from critical low levels. Application of the numerical model revealed that the initial drop was closely related to the change of lubrication regime. Only after a slow recovery did the coefficient of adhesion reach the boundary regime where it stabilized. Compared to commercial TOR lubricants, the custom-made composition showed good resilience to low adhesion. The last paper tested the boundary friction properties of TOR lubricant, FM and solid FM. It was found, that independently of the used product, the drop in coefficient of friction occurred at the same weight amount applied. Interestingly, the application of FM without drying the substance resulted in a higher coefficient of friction even after application of an excessive amount. The liquid state of this substance probably allows the movement of solid particles that results in more asperity or hard particle interaction.

This thesis contains original research expanding on knowledge regarding friction

management in wheel and rail contact. The results are confronted with currently published research. Further work should be focused on extending the model by time-dependent changes in the coefficient of adhesion. This would provide information about the redistribution and time effectiveness of the applied product. The main contributions of this thesis can be summarized in the following points:

- Numerical model considering both the boundary and elastohydrodynamic lubrication regime that can predict the coefficient of adhesion based on simple rheological test inputs.
- The use of large particles with high hardness does not improve resilience to low adhesion conditions after the application of TOR product.
- Low frictional values occur at the same amount of product present in the contact, regardless of the type of product used.

8   LIST OF PUBLICATIONS

Publications related to the topic of this thesis

KVARDA, D., R. GALAS, M. OMASTA, L.B. SHI, H.H. DING, W.J. WANG, I. KRUPKA and M. HARTL. Asperity-based model for prediction of traction in water-contaminated wheel-rail contact. *Tribology International*, 2021, 157, 1–11. **(IF 5.620)**

KVARDA, D., S. SKURKA, R. GALAS, M. OMASTA, L.B. SHI, H.H. DING, W.J. WANG, I. KRUPKA and M. HARTL. The effect of top of rail lubricant composition on adhesion and rheological behaviour. *Engineering Science and Technology, an International Journal*. 2022, 35, 1–9. **(IF 4.36)**

KVARDA, D., R. GALAS, M. OMASTA, M. DZIMKO, I. KRUPKA and M. HARTL. Shear properties of top-of-rail products in numerical modelling. *Proceedings of the Institution of Mechanical Engineers, Part F: Journal of Rail and Rapid Transit*. 2022, 0, 1–10. **(IF 1.87)**

Other publications

GALAS, R., D. KVARDA, M. OMASTA, I. KRUPKA and M. HARTL. The role of constituents contained in water–based friction modifiers for top–of–rail application. *Tribology International*. 2018, 117, 87–97. **(IF 5.620)**

SHI, L.B., Q. LI, D. KVARDA, R. GALAS, M. OMASTA, W.J. WANG, J. GUO and Q.Y. LIU. Study on the wheel/rail adhesion restoration and damage evolution in the single application of alumina particles. *Wear*. 2019, 426-427, 1807–1819. **(IF 4.695)**

SHI, L.B., C. WANG, H.H. DING, D. KVARDA, R. GALAS, M. OMASTA, W.J. WANG, Q.Y. LIU and M. HARTL. Laboratory investigation on the particle-size effects in railway sanding: Comparisons between standard sand and its micro fragments. *Tribology International*. 2020, 146, 1–12. **(IF 5.620)**

REMESOVA, M., S. TKACHENKO, D. KVARDA, I. ROCNAKOVA, B. GOLLAS, M. MENELAOU, L. CELKO and J. KAISER. Effects of anodizing conditions and the addition of Al2O3/PTFE particles on the microstructure and the mechanical properties of porous anodic coatings on the AA1050 aluminium alloy. *Applied Surface Science*. 2020, 513, 1–10. **(IF 7.392)**

LI, Q., B.N. WU, H.H DING, R. GALAS, D. KVARDA, Q.Y. LIU, Z.R. ZHOU, M. OMASTA and W.J. WANG. Numerical prediction on the effect of friction modifiers on adhesion behaviours in the wheel-rail starved EHL contact. *Tribology International*. 2022, 170, 1–11. **(IF 5.620)**

NAVRATIL, V., R. GALAS, M. KLAPKA, D. KVARDA, M. OMASTA, L.B. SHI, H.H. DING, W.J. WANG, I. KRUPKA and M. HARTL. Wheel squeal noise in rail transport: the

effect of friction modifier composition. *Tribology in Industry.* 2022, 44, 361–373.

LI, Q., S.Y. ZHANG, B.N. WU, Q. LIN, H.H DING, R. GALAS, D. KVARDA, M. OMASTA, W.J. WANG and Z.F. Wen. Analysis on the effect of starved elastohydrodynamic lubrication on the adhesion behavior and fatigue index of wheel-rail contact. *Wear*. 2022, 510-511, 1–12. **(IF 4.695)**

9 LITERATURE

[1]   CARTER, F., I. J. MCEWEN and C. PRITCHARD. On the Action of a Locomotive Driving Wheel. In: *Proceedings of the Royal Society A: Mathematical, Physical and Engineering Sciences*. 1926, 151–157.

[2]   HAINES, D. J. and E. OLLERTON. Contact Stress Distributions on Elliptical Contact Surfaces Subjected to Radial and Tangential Forces. *Proceedings of the Institution of Mechanical Engineers*. 1963, 177(1), 95–114.

[3]   STOCK, R., L. STANLAKE, C. HARDWICK, M. YU, D. EADIE and R. LEWIS. Material concepts for top of rail friction management – Classification, characterisation and application. *Wear*. 2016, 366–367, 225–232.

[4]   HARMON, M. and R. LEWIS. Review of top of rail friction modifier tribology. *Tribology - Materials, Surfaces & Interfaces*. 2016, 5831, 1–13.

[5]   KALOUSEK, J. and E. MAGEL. Modifying and managing friction. *Railway Track and Structures*. 1997, 93(5), 5–6.

[6]   EGANA, J. I., J. VINOLAS and N. GIL-NEGRETE. Effect of liquid high positive friction (HPF) modifier on wheel-rail contact and rail corrugation. *Tribology International*. 2005, 38(8), 769–774.

[7]   MATSUMOTO, A., Y. SATO, H. OHNO, M. TOMEOKA, K. MATSUMOTO, T. OGINO, M. TANIMOTO, Y. OKA and M. OKANO. Improvement of bogie curving performance by using friction modifier to rail/wheel interface Verification by full-scale rolling stand test. *Wear*. 2005, 258(7–8), 1201–1208.

[8]   OLDKNOW, K. D., D. T. EADIE and R. STOCK. The influence of precipitation and friction control agents on forces at the wheel/rail interface in heavy haul railways. *Journal of Rail and Rapid Transit*. 2012, 227(1), 86–93.

[9]   EADIE, D. T., D. ELVIDGE, K. D. OLDKNOW, R. STOCK, P. POINTNER, J. KALOUSEK and P. KLAUSER. The effects of top of rail friction modifier on wear and rolling contact fatigue: Full-scale rail-wheel test rig evaluation, analysis and modelling. *Wear*. 2008, 265(9–10), 1222–1230.

[10]   SEO, J.-W., H.-K. JUN, S.-J. KWON and D.-H. LEE. Effect of Friction Modifier on Rolling Contact Fatigue and Wear of Wheel and Rail Materials. *Tribology Transactions*. 2016, 0(0), 1–12.

[11]   GALAS, R., D. KVARDA, M. OMASTA, I. KRUPKA and M. HARTL. The role of

constituents contained in water–based friction modifiers for top–of–rail application. *Tribology International*. 2018, 117, 87–97.

[12] GALAS, R., M. OMASTA, I. KRUPKA and M. HARTL. Laboratory investigation of ability of oil-based friction modifiers to control adhesion at wheel-rail interface. *Wear*. 2016, 368–369, 230–238.

[13] STOCK, R., D. T. EADIE, D. ELVIDGE and K. D. OLDKNOW. Influencing rolling contact fatigue through top of rail friction modifier application - A full scale wheel-rail test rig study. *Wear*. 2011, 271(1–2), 134–142.

[14] EADIE, D. T., K. D. OLDKNOW, L. MAGLALANG, T. MAKOWSKY, R. REIFF, P. SROBA and W. POWELL. Implementation of wayside Top of rail friction control on North American heavy haul freight railways. In: *Proceedings of the seventh World Congress on Rail- way Research*. 2006, 2–11.

[15] SPIRYAGIN, M., M. SAJJAD, D. NIELSEN, Y. Q. SUN, D. RAMAN and G. CHATTOPADHYAY. Research methodology for evaluation of top-of-rail friction management in Australian heavy haul networks. In: *Proceedings of the Institution of Mechanical Engineers, Part F: Journal of Rail and Rapid Transit*. 2014, 228(6), 631–641.

[16] EADIE, D. T., M. SANTORO, K. D. OLDKNOW and Y. OKA. Field studies of the effect of friction modifiers on short pitch corrugation generation in curves. *Wear*. 2008, 265(9–10), 1212–1221.

[17] EADIE, D. T. and M. SANTORO. Top-of-rail friction control for curve noise mitigation and corrugation rate reduction. *Journal of Sound and Vibration*. 2006, 293(3–5), 747–757.

[18] VUONG, T. T., P. A. MEEHAN, D. T. EADIE, K. D. OLDKNOW, D. ELVIDGE, P. A. BELLETTE and W. J. DANIEL. Investigation of a transitional wear model for wear and wear-type rail corrugation prediction. *Wear*. 2011, 271(1–2), 287–298.

[19] ISHIDA, M., M. AKAMA, K. KASHIWAYA and A. KAPOOR. The current status of theory and practice on rail integrity in Japanese railways-rolling contact fatigue and corrugations. *Fatigue and Fracture of Engineering Materials and Structures*. 2003, 26(10), 909–919.

[20] GRASSIE, S. L. Rail corrugation: Advances in measurement, understanding and treatment. *Wear*. 2005, 258(7–8), 1224–1234.

[21] EADIE, D. T., M. SANTORO and W. POWELL. Local control of noise and vibration with KELTRACK friction modifier and Protector trackside application: An integrated solution. *Journal of Sound and Vibration*. 2003, 267(3), 761–772.

[22] LIU, X. and P. A. MEEHAN. Investigation of squeal noise under positive friction characteristics condition provided by friction modifiers. *Journal of Sound and Vibration*. 2016, 371, 393–405.

[23] EADIE, D. T., M. SANTORO and J. KALOUSEK. Railway noise and the effect of top of rail liquid friction modifiers: Changes in sound and vibration spectral distributions in curves. *Wear*. 2005, 258(7–8), 1148–1155.

[24] EADIE, D. T., J. KALOUSEK and K. CHIDDICK. The role of high positive friction (HPF) modifier in the control of short pitch corrugations and related phenomena. *Wear*. 2002, 253(1–2), 185–192.

[25] AREIZA, Y. A., S. I. GARCÉS, J. F. SANTA, G. VARGAS and A. TORO. Field measurement of coefficient of friction in rails using a hand-pushed tribometer. *Tribology International*. 2014, 82, 274–279.

[26] KALOUSEK, J. and K. L. JOHNSON. An Investigation of Short Pitch Wheel and Rail Corrugations on the Vancouver Mass Transit System. *Proceedings of the Institution of Mechanical Engineers, Part F: Journal of Rail and Rapid Transit*. 1992, 206(2), 127-135.

[27] MATSUMOTO, A., Y. SATO, H. ONO, Y. WANG, M. YAMAMOTO, M. TANIMOTO and Y. OKA. Creep force characteristics between rail and wheel on scaled model. *Wear*. 2002, 253(1–2), 199–203.

[28] MATSUMOTO, K., Y. SUDA, T. IWASA, T. FUJII, M. TOMEOKA, M. TANIMOTO, Y. KISHIMOTO and T. NAKAI. A Method to Apply Friction Modifier in Railway System. In: *JSME International Journal Series C*. 2004, 47(2), 482-487.

[29] TOMEOKA, M., N. KABE, M. TANIMOTO, E. MIYAUCHI and M. NAKATA. Friction control between wheel and rail by means of on-board lubrication. *Wear*. 2002, 253(1–2), 124–129.

[30] ISHIDA, M., T. BAN, K. IIDA, H. ISHIDA and F. AOKI. Effect of moderating friction of wheel/rail interface on vehicle/track dynamic behaviour. *Wear*. 2008, 265(9–10), 1497–1503.

[31] HARRISON, H., T. MCCANNEY and J. COTTER. Recent developments in coefficient of friction measurements at the rail/wheel interface. *Wear*. 2002, 253(1–2), 114–123.

[32] LUNDBERG, J., M. RANTATALO, C. WANHAINEN and J. CASSELGREN. Measurements of friction coefficients between rails lubricated with a friction modifier and the wheels of an IORE locomotive during real working conditions. *Wear*. 2015, 324–325, 109–117.

[33] GALAS, R., M. OMASTA, M. KLAPKA, S. KAEWUNRUEN, I. KRUPKA and M. HARTL. Case study: The influence of oil-based friction modifier quantity on tram braking distance and noise. *Tribology in Industry*. 2017, 39(2), 198–206.

[34] HARDWICK, C., R. LEWIS and R. STOCK. The effects of friction management materials on rail with pre existing rcf surface damage. *Wear*. 2017, 384–385, 50–60.

[35] LEWIS, R., E. A. GALLARDO, J. COTTER and D. T. EADIE. The effect of friction modifiers on wheel/rail isolation. *Wear*. 2011, 271(1–2), 71–77.

[36] HARDWICK, C., S. LEWIS and R. LEWIS. The effect of friction modifiers on wheel/rail isolation at low axle loads. *Proceedings of the Institution of Mechanical Engineers, Part F: Journal of Rail and Rapid Transit*. 2014, 228(7), 768–783.

[37] SONG, J., L. SHI, H. DING, R. GALAS, M. OMASTA, W. WANG, J. GUO, Q. LIU and M. HARTL. Effects of solid friction modifier on friction and rolling contact fatigue damage of wheel-rail surfaces. *Friction*. 2021.

[38] GODET, M. The third-body approach: A mechanical view of wear. *Wear*. 1984, 100(1–3), 437–452.

[39] HOU, K., J. KALOUSEK and E. MAGEL. Rheological model of solid layer in rolling contact. *Wear*. 1997, 211(1), 134–140.

[40] LU, X., J. COTTER and D. T. EADIE. Laboratory study of the tribological properties of friction modifier thin films for friction control at the wheel/rail interface. *Wear*. 2005, 259(7–12), 1262–1269.

[41] EVANS, M., W. A. SKIPPER, L. E. BUCKLEY-JOHNSTONE, A. MEIERHOFER, K. SIX and R. LEWIS. The development of a high pressure torsion test methodology for simulating wheel/rail contacts. *Tribology International*. 2021, 156, 1–13.

[42] BUCKLEY-JOHNSTONE, L. E., G. TRUMMER, P. VOLTR, A. MEIERHOFER, K. SIX, D.I. FLETCHER and R. LEWIS. Assessing the impact of small amounts of water and iron oxides on adhesion in the wheel/rail interface using High Pressure Torsion testing. *Tribology International*. 2019, 135, 55–64.

[43] SIX, K., A. MEIERHOFER, G. MUULLER and P. DIETMAIER. Physical processes in wheel-rail contact and its implications on vehicle-track interaction. *Vehicle System Dynamics*. 2015, 53(5), 635–650.

[44] SIX, K., A. MEIERHOFER, G. TRUMMER, C BERNSTEINER, C. MARTE, G. MÜLLER, B. LUBER, P. DIETMAIER and M. ROSENBERGER. Plasticity in wheel–rail contact and its implications on vehicle–track interaction. *Proceedings of the Institution of*

Mechanical Engineers, Part F: Journal of Rail and Rapid Transit. 2017, 231(5), 558–569.

[45] MEYMAND, S. Z., A. KEYLIN and M. AHMADIAN. A survey of wheel-rail contact models for rail vehicles. *Vehicle System Dynamics*. 2016, 54(3), 386–428.

[46] VOLLEBREGT, E. A. H., K. SIX and O. POLACH. Challenges and progress in the understanding and modelling of the wheel–rail creep forces. *Vehicle System Dynamics*. 2021, 59(7), 1026–1068.

[47] HERTZ, H. Über die Berührung fester elastischer Körper und über die Härte. *Jorunal für reine und agewandte Mathematik*. 1882, 92, 157–171.

[48] KALKER, J. J. *Three-Dimensional Elastic Bodies in Rolling Contact*. Netherlands: Springer, 1990. 334 p. ISBN 9789048140664.

[49] PIOTROWSKI, J. and H. CHOLLET. Wheel-rail contact models for vehicle system dynamics including multi-point contact. *Vehicle System Dynamics*. 2005, 43(6–7), 455–483.

[50] VERMEULEN, P. J. and K. L. JOHNSON. Contact of Nonspherical Elastic Bodies Transmitting Tangential Forces. *Journal of Applied Mechanics*. 1964, 31(2), 338–340.

[51] POLACH, O. A Fast Wheel-Rail Forces Calculation Computer Code. *Vehicle System Dynamics*. 1999, 33, 728–739.

[52] KALKER, J. J. Simplified Theory of Rolling Contact. *Delft Progress Report*. 1973, 1, 1–10.

[53] KALKER, J. J. A Fast Algorithm for the Simplified Theory of Rolling Contact. *Vehicle System Dynamics: International Journal of Vehicle Mechanics and Mobility*. 1982, 11(1), 1–13.

[54] KALKER, J. J. *On the rolling contact of two elastic bodies in the presence of dry friction*. Delft, 1967. PhD thesis. Delft University of Technology. Faculty of Electrical Engineering, Mathematics and Computer Science.

[55] LOGSTON, C. F. and G. S. ITAMI. Locomotive Friction-Creep Studies. *Journal of Engineering for Industry*. 1980, 102(3), 275–281.

[56] ERTZ, M. and F. BUCHER. Improved Creep Force Model for Wheel/Rail Contact Considering Roughness and Temperature. *Vehicle System Dynamics*. 2002, 37, 314–325.

[57] SHEN, Z. Y., J. K. HEDRICK and J. A. ELKINS. A Comparison of Alternative Creep Force Models for Rail Vehicle Dynamic Analysis. *Vehicle System Dynamics*. 1983, 12(1–

3), 79–83.

[58] POLACH, O. Creep forces in simulations of traction vehicles running on adhesion limit. *Wear*. 2005, 258(7–8), 992–1000.

[59] SPIRYAGIN, M., O. POLACH and C. COLE. Creep force modelling for rail traction vehicles based on the Fastsim algorithm. *Vehicle System Dynamics*. 2013, 51(11), 1765–1783.

[60] LOGSTON, C. F. and G. S. ITAMI. Locomotive Friction-Creep Studies. *Journal of Engineering for Industry*. 1980, 102(3), 275–281.

[61] ROVIRA, A., A. RODA, R. LEWIS and M. B. MARSHALL. Application of Fastsim with variable coefficient of friction using twin disc experimental measurements. *Wear*. 2012, 274–275, 109–126.

[62] MEIERHOFER, A., C. HARDWICK, R. LEWIS, K. SIX and P. DIETMAIER. Third body layer-experimental results and a model describing its influence on the traction coefficient. *Wear*. 2013, 314, 148–154.

[63] MEIERHOFER, A. *A new Wheel-Rail Creep Force Model based on Elasto-Plastic Third Body Layers*. Graz, 2015. PhD thesis. Graz University of Technology, Institute of Applied Mechanics.

[64] VOCE, E. The Relationship between Stress and Strain for Homogeneous Deformation. *Journal of the Institute of Metals*. 1948, 74, 537–562.

[65] CHEN, H., A. YOSHIMURA and T. OHYAMA. Numerical analysis for the influence of water film on adhesion between rail and wheel. *Proceedings of the Institution of Mechanical Engineers, Part J: Journal of Engineering Tribology*. 1998, 212(5), 359–368.

[66] CHEN, H., M. ISHIDA, A. NAMURA, K. S. BAEK, T. NAKAHARA, B. LEBAN and M. PAU. Estimation of wheel/rail adhesion coefficient under wet condition with measured boundary friction coefficient and real contact area. *Wear*. 2011, 271(1–2), 32–39.

[67] CHEN, H., A. NAMURA, M. ISHIDA and T. NAKAHARA. Influence of axle load on wheel/rail adhesion under wet conditions in consideration of running speed and surface roughness. *Wear*. 2016, 366–367, 303–309.

[68] CHEN, H., T. BAN, M. ISHIDA and T. NAKAHARA. Adhesion between rail/wheel under water lubricated contact. *Wear*. 2002, 253(1–2), 75–81.

[69] CHEN, H., T. BAN, M. ISHIDA and T. NAKAHARA. Experimental investigation of influential factors on adhesion between wheel and rail under wet conditions. *Wear*. 2008,

265(9–10), 1504–1511.

[70]   GREENWOOD, J. A. and J. B. P. WILLIAMSON. Contact of nominally flat surfaces. *Proceedings of the Royal Society of London. Series A. Mathematical and Physical Sciences*. 1966, 295(1442), 300–319.

[71]   WU, B., Z. WEN, H. WANG and X. JIN. Numerical analysis on wheel/rail adhesion under mixed contamination of oil and water with surface roughness. *Wear*. 2014, 314(1–2), 140–147.

[72]   GREENWOOD, J. A. and J. H. TRIPP. The Contact of Two Nominally Flat Rough Surfaces. *Proceedings of the Institution of Mechanical Engineers*. 1970, 185(1), 625–633.

[73]   WU, B., Z. WEN, T. WU and X. JIN. Analysis on thermal effect on high-speed wheel/rail adhesion under interfacial contamination using a three-dimensional model with surface roughness. *Wear*. 2016, 366–367, 95–104.

[74]   ZHAO, Y., D. M. MAIETTA and L. CHANG. An Asperity Microcontact Model Incorporating the Transition From Elastic Deformation to Fully Plastic Flow. *Journal of Tribology*. 2000, 122(1), 86–93.

[75]   WU, B., T. WU and B. AN. Numerical investigation on the high-speed wheel/rail adhesion under the starved interfacial contaminations with surface roughness. *Lubrication Science*. 2020, 32(3), 93–107.

[76]   TOMBERGER, C., P. DIETMAIER, W. SEXTRO and K. SIX. Friction in wheel-rail contact: A model comprising interfacial fluids, surface roughness and temperature. *Wear*. 2011, 271(1–2), 2–12.

[77]   SHI, L. B., C. WANG, H. H. DING, D. KVARDA, R. GALAS, M. OMASTA, W. J. WANG, Q. Y. LIU and M. HARTL. Laboratory investigation on the particle-size effects in railway sanding: Comparisons between standard sand and its micro fragments. *Tribology International*. 2020, 146, 1–12.

[78]   WANG, C., L. B. SHI, H. H. DING, W. J. WANG, R. GALAS, J. GUO, Q. Y. LIU, Z. R. ZHOU and M. OMASTA. Adhesion and damage characteristics of wheel/rail using different mineral particles as adhesion enhancers. *Wear*. 2021, 477, 1–12.

[79]   ERTZ, M. and K. KNOTHE. A comparison of analytical and numerical methods for the calculation of temperatures in wheel/rail contact. *Wear*. 2002, 253(3–4), 498–508.

[80]   HERTZ, H. Über die Berührung fester elastischer Körper. *Journal für die reine und angewandte Mathematik*. 1881, 171(92), 156–171.

[81]   BREWE, D. E. and B. J. HAMROCK. Simplified Solution for Elliptical-Contact Deformation Between Two Elastic Solids. *Journal of Lubrication Technology*. 1977, 99(4), 485–487.

[82]   JOHNSON, K. L. *Contact Mechanics*. Cambridge University Press, 1985. ISBN 9780521255769.

[83]   ESFAHANIAN, M. and B. J. HAMROCK. Fluid-Film Lubrication Regimes Revisited. *Tribology Transactions*. 1991, 34(4), 628–632.

[84]   HAMROCK, B. J. and D. DOWSON. *Isothermal Elastohydrodynamic Lubrication of Point Contacts: Part III—Fully Flooded Results*. NASA Technical Note, 1976.

[85]   ROELANDS, C. *Correlational Aspects of the Viscosity-Temperature Pressure Relationship of Lubricating Oils*. Delft, 1966. PhD thesis. Technical University of Delft.

[86]   BHUSHAN, B. Contact mechanics of rough surfaces in tribology: Multiple asperity contact. *Tribology Letters*. 1998, 4(1), 1–35.

[87]   GUPTA, V., G. T. HAHN, P. C. BASTIAS and C. A. RUBIN. Calculations of the frictional heating of a locomotive wheel attending rolling plus sliding. *Wear*. 1996, 191(1–2), 237–241.

[88]   EISENBERG, D. and W. KAUZMANN. *The structure and Properties of Water*. New York: Oxford University Press, 2007. 296 p. ISBN 9780198570264

[89]   MILAN, J. C.G., M. A. CARVALHO, R. R. XAVIER, S. D. FRANCO and J. D.B. DE MELLO. Effect of temperature, normal load and pre-oxidation on the sliding wear of multi-component ferrous alloys. *Wear*. 2005, 259(1–6), 412–423.

[90]   PEARSON, S. R., P. H. SHIPWAY, J. O. ABERE and R. A.A. HEWITT. The effect of temperature on wear and friction of a high strength steel in fretting. *Wear*. 2013, 303(1–2), 622–631.

LIST OF FIGURES AND TABLES

List of figures

List of tables

LIST OF SYMBOLS AND ABBREVIATIONS

a	m	Contact semi-axis in x direction
b	m	Contact semi-axis in y direction
c	J/(kg·K)	Specific heat capacity
C_{11}	–	Kalker's coefficients
D	–	Ellipticity parameter
E^*	Pa	Reduced elastic modulus
E'	Pa	Effective elastic modulus
E_1	Pa	Elastic modulus for body 1
E_2	Pa	Elastic modulus for body 2
f	–	Coefficient of friction
F	N	Force
F_{EHL}	N	Load carried by EHL film
F_F	N	Frictional force
F_N	N	Normal force
F_T	N	Tangential adhesion force
G	Pa	Shear modulus
h	m	Surface separation
H	Pa	Mean pressure related to hardness
h_c	m	Central film thickness
k	–	Axis ratio
K	–	Roughness parameter
L	m/Pa	Coefficient of flexibility
L_e	m/Pa	Elastic third body layer flexibility coefficient
L_K	m/Pa	Kalker's flexibility coefficient
L_p	m	Plasticity parameter

$L_{\mu e}$	m	Frictional elasticity parameter
$L_{\mu p}$	m	Frictional plasticity parameter
m	–	Number of discretization points in x direction
M_k	N·m	Torque
n	–	Number of discretization points in y direction
p	Pa	Pressure
p_a	Pa	Asperity pressure
$\dot{q}$	N/(m·s)	Frictional power dissipation rate
R	m	Reduced contact radius
r_1	m	Inner radius of annulus contact area
r_{1x}	m	Longitudinal radius of body 1
r_{1y}	m	Lateral radius of body 1
r_2	m	Outer radius of annular contact area
r_{2x}	m	Longitudinal radius of body 2
r_{2y}	m	Lateral radius of body 2
r_e	m	Effective radius of annulus contact area
r_x	m	Reduced radius in longitudinal direction
r_y	m	Reduced radius in lateral direction
s	m/s	Slip velocity
S	m^2	Contact area
$slip$	–	Slip ratio
t	s	Time
T	K	Temperature
T_A	K	Ambient temperature
U	–	Dimensionless speed parameter
u_1	–	Deformation of surface for body 1
u_2	–	Deformation of surface for body 2

v	m/s	Rolling speed
v_1	m/s	Velocity of body 1
w	m/s	Rigid slip
W	–	Dimensionless load parameter
W_{BL}	–	Dimensionless load parameter for boundary friction
W_{EHL}	–	Dimensionless load parameter for EHL friction
x	m	Coordinate in x direction
$\dot{x}_1$	m/s	Surface velocity of body 1
$\dot{x}_2$	m/s	Surface velocity of body 2
y	m	Coordinate in y direction
z	m	Coordinate in z direction
Z	–	Roelands pressure-viscosity coefficient
α	1/Pa	Barus pressure-viscosity coefficient
β	m	Curvature of asperity peaks
γ	$1/m^2$	Density of asperity peaks
ε	–	Error
η	Pa·s	Viscosity
η_0	Pa·s	Viscosity at ambient conditions
θ	–	Elliptical integral
Λ	–	Film parameter
λ	W/(m·K)	Thermal conductivity
μ	–	Coefficient of adhesion
μ_{BL}	–	Coefficient of adhesion in boundary friction
μ_{c1}	–	Elasticity limiting coefficient of friction
μ_{c1}^T	–	Elasticity limiting temperature coefficient
μ_{c2}	–	Plasticity limiting coefficient of friction
μ_{c2}^T	–	Plasticity limiting temperature coefficient

μ_{EHL}	–	Coefficient of adhesion in EHL friction
v_1	–	Poisson ration for body 1
v_2	–	Poisson ratio for body 2
ρ	kg/m^3	Density
σ	Pa	Normal stress
τ	Pa	Shear stress
τ_{BL}	Pa	Shear stress in boundary friction
τ_{c1}	Pa	Elasticity limiting shear stress
τ_{c2}	Pa	Plasticity limiting shear stress
τ_{EHL}	Pa	Shear stress in EHL friction
ω_1	rad/s	Angular velocity of body 1
ψ	m	Standard deviation of asperity height

FM	Friction modifier
HPF	High positive friction modifier
HPT	High pressure torsion
LCF	Low coefficient of friction modifier
MTM	Mini traction machine
SRR	Slide-to-roll ratio
TOR	Top of rail
VHPF	Very high positive friction modifier